Università degli Studi del Piemonte Orientale
"Amedeo Avogadro"

Dipartimento di Scienze del Farmaco

Dottorato di Ricerca in Biotecnologie Farmaceutiche ed Alimentari
XXVIII ciclo a.a. 2012-2015

A JOURNEY THROUGH THE CHEMISTRY OF DIAGNOSTIC IMAGING PROBES

Arianna Maria Giani

Supervisor: Prof. Giovanni Battista Giovenzana

PhD program co-ordinator: Prof. Menico Rizzi

Contents

CHAPTER 1

1.0 MOLECULAR IMAGING

“Imaging” refers to the generic process through which it is possible to observe an area of a living organism not visible from the outside and it is widely employed in clinical diagnostics in order to detect and locate physiological and pathological phenomena.
In "*vivo*" medical imaging has made wide improvement through advances in the engineering of imaging devices and developments in the chemistry of probes. Over the past years, the National Cancer Institute recognized Molecular Imaging as an extraordinary tool for studying diseases noninvasively and quantitatively at the molecular level.[1]

Molecular imaging is a scientific discipline and it is a result of combined advances in chemistry, biology, physics and engineering. It can be defined as the visualization, characterization, and measurement of biological processes at the molecular and cellular levels in humans and other living systems and molecular imaging agents are probes used to visualize, characterize, and measure biological processes. These two definitions were stated by the Society of Nuclear Medicine in 2007 as a way to highlight the interdisciplinary nature of this new field of research.[2]

Molecular imaging employs contrast agents or probes of different nature to gain more information. The advantages of using more specific molecular probes are evident for personalized medicine and for accelerating the time and the quality of the diagnosis. At the state of art, however, most of these molecules are non-targeted reagents.[3]

1.1 BASIC PRINCIPLES OF IMAGING MODALITIES: BASIC OF DIAGNOSTIC IMAGING TECHNIQUES

Imaging modalities can be simply divided into two categories:

- ✓ Morphological and anatomical techniques including Computed Tomography (CT), Magnetic Resonance Imaging (MRI) and Ultrasound Sonography (US). They are characterized by high spatial resolution but they are not able to give any information about little changes at the tissue or cell levels. As a matter of fact, these techniques are able to give images of the body that allow to detect coarse changes in a tissue such as tumours in advanced stages.
- ✓ Molecular Imaging techniques include Single Photon Emission Computed Tomography (SPECT), Positron Emission Tomography (PET), Optical Imaging (OI) and Photoacoustic Tomography (PAT). Thanks to the use of radiopharmaceuticals, luminophores and choromophores injected at nanomolar blood concentration they allow to detect subtle changes inside a tissue in a pathological situation (for example early stage tumours). Unfortunately nuclear techniques as SPECT and PET do not possess a great spatial resolution and Optical Imaging techniques suffer from a limited tissue penetration.

Combining morphological/anatomical and molecular imaging modalities, it is possible to obtain a better imaging of the pathophysiological changes in early disease phases with high structural resolution (for example, PET–CT and PET–MRI technology).

Technique	Labels	Signal measured	Strengths	Weaknesses	Cost	Throughput	Sensitivity ([M] of label detected)	Resolution
CT	None	X-rays	Fast, cross-sectional images	Poor resolution of soft tissues	High	Low	10^{-6}	50µm
MRI	Can use isotope-labelled molecular tracers	Alterations in magnetic fields	Harmless, high-resolution of soft tissues	Cannot follow many labels	High	Low	10^{-9}-10^{-6}	50µm
US	Microbubbles, which can be combined with targeted contrast agents	Sound waves	Quick, harmless	Poor image contrast	Low	High	10^{-8}	50µm
SPECT	Radiolabelled molecules	γ-rays	Can distinguish between radionuclides, so more processes can be imaged at once	Requires radioactivity	High	Low	10^{-14}	1-2mm
PET	Radiolabelled molecules	2 γ-rays from positron annihilation	Highly sensitive	Can detect only one radionuclide, implies radioactivity	High	Low	10^{-15}	1-2mm
OI	Genetically engineered proteins and fluorescently labelled probes	Light, particularly in the infrared	Easy, non-damaging technique readily adapted to study specific molecular events	Poor depth penetration	Low	High	10^{-12}	50µm
PAT	Probes that absorb light and create sound signals	Sound waves	Better depth resolution than light	Information processing and machines still being optimized	Low	High	10^{-8}	50µm

Table 1. Imaging techniques currently used in the context of biomedical research and/or medical diagnosis

1.1.1 Computed Tomography

Computed tomography (CT) was introduced in the clinical practice in 1972 and rapidly became a very important tool in the radiological diagnosis. For example CT of the brain became the procedure of choice for evaluation of brain tumours. It replaced invasive procedures such as pneumoencephalography and the progressive improvement of the image quality, reduction of costs, and reduction of scan times has resulted in significant expansion of CT applications.[4] CT is a medical imaging method that combines multiple X-ray projections taken from different angles to produce detailed cross-sectional images of areas inside the body. CT images allow to obtain very precise 3D views of certain parts of the body, such as soft tissues, blood vessels, lungs, brain, heart, abdomen, pelvis and bones. It is often used to locate bone and traumatic injuries, vascular condition/blood flow, abdominal aortic aneurysms, pulmonary embolism, cardiovascular disease and to measure the size and location of tumours.

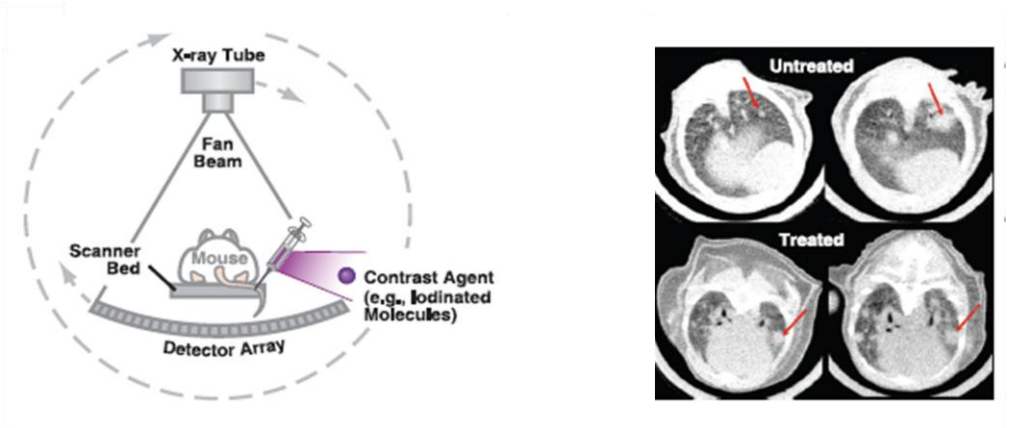

Figure 1. Schematic principle of CT is reported.[5]

1.1.2 Magnetic Resonance Imaging

Magnetic resonance imaging (MRI) is a medical imaging technique commonly used to visualize structures and functions of the body providing detailed images in any plane using intravenous contrast agent.[6]

This technique is based on the principles of nuclear magnetic resonance. A powerful magnetic field aligns the nuclear magnetization of hydrogen atoms of the body water molecules. Radio frequency (RF) fields are used to systematically alter the alignment of this magnetization inducing the hydrogen nuclei to produce a rotating magnetic field detectable by the scanner.[7]

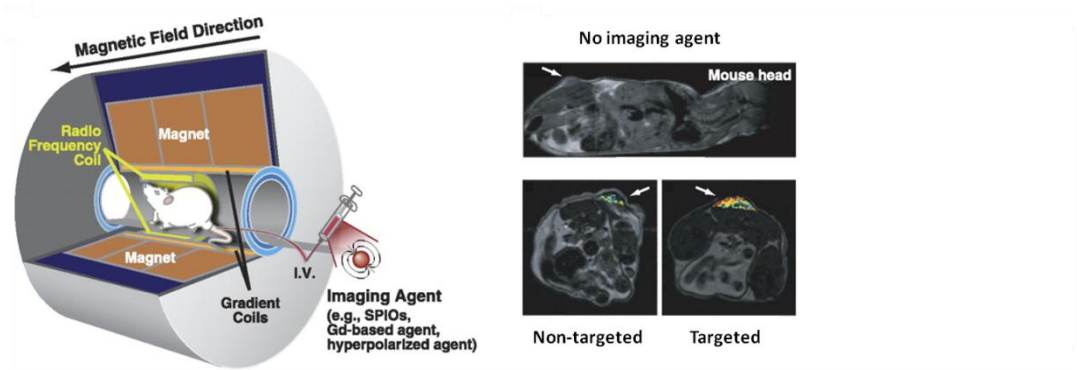

Figure 2. Schematic illustration of MRI: a mouse is placed inside a magnet. Unpaired nuclear spin within the body either align parallel or anti-parallel with the direction of the magnetic field. MR signal is generated from a very small difference in number of parallel versus anti-parallel spins. MRI images with or without contrast agents are reported. [5]

1.1.3 Ultrasound Sonography

Ultrasound (US) imaging is based on the use of the sound at frequency higher than 20 KHz to obtain projections of the organism. Ultrasound contrast agents (UCAs) can be used to improve US-imaging and are based on materials characterized by different acoustic properties respect to other tissues. The most common approach is the use of intravenous injections of small air or gas bubbles (microbubbles) that

improve the Doppler signal from blood vessels. One of its most important application is the study of angiogenesis; it can be indeed used to image microcirculation.[8]

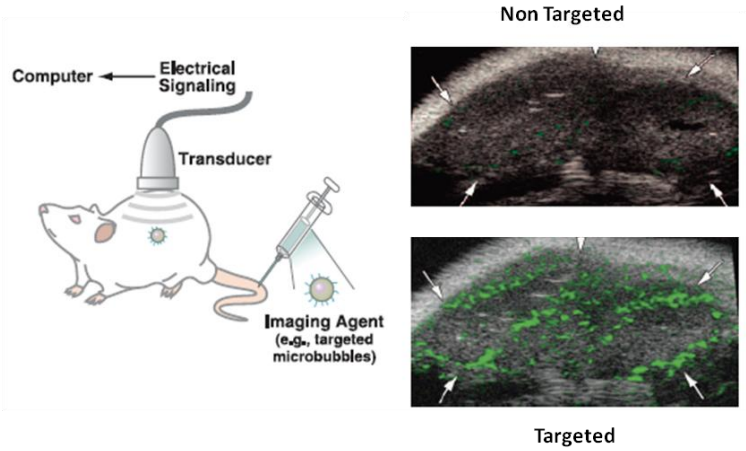

Figure 3. Schematic illustrating the general principles of molecular imaging using US. US images demonstrating the significant advantage of using microbubbles targeted to vascular endothelial growth factor receptor type 2 (VEGFR2) compared with non-targeted microbubbles for visualizing tumour angiogenesis in mice. [5]

1.1.4 Single Photon Emission Computed Tomography

Single Photon Emission Computed Tomography (SPECT) is a medical imaging technique commonly used to obtain 3D biotopological data of the body. SPECT use γ-rays to collect images through a gamma-camera that provides a series of two-dimensional views of the distribution in the body of a radionuclide previously administered to the patient. The radionuclide may be introduced into the patient, normally through injection into the bloodstream or seldom *per os*.

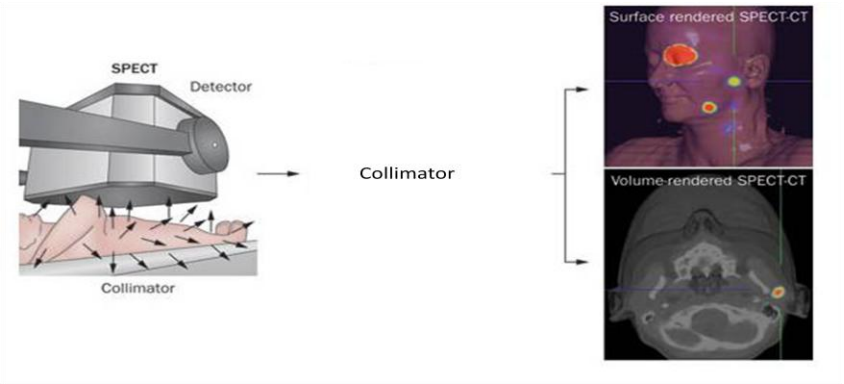

Figure 4. SPECT principles. The radiotracer previously administrated to the patient decay emitting photons. Produced photons transfer energy to the gamma-camera detector. Because photons are emitted in all directions, a collimator is used to collect only photons that are travelling perpendicular to the detector surface. These detectors are made of a high density material, such as lead or steel, through which there are multiple parallel holes. To collect a tomographic image, the gamma camera rotates around the body, collecting a set of overlapping planar images that are elaborated through a 'back projection' technique.

1.1.5 Positron Emission Tomography

Positron Emission Tomography (PET) is one of the most recent techniques used in medical diagnostics and it is able to give functional imaging of the body. This technique exploits positrons issued following radioactive decay of the previously administered tracer. PET is very useful to locate functional changes inside an organ or an entire apparatus and it is essential for early diagnosis. In fact, physiological changes take place before structural alterations in a pathological condition.

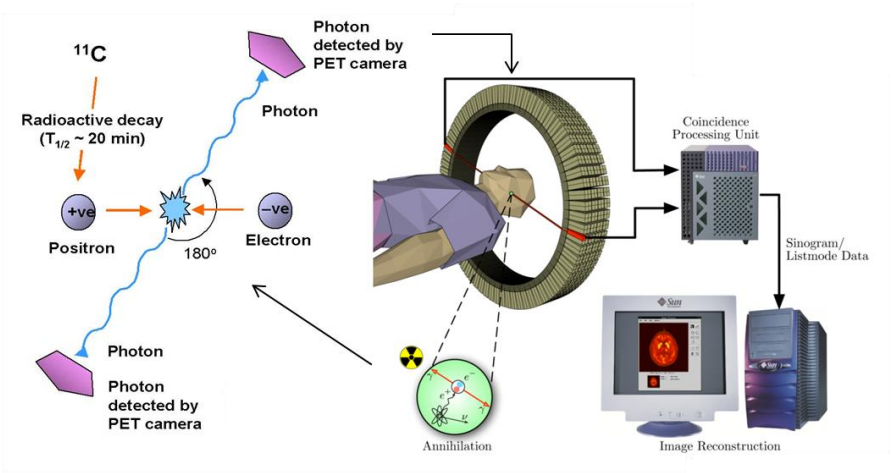

Figure 5. PET scanners detect the simultaneous outcoming of two photons of a characteristic energy from opposed detectors (lower panels), a process is termed 'coincidence'. The photons have an energy of 511 keV, which is the energy released from an electron-positron annihilation reaction. A tomographic image is obtained by combining many 'lines of coincidence'.

1.1.6 Optical Imaging

Optical imaging uses light to visualize the body, and so it is sensitive to compounds and structures in tissues that are able to provide optical contrast. The acquired image depends on the light wavelength applied and the instrumental mode of detection. Generally, light tissue interaction is characterized by the processes of absorption, photon scattering and fluorescence emission. Optical contrast mechanisms include absorption, fluorescence, luminescence and scattering. Optical imaging combines different modalities with a great potential for biomedical imaging. These techniques are used in molecular imaging to visualize and quantify altered molecular mechanism in a non-invasive and ionising radiation-free manner, using relatively simple apparatus.[9-10]

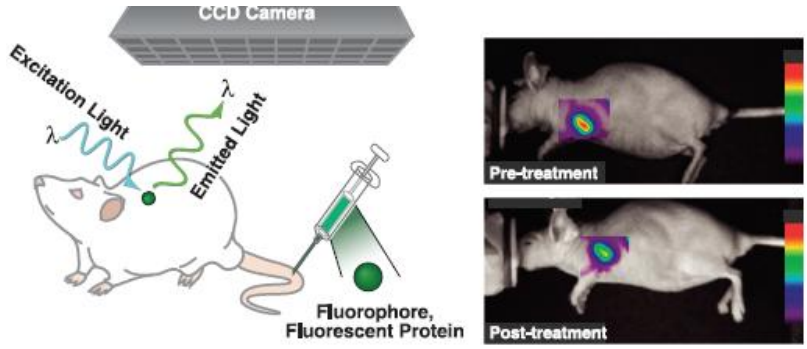

Figure 6. General principles of molecular imaging using optical fluorescence [5]

1.1.7 Photoacoustic Tomography

First reported by Alexander Graham Bell in 1880 [11], the photoacoustic effect can be exploited for imaging purposes. It can be described as the production of sound waves resulting from the absorption of light. One of the main advantages of PAT is its depth of penetration (from 6 mm to 5 cm), which is superior to that of most optical techniques. In addition, the spatial resolution of PAT is not negatively influenced by increases in depth of penetration, as is typically the situation with other optical modalities and US.

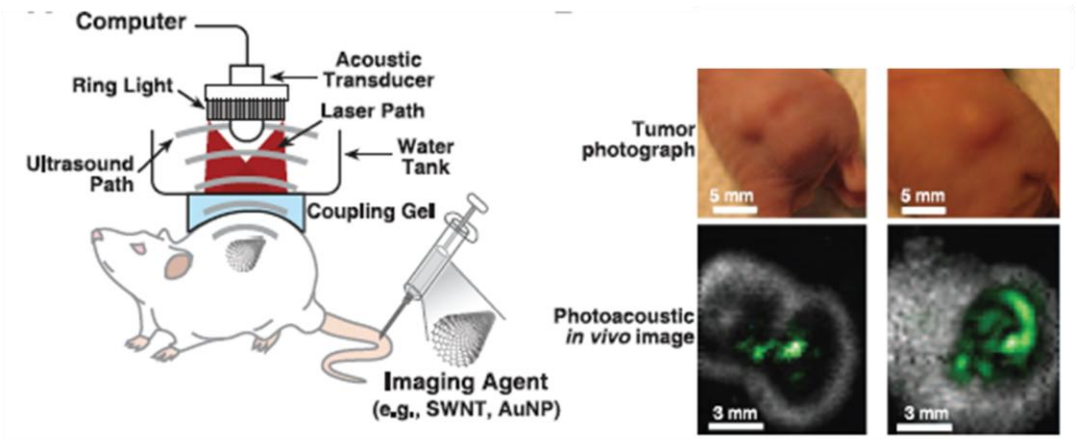

Figure 7. Schematic representation of the basic concept of PAI.[5]

1.2 OPTICAL IMAGING

Optical Imaging is a light-based technology with a great potential to improve the *in vivo* and *in vitro* diagnosis and treatment of various diseases. It offers a number of important advantages over existing radiological imaging techniques using non-ionising radiation. Moreover, the use of dedicated "probes" offers the possibility to study selected biological pathways at the functional and molecular level in a living system or in a model tissue or cell.

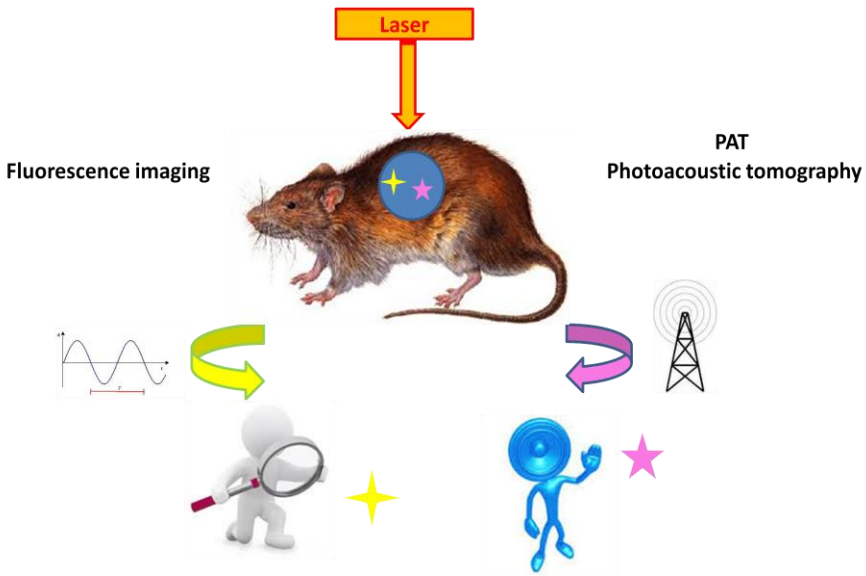

Figure 8. Optical Imaging principles

The principles underlying selected techniques of molecular imaging are shown in Figure 8. The target is irradiated by a high intensity light source, usually a laser. The image can be obtained by detecting the luminescence of suitable fluorescent agents (fluorescence imaging), previously administered. In a different technique (PAT) the laser irradiation is modulated in the KHz range, and an acoustic signal is

detected, arising from the sound waves resulting by the local expression following the absorption of radiation by selected probes. In both imaging techniques, the molecular probe must be endowed with a strong ability to absorb the radiation of the source. Laser sources in the red and infrared region are preferred due to their significant penetration depth in tissues. In fluorescence imaging, the molecular probe must receive the absorbed energy in the form of a longer-wavelength radiation. In PAT, the molecular probe must undergo to a nonradiative decay, releasing thermal energy leading to adiabatic expansion of the local environment.

1.2.1 General requirement for fluorescent probes in Optical Imaging

A successful optical molecular probe for medical imaging should have several adjective properties such as brightness, bio- and photostability, and specific wavelengths and pharmacokinetics [12]

- ✓ WAVELENGTH: fluorophores require excitation light to emit a signal. Excitation in the ultraviolet cannot be used because may cause direct tissue damage,[13] blue or green excitation light have poor tissue penetration and fluorophores which need excitation with about 600 nm (yellow light) are not applicable due to the presence of endogenous molecules responding at the same wavelength. In fact the tissue autofluorescence at these wavelengths could be too high to be distinguished from the exogenous fluorophore signal.[14] The best excitation wavelength of a fluorophore is between near-infrared and the deep red range due to a good tissue penetration and low autofluorescence.[15]

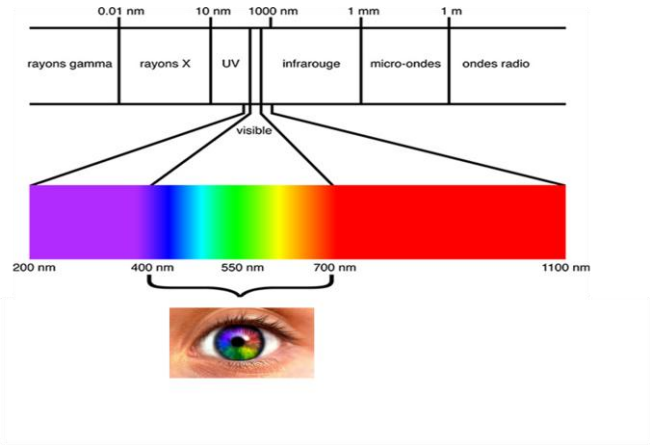

Figure 9. Electromagnetic spectrum

- ✓ BRIGHTNESS: of course, the brighter the agent, better will be signal-to-noise ratio. To be able to increase the brightness, the size of the fluorophore must be larger. However, in this situation different problems ensues such as a difficult conjugation and higher toxicity.[12]
- ✓ STABILITY: the in vivo stability is another crucial point. Once internalized into the lysosome, most of the fluorophores, such as fluorescein, BODIPY, and cyanine derivatives except rhodamines, lose fluorescence in several days. Rhodamine is an exception because it can keep fluorescence for longer than a week. [16-17] Furthermore, photodegradation is a very usual phenomenon for this type of molecules. Although the stability is essential some level of degradation is desirable so that the product could be easily conjugated, metabolized and excreted.
- ✓ PHARMACOKINETICS: fluorophores are often conjugated with biomolecules such as proteins, sugars and antibodies. Most of small-molecules fluorophores may alter the pharmacokinetics of targeting portions to which they are conjugated. Pharmacokinetic and toxicological studies are vital to understand biological half-life, specific tissue accumulation and toxicity.

1.2.2 Classification

Fluorophores can be divided into three major classes:

- ✓ SMALL-MOLECULE FLUOROPHORES: are synthetic fluorophores with various core structures including fluorescein, BODIPY, rhodamine, and cyanine derivatives. All of these are commercial available, with molecular ranges between 300 to 2000 Da and cover the emission spectrum from blue to NIR.[18]
- ✓ GENETICALLY ENCODED FLUORESCENT PROTEINS: they are artificial proteins with emission wavelengths not found in nature, including infrared. [19] In particular three proteins can be cited including green fluorescent protein (GFP), yellow fluorescent protein (YFP), and red fluorescent protein (RFP). Some of them have unique features among which a large Stokes shift.[20]
- ✓ NANOCRYSTALS: are synthetic materials characterised by a broad excitation range, a narrow emission peak, resistance to photodegradation, and extremely high brightness.[21] Numerous nanocrystals with unique optical properties have been reported. They are new products belonging to the field of nanotechnologies, however the pharmacokinetic and pharmacodynamic will be investigated together with many toxicological studies to report any shadows about their use.

1.2.3 Small-Molecule Fluorophores

- ✓ Fluorescein is a synthetic organic compound soluble in water and alcohol. It is widely employed as a fluorescent tracer for many optical applications. Fluorescein is a fluorophore commonly used in microscopy, in forensics to

detect latent blood stains and it is a very important for Fundus Angiography.

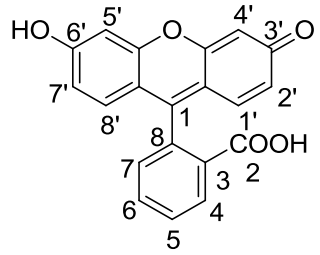

Figure 13. Fluorescein structure

Fluorescein is used to perform retinal angiography to investigate ocular pathologies.[22]

- ✓ BODIPY dyes have been described for the first time in 1968 by Treibs and Kreuzer.[23] BODIPY dyes are notable for their uniquely Stokes shift, high fluorescence quantum yields and high solubility in many organic solvents. The combination of these qualities makes BODIPY fluorophore an important tool in a variety of imaging applications. With derivatives that span the entire visible spectrum BODIPY dyes are proving to be extremely versatile. Some of these compounds have very excellent spectral characteristics and they are largely better than fluorescein. [24] They are used for *in vitro* clinical diagnostics or biological, pharmacological and biochemistry research. Most of these dyes are used to generate fluorescent conjugates such as enzymes, fatty acids, phospholipids, lipopolysaccharides and receptor ligands. In addition, oligonucleotide conjugates BODIPY dyes have been reported to be useful for DNA sequencing,[25,26,27] nucleic acid hybridization [28] and other applications.

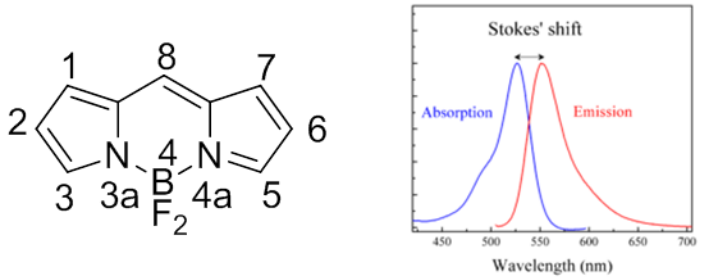

Figure 10. The structure and numbering of the BODIPY fluorophore, 4,4-difluoro-4-bora-3a,4a-diaza-*s*-indacene is reported. Stokes shift is the difference (in wavelength or frequency units) between positions of the band maxima of the absorption and emission spectra.

- ✓ Cyanines represent one of the subclasses of the huge family of polymethine dyes.[29,30] Cyanines have been used as sensitizer for emulsion photography and in advanced photonic materials,[31,32] as well as photodynamic therapy agents or probes for near-infrared imaging.[33,34] These dyes embody a π-conjugated bridge composed of an odd number of sp^2 carbon atoms linking electron-donating or -accepting groups. Photophysical properties are unequivocally related to the bridge length and to a minor extent to the terminal substituents.

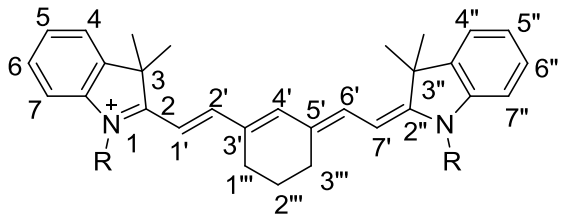

Figure 11. General structure of cyanines

- ✓ Rhodamine dyes are widely employed as fluorescent markers for labeling proteins, nucleic acids, lipids, carbohydrates, toxins, hormones and other biomolecules. They are used owing to their photostability, high extinction, high fluorescent quantum yields, and low degree of triplet formation. [35,36]

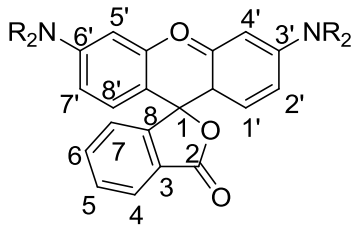

Figure 12. General structure of Rhodamine derivatives

Rhodamine derivatives are used for detecting nucleic acids,[37] for measuring membrane potential,[38] photodynamic therapy,[39] and apoptosis assays.[40]

1.3 MRI: CONCEPTS

Magnetic resonance imaging (MRI) is one of the most significant developments in medical imaging and it is based on the principles of nuclear magnetic resonance, discovered by Bloch and Purcell in 1946, for which they were awarded the 1952 Nobel Prize.[41,42] Since 1970s, MRI has evolved into an indispensable modality for routine clinical diagnosis and widely used tool for "*in vivo*" biomedical research. MRI was used at first for imaging the body and its role in biomedical research has expanded significantly in the past 20 years due to its ability to provide physiological and functional information. Although MRI is becoming mature, advances are still being made and promise to further expand its utility to many applications.[43] MRI is attractive in clinical medicine because it provides images with exquisite soft tissue contrast and it is non-invasive. The use of MRI eliminates the need for invasive diagnostic procedures, and it has been shown to provide physiological information earlier in clinical investigation. The technique also offers fast scan times, the capacity to produce excellent quality and high-resolution images. It has the greatest spatial resolution and clinical potential, and can image structures in the millimeter range without the use of ionising radiation such as that used in X-ray and CT scanning. [44] In 1973, Lauterbur applied the NMR principles to a combination of a strong constant magnetic field and weaker and variable magnetic field gradients. This allowed to identify the position of a particular nucleus, as the strength of the field is proportional to the radiofrequency. [45] Lauterbur did not make any hypothesis as to the potential application for this research, although a comment was made that there was a signal difference between cancerous tissue and normal tissue. Nevertheless, clear potential for the use in clinical imaging was realized, and as soon as few years after this idea was reported, prototype MRI machines were invented. In 1980, medical MRI scans started and since then MRI has become an essential tool for diagnoses in medicine. [45]

The simplest form of NMR imaging involves the application of a linear magnetic field gradient in addition to the main static field in order to “spatially encode” nuclei in the subject with different resonant frequencies. The free introduction decay signal (FID) following a radio frequency pulse is Fourier transformed to yield a one-dimensional projection of signal amplitude along a particular line through the subject. Briefly, the net macroscopic magnetization of proton spins, which is aligned parallel with the applied field along the *z* axis, is perturbed by application of one or more radio frequency pulses. The component of the magnetization along the *z* axis “relaxes” back to its equilibrium value with an exponential time constant, T_1, the longitudinal (or spin-lattice) relaxation time. The time dependence of the magnetization perpendicular to the *z* axis is characterized similarly by T_2, the transverse (or spin-spin) relaxation time, which measures the time for the decay of the transverse magnetization to its equilibrium value of zero. In image data acquisition, the pulses are rapidly repeated for each projection. Tissues with short T_1, values generally yield greater image intensity than those with longer values since the steady-state magnetization along the *z* axis is greater in the tissue with the fastest relaxation. On the other hand, short T_2 values are always associated with lower signal intensity since this diminishes the net transverse magnetization available for detection. Under conditions normally employed, the dominant effect of a paramagnetic agent in NMR imaging is to increase the signal intensity of the tissue containing the agent.

1.3.1 Spin-Lattice Relaxation (T_1)

When a RF pulse is applied, **M** tips towards the xy plane while processing around the steady external magnetic field $\mathbf{B_0}$. When this perturbation is terminated, the nuclear spin system will "relax" to the equilibrium by dissipating the excess energy to its surroundings via thermal exchange. This process is called spin-lattice

relaxation and the equilibrium condition is reached by a first order process characterized by a time constant, T_1, the spin-lattice relaxation time.

1.3.2 Spin-Spin Relaxation (T_2)

When the RF pulse is applied, the moments in the xy plane begin to lose their precessing phase coherence, due to the natural processes that cause nuclei to exchange energy with each other. As a result of this process, called spin-spin relaxation, the net **Mxy** magnetization decays to zero exponentially with time, characterized by the time constant T_2. SI_1 and SI_2 represent the signal intensities of two adjacent regions on an MR image. The magnitude of the detected signal depends upon the spin density (number of protons available), T_1 and T_2 characteristics of tissues, chemical shift, temperature, and flow phenomena. Among these parameters, the relaxation characteristics are most influential to the signal intensity. With conventional MR imaging techniques, however, the relaxation characteristics of the normal and pathological conditions are often very small, making the accurate diagnosis based on the contrast from the MR image difficult. Therefore, it is important to increase the contrast between the normal tissue and pathological conditions on an MR image to improve the diagnostic accuracy. Since the variation of relaxation characteristics has a profound effect on the tissue contrast, the selective enhancement of tissue contrast can be achieved by the administration of MR contrast agents, which change the local environment of protons and thereby change their relaxation characteristics. [46]

1.3.3 Contrast agents

MRI contrast agents (MRI CAs) are chemical compounds able to alter the relaxation times of water protons in tissues where they are distributed. Contrast agents are today used in up 50% of all MRI scans in the clinic. These molecules contain paramagnetic metal ion that increase the relaxation of water protons. The relaxation rate (r_i) represents the efficiency of a contrast agent and is defined by the eq. 1 where ($1/T_i$) indicate the relaxation time of the solution of the contrast agent, $(1/T_i)_0$ that of water, [CA] the c0ntrast agent millimolar concentration.

$$\text{Eq. 1} \qquad (1/T_i) = (1/T_i)_0 + r_i[CA]$$

In Fig. 3 essential parameters influencing the relaxivity are reported. Contrast agents enhance both longitudinal ($1/T_1$) and transverse ($1/T_2$) relaxation rates. Factors include the number of inner-sphere water molecules (q), the rotational tumbling time (τ_R), and the residence lifetime of inner-sphere water molecules (τ_M). A larger inner-sphere hydration (*i.e.*: higher q values) leads to larger relaxivity values. Outer-sphere relaxivity also contributes to the overall relaxivity of a contrast agent. Values such as a (distance of closest approach of outer-sphere water molecules) and τ_D (diffusional correlation time of outer-sphere water molecules) can contribute to relaxivity.[47,48]

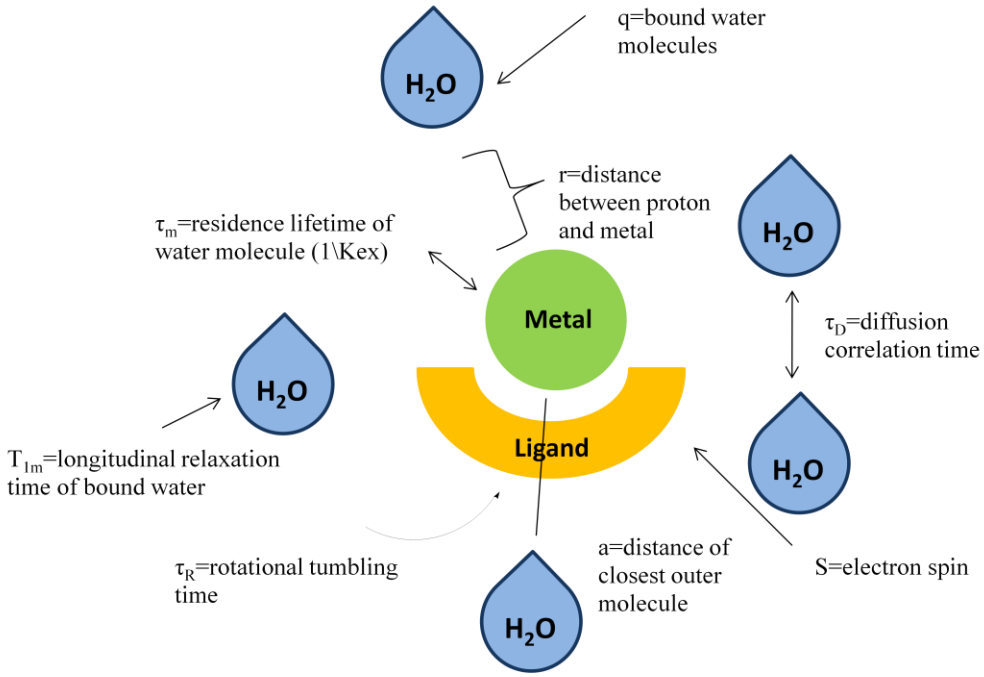

Figure 14. Variables contributing to contrast agent relaxivity

1.3.4 General features for MR Contrast Agents

In addition to nuclear relaxation properties, imaging contrast agents should be biocompatible, aside from standard pharmaceutical features such as water solubility and stability. The principal features requested to a good MRI contrast agent are:

- ✓ RELAXIVITY: the efficiency with which the paramagnetic complex enhances the proton relaxation rates of water, referred to as relaxivity, must be sufficient to significantly increase the relaxation rates of the target tissue. The dose of the complex at which such alteration of tissue relaxation rates occurs must be non-toxic.

- ✓ *"IN VIVO"* DISTRIBUTION: Ideally, to be of diagnostic value, the complex should be localized for a period of time in a target tissue. This is a basic requisite in any procedure of imaging based on complexes where detection of the agent is usually a simple function of its tissue concentration.
- ✓ TOXICITY OF METAL COMPLEXES: the "in vivo" stability and the tissues clearance behaviour of intravenous metal complexes affect their acute and chronic toxicity. It is well known that the free lanthanide ions are relatively toxic at doses required for NMR relaxation rate changes thus, the dissociation of the complex must not occur. [49] It is clear that the integrity of the gadolinium(III) complex must be maintained in vivo in order to create a safe and efficacious MRI agent.

  Toxic effects from a metal complex can derive from:

  - The free metal ion and the free ligand: In the latter two cases, metabolites may be more toxic than the starting compound. The decomplexation of the metal from the ligand generally leads to a higher toxicity due to the presence of the free metal in the body. [30] Dissociation of Gd(III) from an MRI contrast agent is highly undesirable. Free metal and unchelated ligands are generally more toxic than the complex itself. Free Gd(III) is known to bind strongly to serum proteins. In addition the released metal is irreversibly accumulates in the bones. The free ion manages to coordinate oxygen, nitrogen, or sulphur normally present in cell membranes macromolecules resulting in alterations of the dynamic equilibria necessary to life. Gd(III) can interfere and compete with Ca(II) binding sites whereas the toxicity of free ligands can be explained from the sequestration of common metal ions present in the body such as Ca(II).

- The complex: The toxicity of intact metal complexes can derive from a wide variety of effects. The injection of large quantities of the ionic complexes and appropriate counter ions induces a difference in osmolarity between intracellular and extracellular compartments. Water is drawn out of cells as a result of the osmotic gradient, causing cellular and circulatory damages. Other possible mechanisms of chelate toxicity include enzyme inhibition, nonspecific protein conformational effects, or alteration of membrane potentials. [50]

1.3.5 *In vivo* stability of metal complexes

The complex should be efficiently excreted from the body minutes or hours after administration; stability is required only for its lifetime. A wide range of coordinating molecules, proteins and metal ions can compete for either the paramagnetic metal ion or its multidentate ligand. An important thermodynamic point for trivalent metal ions in serum is their precipitation after the interaction with common anions like hydroxide, phosphate, or carbonate. Both phosphate and carbonate are significant with respect to in this parameter. Martell defined the solubilisation constant K_{sol},(eq. 2) as the degree of conversion of the free ligand to the metal chelate where T_L is the total concentration of the ligand. Low values of K_{sol} show incapacity of a ligand to solubilize the ion; alternatively, it would predict that the complex would be unstable with respect to metal ion precipitation. Very high values of K_{sol} would occur for a thermodynamically stable complex where no precipitate would be present. [51]

Eq.2 $$K_{sol} = [ML] / T_L$$

1.3.6 Clinically approved Gadolinium, Manganese and Iron chelates

- ✓ INTRAVENOUS AGENT: Acyclic and macrocyclic polyaminocarboxylic ligands form stable complexes with gadolinium leading to the clinically employed Magnevist®, Dotarem®, Omniscan® and Prohance® (Figure 15). Macrocyclic chelates are characterized by a superior thermodynamic and kinetic inertness with respect to the acyclic counterparts. In recent years, complexes of acyclic chelating agents were demonstrated to slowly dissociate and to be linked with pathologies such as Nephrogenic Systemic Fibrosis, observed in patient with kidney failure exposed to these CAs.[52]

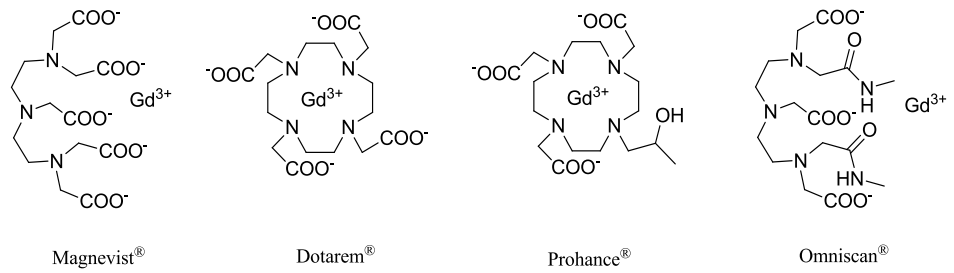

Figure 15. Common commercially available probes

Manganese(II) can be used as an alternative paramagnetic metal ion complexed to a ligand too. Being an endogenous metal ion, its eventual release from corresponding chelates raises less concerns than with gadolinium. A paramagnetic complex based on this metal ion was previously formulated and commercialised for liver imaging: Teslascan® (Figure 16).

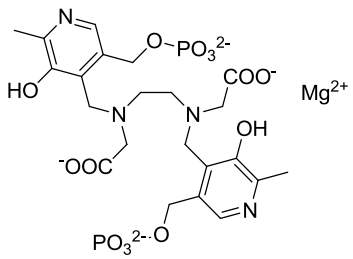

Figure 16. Teslascan®

Another class of intravenous contrast agents includes nanoparticles formed by iron oxides that constitute superparamagnetic centers. Their large magnetic influence causes distortion of the local magnetic field followed by an important signal loss (T_2). Currently, the most used contrast agents are based on supermagnetic iron oxide (SPIO). After injection they are selectively absorbed by reticuloendothelial cells located in the liver, spleen and bone marrow.

- ✓ ORAL AGENTS: oral agents are used for studying abdominal and pelvic structures. They are generally solutions of metal-chelate complexes (Magnevist®) or paramagnetic metal ions (ex.: ferric ammonium citrate).

1.3.7 Classification of MRI contrast agents

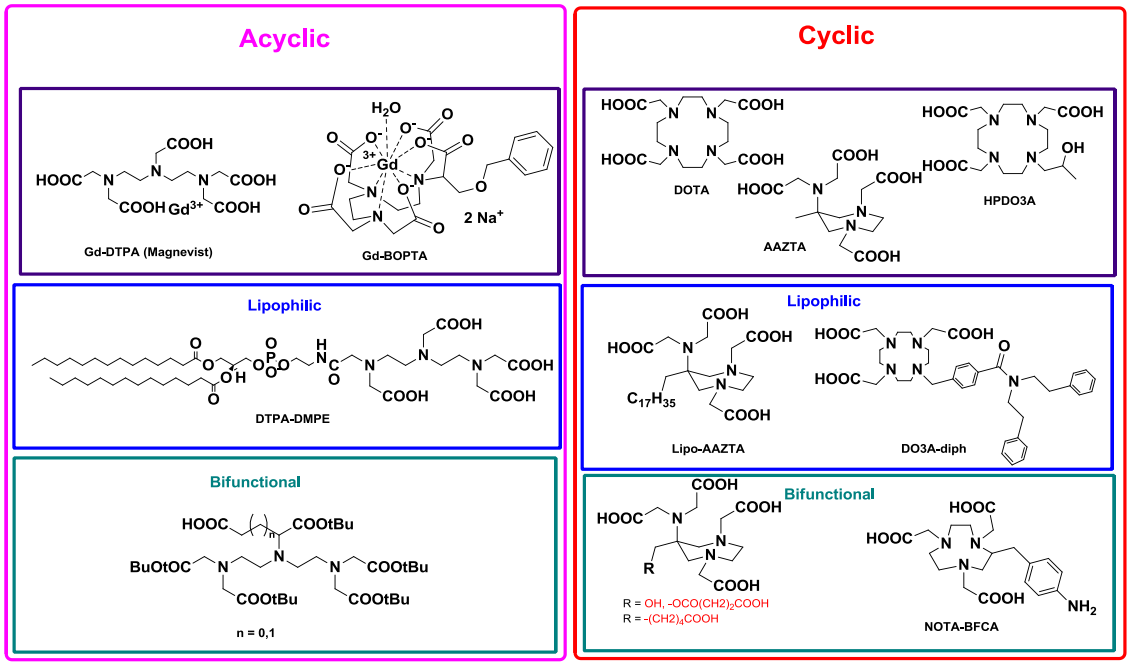

Figure 17. Schematic classification of chelating agents for MRI

- ✓ ACYCLIC CHELATING AGENTS: DTPA was one of the first chelating agents employed in clinical diagnostics with Gd (Gd-DTPA), also known as Magnevist®. It is defined as linear or acyclic octadentate ligand which coordinates Gd(III) permitting the coordination of only one molecule of water in the inner coordination sphere. Several octadentate ligands based to the DTPA scaffold were synthesized, substituting acetate moiety with different amides (DTPA-BMA) obtaining Gd-DTPA-bisamides complexes with relaxivity properties similar to DTPA. The linear structure entails low values of stability constant, while the high denticity is responsible of the relatively low values of relaxivity. Starting from the last observation, ligands characterized by lower denticity were recently investigated showing enhanced relaxivity properties.
- ✓ CYCLIC CHELATING AGENTS: macrocyclic ligands as DOTA are preferable to the DTPA-like open-chain ones, as the latter show lower thermodynamic stability and kinetic inertness. During the last decades, the research in the field of cyclic chelating agents for lanthanides were widely explored: in this framework DO3A and its derivates as HP-DO3A were investigated leading to interesting results and clinically employed derivatives. Recently a new mesocyclic heptadentate ligand with efficient chelating properties was synthesized, *i.e.*: AAZTA. Its efficient size-match with small transition metal ions and lanthanides, the satisfactory thermodynamic and kinetic inertness award to this ligand interesting diagnostic application not exclusively in MRI, but also in PET, and SPECT techniques.
- ✓ LIPOPHILIC CHELATING AGENTS: the introduction of a lipophilic alkyl chain on the skeleton of the common contrast agents supports the self-assembly into micelles or other lipid-based nanoassemblies that exhibit enhanced values of r_1. In addition to this, lipophilic CAs can further form supramolecular adducts with HSA, LDL and HDL with significant

increments in the relaxivity due to the reduced and lower mobility of the systems: example of lipophilic MRI-CAs are Gd-DTPA-DMPE and Gd-AAZTA-C_{17} with potential applications for *in vivo* imaging of tumours and cardiovascular diseases.

- ✓ BIFUNCTIONAL CHELATING AGENTS (BFCAs): they were introduced with the aim to add more selectivity to the contrast agents linking itself to a targeting vector. The most common BFCAs derive from cyclic and acyclic polyaminopolycarboxylic acids similar to DTPA, DOTA and AAZTA, on which a suitable versatile and reactive functional group is added, without altering the chelating properties of the coordination cage.

1.4 NUCLEAR MEDICINE IMAGING: SPECT AND PET

Nuclear medicine imaging is based on the principle of tracers and primarily gives images of function, including physiology, biochemistry or metabolism, by analyzing the dynamic behaviour of molecules in organs and tissues. Nowadays SPECT and PET are the dominant imaging techniques in nuclear medicine. Changes in function often anticipate changes in anatomy in various disease conditions. Accordingly, nuclear medicine imaging may be useful for early diagnosis of disease and for assessment of treatment effects in the early post-therapeutic stage. Single-photon emission computed tomography (SPECT) and positron emission tomography (PET) were the first molecular imaging modalities used clinically. [53]

PET requires the injected drug to be labelled with a positron-emitting radionuclide. When radionuclide decays, it expels a positron from its nucleus, which travels a short distance before being destroyed with an electron to release two γ rays (moving in the opposite direction), detected by the PET scanner.

SPECT requires the use of a contrast agent labelled with a γ-emitting radionuclide. These γ rays are recorded by the detectors of a dedicated gamma camera and after that the signal is processed, it can be converted into an image identifying the tracer localization. In both situations after an enough acquisition time, the data are elaborated by computer using complicated algorithms to produce images of the radiotracer's location within the organism. PET and SPECT use radiopharmaceutical compounds to provides images. Radiopharmaceuticals are drugs containing a radionuclide, and are used routinely in nuclear medicine for the diagnosis or therapy of various diseases. [54] Intravenous injection is the favourite modality to administer radiopharmaceuticals. They are mostly small organic or inorganic compounds with a definite composition.

Radiopharmaceuticals are above all small organic or inorganic compounds but they can also be biomolecules such as monoclonal antibodies and antibody fragments labelled with a radionuclide.

Diagnostics and therapeutics are the two main classes of radiopharmaceuticals. Another kind of classification may be associated to the type of biodistribution: those whose distribution into the body is determined only by their chemical and physical properties; and those whose distribution is determined by their receptor binding or biological interactions. [54]

Radiopharmaceutical	Trade name	Primary uses
Indium-111 pentetate	Indium-111 DTPA®	Imaging of CSF kinetics
Indium-111 oxyquinoline	Indium-111 oxine®	Labeling leukocytes and platelets
Samarium-153 EDTMP	Quadramet®	Palliative treatment of bone pain
Tc-99m Bicisate (ECD)	Neurolite®	Cerebral perfusion imaging
Tc-99m Disofenin (DISIDA)	Hepatolite®	Hepatobiliary imaging
Tc-99m Exametazine (HMPAO)	Ceretec®	Cerebral perfusion imaging
Tc-99m Gluceptate	Glucoscan®	Renal imaging
Tc-99m Lidofenin (HIDA)	Technescan® HIDA	Hepatobiliary imaging
Tc-99m Mertiatide	Technescan® MAG3	Renal imaging
Tc-99m Oxidronate (HDP)	Osteoscan® HDP	Bone imaging
Tc-99m Pentetate (DTPA)	Technеplex®, Technescan®	Renal imaging and function studies
Tc-99m Sestamibi	Cardiolite®, Miraluma®	Myocardial perfusion imaging
Tc-99m Succimer (DMSA)	DMSA®	Breast tumor imaging Renal imaging
Tc-99m Teboroxime	Cardiotec®	Myocardial perfusion imaging
Tc-99m Tetrofosmin	Myoview®	Myocardial perfusion imaging

Table 2. List of selected examples of commercial "small molecule" radiopharmaceuticals, along with their medical applications.

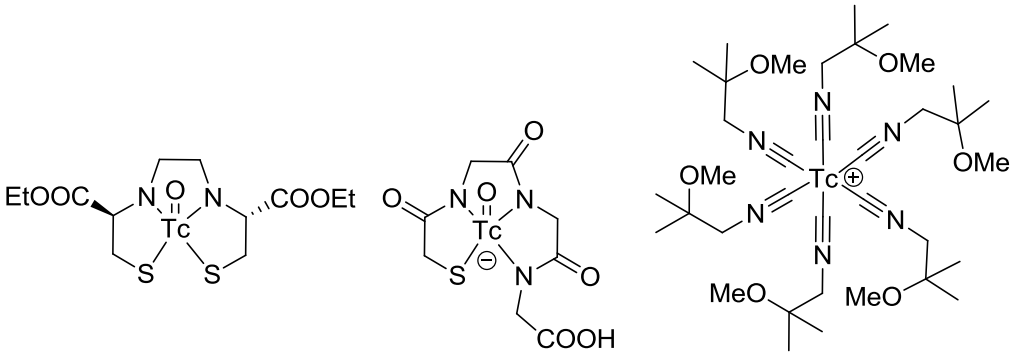

^{99m}Tc-Bicisate ^{99m}Tc-MAG$_3$ ^{99m}Tc-Sestamibi

Figure 18. Structures of selected radiopharmaceuticals based on small metal complexes.

Diagnostic radiopharmaceuticals are molecules labelled with positron-emitting isotopes for positron emission tomography (for PET) or gamma-emitting isotopes for single photon emission computed tomography (for SPECT). As a rule, diagnostic radiotracers do not have pharmacological effect and they are dosed in the range of 10^{-6} to 10^{-8} M.

The first ^{99}Mo/^{99m}Tc generator has been developed in 1959 by the Brookhaven National Laboratory,[55] and $^{99m}TcO_4^{2-}$ has been used for diagnosis of thyroid disease due to the similarity with iodide. Subsequently a lot of ^{99m}Tc complexes have been designed, synthesized and studied as fundamental radio-probes for nuclear medicine. [55,56]

1.4.1 Target-specific radiopharmaceuticals

Currently, one of the biggest issues in the molecular imaging research is the probe specificity. Development of targeted-specific radiopharmaceuticals will be the future in this field. In this strategy, radiotracers are conveyed to the diseased tissue where will interact with a specific receptor. Image quality may be increased by channelling a large amount of radiotracer in the desired tissue, then the toxicity may be reduced. The high specificity of receptor binding results in selective uptake and distribution of the radiolabelled receptor ligand at diseased tissues. A number

of biomolecules, including monoclonal antibodies, antibody fragments and small peptides, have been studied as ‘‘carriers’’ for radionuclides and a part of these have been approved by FDA for diagnosis or treatment of various diseases.

Radiopharmaceutical	Trade name	Primary uses
Indium-111 capromab pendetide	ProstaScint1®	ProstaScint1 Imaging of prostate cancer
Indium-111 pentetreotide	Octreoscan ®	Imaging of neuroendocrine tumors
Indium-111 satumomab pendetide	OncoScint®	Imaging of metastatic disease associated with colorectal and ovarian cancer
Tc-99m Apcitide	AcuTect ®	Synthetic peptide for imaging DVT (deep vein thrombosis)
Tc-99m Arcitumomab	CEA-Scan®	Monoclonal antibody for colorectal cancer
Tc-99m Depreotide	Neotect	Somatostatin receptor-bearing pulmonary masses
Y-90 Ibitumomab tiuxetan	Zevalin	Treatment of non-Hodgkin’s lymphoma
I-131 Tositumomab	Bexxar ® HIDA	Treatment of non-Hodgkin’s lymphoma

Table 3. Selected target-specific diagnostic and therapeutic radiopharmaceuticals

.

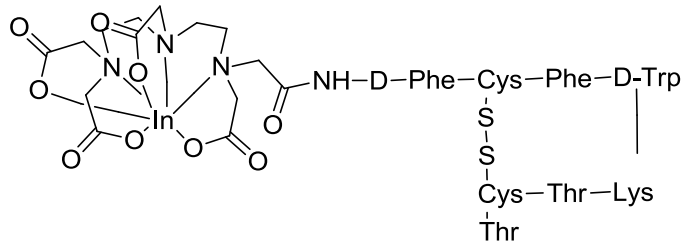

Figure 19. Structures of selected target-specific radiopharmaceuticals

1.4.2 Coordination chemistry and design of radiopharmaceuticals

The general strategies for the design of a radiopharmaceutical are:

- ✓ Integrated approach: the substitution of a part of a known strong affinity receptor ligand with an "unnatural" metal chelate is the basic principle of integrated approach. In this way the conformation, size changes and receptor binding affinity remain unchanged. Unluckily this method often is complicated and the final receptor binding affinity is too low.[57]
- ✓ Bifunctional approach: The bifunctional approach uses a high affinity receptor ligand as the targeting biomolecule such as monoclonal antibodies, small peptides, peptidomimetics, or nonpeptide receptor ligands. The typology and oxidation state of the radiometal are essential criteria to select macromolecules. This approach is the most used to design and development of target-specific radiopharmaceuticals.[54]
- ✓ Hybrid approach: the radiometal is chelated by a tripeptide sequence (such as Gly-Gly-Gly, Cys-Gly-Gly, or Cys-Gly-Cys) containing an N_4, N_3S, or N_2S_2 donor set.[54] the tripeptide sequence can be included in a bigger peptide structure that can be linear or cyclic. Though this method has been used to obtain ^{99m}Tc-and^{188}Re-labeled a-melanocyte-stimulating hormone peptide analogues the efficacy of this approach for the production of a big quantity of final radiopharmaceutical for the commercial market is yet to be proved.[58,59]

1.4.3 Radiometals

Traditionally non-metals isotopes as ^{18}F, ^{15}O, ^{13}N, and ^{11}C are used for PET investigation. They are produced by means of a cyclotron.

^{18}F-FDG is the radiolabeled analogue of glucose and today it is the most important tracer used for PET analysis. Because the supply of glucose is increased in many malignancies, the use of ^{18}F-FDG is essential for detecting and monitoring the tumour presence or the therapy efficacy. It is an important tool for the evaluation of glucose metabolism in the heart and brain and it has been recently approved for Alzheimer's diagnosis.

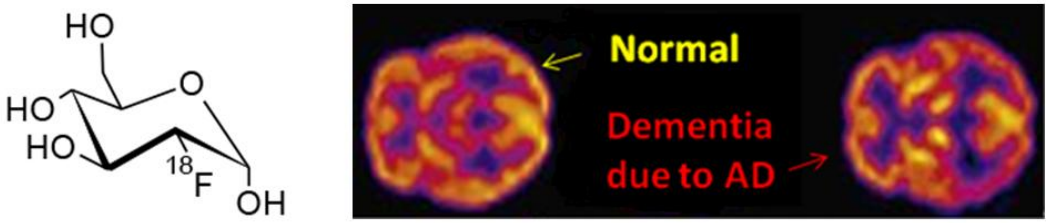

Figure 20. Structure of Fludeoxyglucose (^{18}F). Studies with 18F-FDG in a normal subject and a subject with dementia due to Alzheimer's disease.

Amyvid™ is another example of a molecular imaging agent containing ^{18}F and it is able to bind β-amyloid aggregates, and it is intended for use with PET imaging of the brain. It is a sterile, non-pyrogenic radioactive diagnostic agent for intravenous injection. It is useful to investigate the brain pathology and to estimate β-amyloid plaque density in adult patients with cognitive impairment who are being evaluated for Alzheimer's disease and other causes of cognitive decline.

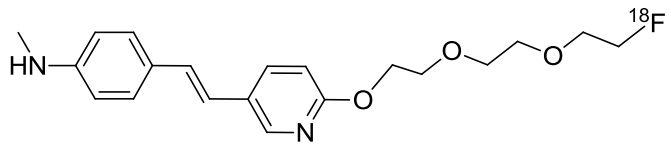

Figure 21. Amyvid™ (E)-4-(2-(6-(2-(2-(2[^{18}F]-fluoroethoxy)ethoxy)ethoxy)pyridine-3-yl)vinyl)-N-methylbenzamine.

Above mentioned isotopes are incorporated into small molecules but owing to their short half-lives and rapid clearance they are not suitable for long term analyses. [53] The time required to purify the radioisotopes, to incorporate it into a carrier agent, the packaging and transport of the resultant radiopharmaceutical across distant locations must be considered and the radiotracer half-life is a central issue. Radionuclides derived from Zr, Y, In, Ga, and Cu isotopes have a longer half-life and they have been investigated as radionuclide labels for biomolecules because they have the potential to combine a nearly optimal decay profile with the biological characteristics of the targeting molecule to become a useful radiopharmaceutical. [60]

Recently PET radioconjugates specific for tumour-associated receptors have been introduced in clinical routine use. They may extend PET applications for *in vivo* quantification of receptor expression and its possible changes during the course of cancer therapy. [61] In this regard the most prominent examples are ^{68}Ga-labeled somatostatin analogues for detect and follow neuroendocrine tumours. [62,63,64]

At the same time other radiometals have witnessed a growing interest for nuclear techniques as zirconium and scandium. In particular the 3.97 hours half-life of ^{44}Sc and its high positron branching of 94.27% and promote the application of ^{44}Sc as radiopharmaceutical for PET. [64] The ligands already used in gadolinium(III)-based magnetic resonance imaging (MRI) contrast agents may be used for the chelation of these radiometals and derivatives of DTPA and DOTA are the first choice. More recently it has been shown that DOTA derivatives are suitable ligands for scandium.[65-66]

1.4.4 Production of radionuclides

The radionuclides most commonly used are generated by a cyclotron or, less commonly, using a linear accelerator. The spectrum of radionuclides that may be produced is dependent of the accelerator energy. Nowadays accelerators with different energies are sold by several industries. ^{18}F is a dominant example of radionuclide used in clinics and produced by accelerator. It is produced by proton bombardment of a stable oxygen-18 (^{18}O) enriched water target, thanks to the nuclear reaction $^{18}O(p,n)^{18}F$.

Radionuclide	Half-life
^{11}C	20.385 min.
^{13}N	9.965 min.
^{15}O	2.037 min.
^{18}F	109.77 min.
^{61}Cu	3.33 hours
^{64}Cu	12.7 hours
^{86}Y	14.74 hours
^{124}I	4.176 days
^{110}In	1.2 hour
^{89}Zr	78.4 hours
^{66}Ga	9.5 hours

Table 4. Data on the half-life of radionuclides are reported

The “generator” is another tool able to provide radionuclides decaying into "daughter" radionuclides with much shorter half-lives. The "parent" radionuclide is chemically bound to an ion exchange column and the ‘daughter’ radionuclide (because of different chemical property) can be eluted and collected. In particular

the $^{68}Ge/^{68}Ge$ generator is remarkable for oncology: its long production useful life combined with the short half-life of ^{68}Ga make it ideal for nuclear medicine practice. [66]

Parent Radionuclide	Half-life	Daughter Radionuclide	Half-life
^{62}Zn	9.26h	^{62}Cu	9.73 min.
^{68}Ge	270.8days	^{68}Ga	67.71min.
^{82}Sr	25.0days	^{82}Rb	1.273 min.

Table 5. Data on the half-life of radionuclides (parent and daughter)

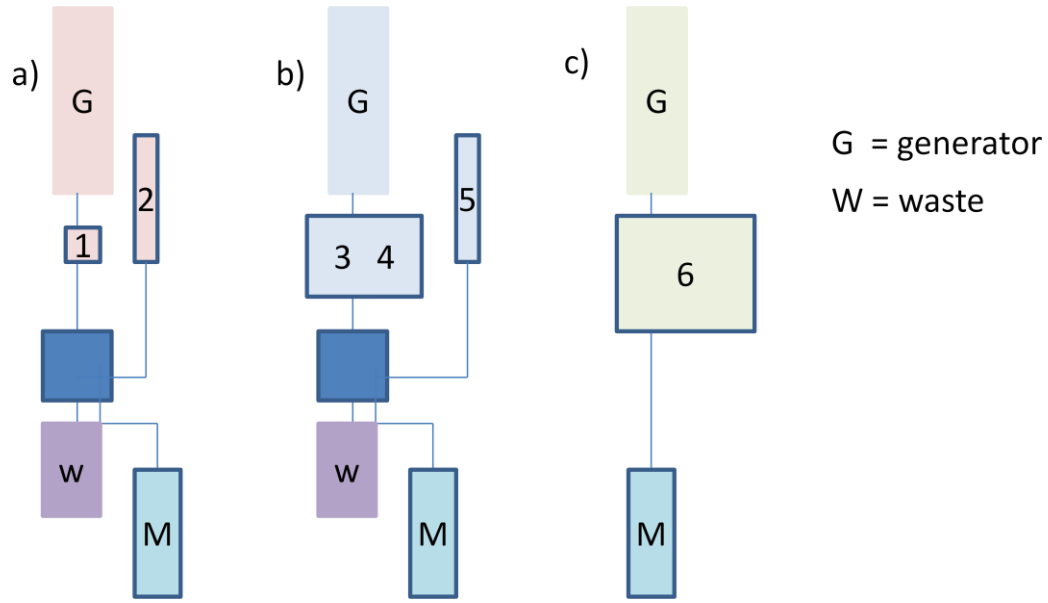

Figure 20. Schematic representation of post-processing technologies for commercial $^{68}Ge/^{68}Ga$ radionuclide generators is shown Figure. [67]

a) Cation exchange-based (Mainz): (1) generator elution through cation-exchange cartridge, (2) desorption of purified ^{68}Ga using HCl/acetone or HCl/ethanol mixtures

b) Anion exchange-based (Hannover/Heidelberg): (3) generator elution into HCl reservoir, (4) second elution through anion-exchange catridge, (5) desorption of purified ^{68}Gd using water
c) Fractionation (Rotterdam): (6) identification of the eluate fraction and use without further purification

Kinetic and thermodynamic stability, redox properties, stereochemistry, coordination chemistry, the charge and lipophilicity are important criteria for the choice of the radiometal. In both production methods the security of final radiometals is essential. Chemico-physical analyses are routinely performed, such as impurity, pH, osmolarity, sterility and toxicity. [61,62,63]

REFERENCES

[1] B. Laxman, D. E. Hall, M. S. Bhojani, D. A. Hamstra, T. L. Chenevert, B. D. Ross and A. Rehemtulla; Proc. Natl. Acad. Sci. USA (2002), 99, 16551

[2] N. Gourtsoyiannis , I. McCall , M. Reiser , B. Silberman , A. Bischof Delaloye , I. Carrió , A. Cuocolo and W. Knapp; Eur Radiol. (2007) Aug;17(8):1926-30.

[3] K. Hisataka, M. Ogawa, R. Alford, P. L. Choyke and Y. Urano; Chem. Rev. (2010), 110, 2620–2640

[4] A. Drevelegas and N. Papanikolaou; Imaging of Brain Tumors with Histological Correlations, Springer, (2011)

[5] M. L. James and S. S. Gambhir; Physiol. Rev. 92: 897–965, (2012)

[6] S. Aime, M. Botta, M. Fasano and E. Terreno; Chem. Soc. Rev.(1998), 27, 19

[7] M. Bottrill, L. Kwok and N. J.Long; Chem. Soc. Rev. (2006), 35, 557

[8] H-D. Liang and M. J. K. Blomley; Br. J. Radiol. (2003), 76, S140-S150

[9] E. M. C. Hillman and S. A. Burgess; Laser & Photon. Rev. (2009), 3, 159

[10] V. Ntziachristos; Annu. Rev. Biomed. Eng. (2006), 8, 1

[11] AG. Bell; Philos. Mag. J. Sci. XI 510–528, (1880).

[12] H. Kobayashi, M. Ogawa, R. Alford, P. L. Choyke and Y. Urano; Chem. Rev. (2010), 110, 2620–2640.

[13] Y. M. W. Janssen; Lab. In. Vest. (1993), 69, 261.

[14] T. Schaeffter; Prog. Drug Res. (2005), 62, 15.

[15] V. Ntziachristos, C. Bremer and R. Weissleder; Eur. Radiol. (2003), 13, 195.

[16] Y.Hama, Y. Urano, Y. Koyama, M. Bernardo, P. L. Choyke and H. Kobayashi; Bioconj. Chem. (2006), 17, 1426.

[17] M. R. Longmire, M. Ogawa, Y. Hama, N. Kosaka, C. A. P. Regino, L. Choyke and H. Kobayashi; Bioconjugate Chem. (2008), 19, 1735.

[18] H. Kobayashi, M. R. Longmire and P. L. Choyke; Adv. Drug Deliv. Rev. (2013) Jul; 65(8): 1112–1119.

[19] R. Heim, A. B. Cubitt and R.Y. Tsien; Nature (1995), 373, 663.

[20] R. Ando, H. Mizuno and A. Miyawaki; Science (2004), 306, 1370.

[21] C. Burda, X. Chen, R. Narayanan and M. A. El-Sayed; Chem. Rev. (2005), 105, 1025.

[22] A. Oishi and F.G. Holz; Am. J. Ophthalmol. (2015) Oct 23.

[23] A. Treibs and F. H. Kreuzer; Justus Liebigs Ann. Chem. (1968), 718, 208.

[24] Handbook of Fluorescent Dyes and Probes, Wiley, (2015)

[25] L.M. Levine, M.L. Michener, M.V. Toth, B.C. Holwerda, Anal. Biochem. 247, 83-88 (1997)

[26] F. Perrin, J. Phys. et Radium (1926), 7(12), 390-401

[27] Weber, G.; in Hercules, D.M. Fluorescence and Phosphorescence Analysis. Principles and Applications, Interscience Publishers (J. Wiley & Sons), New York, pp. 217-240 (1966).

[28] A. Castro, Anal. Chem. (1997), 69(19), 3915-3920.

[29] J. Fabian, H. Nakazumi and M. Matsuoka;. Chem. Rev. (1992), 92, 1197−1226.

[30] A. Mishra, R. K. Behera, B. K. Mishra and G. B. Behera;. Chem. Rev. (2000), 100, 1973− 2011.

[31] J. M. Hales, J. Matichak, S. Barlow, S. Ohira, K. Yesudas, J.-L. Brédas, J. W. Perry and S. R. Marder; Science (2010), 327, 1485−1488.

[32] Q. Bellier, N. S.Makarov, P.A. Bouit, S. Rigaut, K. Kamada, P. Feneyrou, G. Berginc, O. Maury, J. W. Perry and C. Andraud; Phys. Chem. Chem. Phys. (2012), 14, 15299−15307.

[33] X. Wang, J. Sun, W. Zhang, X. Ma, J. Lv and B. Tang; Chem. Sci. (2013), 4, 2551−2556.

[34] C. Hu, W. Sun, J. Cao, P. Gao, J. Wang, J. Fan, F. Song, S. Sun and X. Peng; Org. Lett. (2013), 15, 4022− 4025

[35] M. Beija, C.A.Mafonso and J.M.G. Martinho; Chem. Soc. Rev. (2009), 38, 2410-2433;

[36] M.S.T. Goncalves; Chem. Rev. (2009), 109, 190-212.

[37] O. Seitz and T. Grossmann; Eur. Pat Appl. EP 1860197 (2007).

[38] D. Dickman; PCT Int. Appl. WO 2006054296 (2006).

[39] T. Woo, G. G. Miller and R. Madiyalakan; PCT Int. Appl. WO 2008011707 (2008)

[40] M. Singh and J. W. Gatson; US Pat. Appl. Pub. US 2007141581 (2007).

[41] F. Bloch, W. W. Hansen and M. Packard; Phys. Rev. (1946), 69,127.

[42] E. M. Purcell, H. C. Torrey and R. V. Pound; Phys. Rev. (1946), 69, 37.

[43] X. Hu and D. G. Norris; Annu. Rev. Biomed. Eng. (2004), 6, 157–84.

[44] M. Bottrill, L. Kwok and N. J. Long; Chem. Soc. Rev. (2006), 35, 557.

[45] P. C. Lauterbur; Nature, (1973), 242, 190.

[46] R. B. Lauffer; Chem. Rev. 1907, 87, 901.

[47] E. L. Que and C. J. Chang; Chem. Soc. Rev. (2010), 39, 51.

[48] I. Solomon; Phys. Rev., (1955), 99, 559.

[49] S. Aime , M. Botta, L. Frullano , S. Geninatti , G.B. Giovenzana, R. Pagliarin , G. Palmisano , FR. Sirtori and M. Sisti; J. Med. Chem. (2000);43(21):4017-24.

[50] A. N. Oksendal and P-A Hals; J. Magn. Reson. Imaging, (1993), 3, 15.

[51] A. E. Martell; Inorg. Chimica Acta, (1991).

[52] H.S. Thomsen, S.K. Morcos, T. Almén, M.F. Bellin, M. Bertolotto, G. Bongartz, O. Clement, P. Leander, G. Heinz-Peer, P. Reimer, F. Stacul, A. van der Molen and J. AW. Webb; Eur. Radiol. (2013) Feb;23(2):307-18.

[53] T. J. Wadas, E. H. Wong, G. R. Weisman, and C. J. Anderson; Chem. Rev. (2010), 110, 2858–2902

[54] S. Liu; Chem. Soc. Rev. (2004) 33 445-461.

[55] S. Banerjee, M. R. A. Pillai and N. Ramamoorthy; Semin. Nucl. Med. (2001), 31, 260.

[56] D. Jain; Semin. Nucl. Med. (1999), 29, 221.

[57] R. K. Hom and J. A. Katzenellenbogen; Nucl. Med. Biol. (1997), 24, 485.

[58] M. F. Giblin, S. Jurisson and T. P. Quinn; Bioconjugate Chem. (1997), 8, 347.

[59] Y. B. Miao, D. Whitener, W. W. Feng, N. K. Owen, J. Q. Chen and T. P. Quinn; Bioconjugate Chem. (2003), 14, 1177.

[60] M. J. Welch, C. S. Redvanly; Handbook of Radiopharmaceuticals. John Wiley & Sons Inc.: Hoboken, NJ, (2003).

[61] G. Kramer-Marek and J. Capala; Curr. Pharm. Des. (2012), 18, 2657–2669.

[62] P. W. Miller, N. J. Long, R. Vilar and A. D. Gee; Angew. Chem. Int. Ed. (2008), 47, 8998-9033.

[63] S. Liu; Chem. Soc. Rev. (2004), 33, 445–461.

[64] F. Roesch; Curr. Radiopharm. (2012) 5(3):187-201.

[65]J. Chen, Z. Cheng, T. J. Hoffman, S. S. Jurisson and T. P. Quinn; Cancer Res. (2000), 60, 5649.

[66]A Guide to Clinical PET in Oncology: Improving Clinical Management of Cancer Patients **(**IAEA Tecdoc Series No. 1605. Book)

[67] F. Rosch; J. of Postgraduate Med. (2013) 47(1): 18-25.

CHAPTER 2

2.0 OUTLINE OF THE THESIS

The entire PhD period was devoted to the design, preparation and preliminary evaluation of novel potential probes for diagnostic imaging applications. Rather than selecting a single diagnostic technique among the large number of actually available ones, we decided to focus our research activity on the development of small-sized target compounds, holding specific molecular properties of potential interest for one or (better) more diagnostic techniques. In this contexts were developed the first two topics of this PhD thesis, both involving the study of chelating agents. Chelating agents are widely employed for the coordination of metal ions and when the metal ion plays a role in the diagnostic technique the chelator is essential to allow its safe introduction in the living organism, to mask its toxicity and optionally to enhance specific physico-chemical property and to target the complex towards selected organs and/or tissues. Acyclic chelating agents such as derivatives of the archetypal EDTA and the homolog DTPA are generally a first choice for the chelation of metal ions of diagnostic and therapeutic interest. Unsurpassed thermodynamic inertness of metal complexes of macrocyclic ligands led to the election of this family of chelating agents as the "gold standard" for *in vivo* applications. Nevertheless, their slow kinetic of complex formation is still an open issue in nuclear medicine, where short-lived isotopes are routinely used.

The search for alternative chelating agents is very active because the properties of the currently employed compounds are far to be optimal. Much work has to be done in terms of stability, selectivity and other important features such as the easy conjugation to other molecules, (bio)degradability and not last an easy synthetic access leading to reduced costs.

The first topic of the present thesis involved the design and preparation of a novel chelating agent. The latter was built in a very simple process, taking advantage of a widely available commodity chemical. The structure of the hexadentate ligand includes two amines and four carboxyl groups, placed in a stereochemically controlled fashion on a substituted cyclohexane ring. The unusual arrangement of donor groups of this novel compounds was the subject of the potentiometric determination of its protonation and stability constants. The affinity data registered for different metal ions allowed us to delineate the behaviour of this original chelating agent.

The experience in the potentiometric determination of solution thermodynamic data gained during the period spent in the Department of Inorganic and Analytical Chemistry of the University of Debrecen was directly applied in the second section of the PhD activity. In this task, we explored the possibility to expand the use of a chelating agents previously developed in our research group (AAZTA) for a metal ion recently resurged to the interest of the nuclear medicine community, *i.e.*: Sc^{3+}. The positron emitting isotope ^{44}Sc is characterized by its relatively long half-life, allowing a wider time window for diagnostic imaging purposes; moreover, it can be obtained by a dedicated generator, allowing a more practical and cyclotron-independent *in situ* use. The coordination chemistry of Sc^{3+} is scarcely explored and we were prompted to evaluate the affinity of the chelating agent AAZTA towards this trivalent metal ion, using a combination of potentiometric and spectrophotometric techniques.

An additional topic of the present thesis involved the search for novel molecular scaffolds for optical imaging applications. The latter usually relies on established chromophores or luminophores, with the molecular diversity represented by large variations in the pattern of substituents.

We decided to explore different molecular bases for the development of optical imaging probes and turned our attention to two specific families of compounds: perimidines and aminoquinones.

Perimidines are trinuclear diazaheterocycles synthesised from 1,8-naphthalenediamines and easily functionalised on the pyrimidine moiety, allowing large structural modulations. During the PhD period a series of 2-substituted perimidines was synthesized in order to evaluate its photophysical properties. All the synthesized compounds showed significant fluorescence, and a detailed study of absorption, emission and quantum yield allowed to trace the general properties of perimidines and to learn on the influence of the substituents.

Aminoquinones, aminoquinomethides and derivatives were considered as potential scaffolds for optical imaging applications mainly due to their "push-pull" electronic features, leading to unusually high absorption wavelengths. An easy synthetic access, combined with an almost unlimited variation of the substituents and optional benzo- o hetareno- ring fusion, represent an interesting starting point for the design of chromophores reaching the near-infrared optical window of biological tissues. Exploring the chemistry of aminoquinomethides we met an unprecedented reaction sequence leading to the efficient preparation of highly coloured diaminoquinones, starting from simple compounds as vanillin. The reaction sequence was studied in detail, allowing to outline the likely mechanism and the structural versatility. Preliminary toxicological tests on diaminoquinones showed an almost complete absence of effects on different cellular lines and suggesting the general safety for these compounds.

CHAPTER 3

cis-IPDTA: an Original Polyaminopolycarboxylic Chelating Agent from Isophoronediamine. Synthesis and Thermodynamic Characterization of Metal Complexes

Arianna Maria Giani[a,b], Adrienn Vágner[a] Roberto Negri[b], Zsolt Baranyai[a], Giovanni Battista Giovenzana[b]*

[a] – Department of Inorganic and Analytical Chemistry, University of Debrecen, H-4010, Debrecen, Egyetem tér 1 (Hungary)

[b] – Dipartimento di Scienze del Farmaco, Università degli Studi del Piemonte Orientale "A. Avogadro", Largo Donegani 2/3, I-28100 Novara (Italy)

Abstract

An original diaminotetracarboxylic acid chelating agent (*cis*-**IPDTA**, *cis*-isophoronediamine-*N,N,N',N'*-tetraacetic acid) was prepared starting from commercially available isophoronediamine. Its protonation constants and the stability of selected metal complexes were determined by potentiometric titrations. The coordination behavior of *cis*-**IPDTA** was compared with that of the linear congener **BDTA** and iminodiacetic derivatives.

Introduction

Polyaminopolycarboxylic acids represent the most important class of synthetic chelating agents. They are largely used in a wide range of applications, resulting in

a worldwide estimated consumption in the order of 10^5 tons/year.[1] Despite such impressive commercial interest, this huge market is dominated by just three compounds, **NTA**, **EDTA** and **DTPA**, depicted in Figure 1, with less than a dozen more ligands produced in industrially relevant amounts.[2]

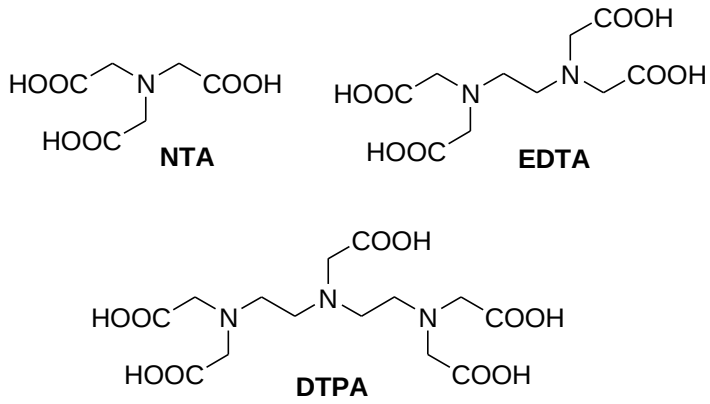

Figure 1: The polyaminopolycarboxylic acid ligands **NTA**, **EDTA** and **DTPA**.

The research in this area is still active as several issues in the design of complexing agents are far to be considered satisfactory, such as the specificity and selectivity towards specific metal ions[3][4] and (bio)degradability.[5] The large scale involved in the different applications of chelating agents lead to the inclusion of the production cost as a critical factor in an overall evaluation of new potential candidates.

In the search of original ligands with improved properties we recently designed and synthesized novel compounds with unusual molecular skeletons as **AAZTA**,[6] a mesocyclic triaminotetracarboxylic acid showing remarkable affinity for several metal ions of diagnostic and therapeutic interests,[7,8] and **NORDATA**, a bicyclic diaminotetracarboxylic derivative featuring a rigid molecular structure.[9]

Furthermore, heterocyclic *s*-triazine derivatives embodying two hydrazino-*N*,*N*-diacetic coordinating residues (**TDITA**s) were assembled resulting in a overall

heptadentate coordinating environment with a selective affinity for mid-series lanthanoids.[10,11]

Isophoronediamine (**IPD**) is a commodity chemical produced in large amounts as an intermediate for the preparation of isophorone diisocyanate, an important building block widely employed for the preparation of polyurethanes and in the modification of alkyd resins. **IPD** is used as such as hardener for epoxy resin and as intermediate in the preparation of the corresponding diisocyanate.[12] Despite its wide availability and low price, this diamine found scarce use in organic synthesis, a recent example being the preparation of a diurea-based catalyst used to perform a stereoselective variant of the Morita-Baylis-Hillmann reaction.[13]

Here we describe the synthesis and the complexation behavior of a new polyaminopolycarboxylic acid-based ligand, *cis*-**IPDTA** (*cis*-isophoronediaminetetraacetic acid), built by placing four coordinating carboxymethyl groups on the nitrogen atoms of the isophoronediamine skeleton.

Experimental section

2.1 - Material and methods

The chemicals used for the experiments were of the highest analytical grade. Isophoronediamine was obtained from Sigma-Aldrich; the resolution of the diastereomeric mixture to obtain diastereomerically pure racemic (±)-*cis*-isophoronediamine is reported in literature.[14] The metal chlorides solutions were prepared from the corresponding commercially available salts (*Aldrich*, 99.9%). The concentration of $CaCl_2$, $MnCl_2$, $Pb(NO_3)_2$, $Cd(NO_3)_2$, $ZnCl_2$, $CuCl_2$ and $LnCl_3$ solutions were determined by complexometric titration with standardized Na_2H_2**EDTA** and *Xylenol Orange* ($ZnCl_2$, $Pb(NO_3)_2$, $CdCl_2$, $LnCl_3$), *murexide* ($CuCl_2$), *Patton & Reeder* ($CaCl_2$) and *Eriochrome Black T* ($MnCl_2$) as indicators. The concentration of the *cis*-**IPDTA** was determined by pH-potentiometric titration

in the presence and absence of a large (40-fold) excess of $CaCl_2$. The pH-potentiometric titrations were made with standardized 0.2000 M KOH. Liquid-phase NMR experiment were recorded on a JEOL ECP300 (7.04 T) spectrometer.

2.2 – Synthesis

2.2.1 - *Tetra-tert-butyl isophoronediamine-N,N,N',N'-tetraacetate* (*cis*-**IPDTA**-(*t*Bu)$_4$)

(±)-*cis*-Isophoronediamine (1.0 g, 5.9 mmol) was dissolved in acetonitrile (30 mL). *tert*-Butyl bromoacetate (3.85 mL, 26.1 mmol, 4.4 eq) and potassium carbonate (8.18 g, 59.3 mmol, 10 eq) were sequentially added and the resulting reaction mixture was stirred at room temperature 24 hours, checking periodically by TLC. The solvent was removed by evaporation under reduced pressure. The resulting oil was redissolved with dichloromethane and washed thrice with a saturated $NaHCO_3$ solution of sodium bicarbonate and twice with brine. The organic phase was dried over anhydrous Na_2SO_4, filtered, and the solvent was removed by evaporation under reduced pressure. The resulting crude oily product was purified by gravimetric chromatography on silica-gel column (petroleum ether/ethyl acetate 95:5 to 9:1), yielding *cis*-**IPDTA**-(*t*Bu)$_4$ (1.45 g, 2.3 mmol, 39%) as a light yellow oil. ^{1}H-NMR ($CDCl_3$, 300 MHz, 298K) δ: 3.42 (*s*, 4H), 3.39 (*s*, 4H), 3.06-2.93 (*m*, 1H), 2.38 (*s*, 2H), 1.62-1.40 (*m*, 2H), 1.43 (*s*, 18H), 1.42 (*s*, 18H), 1.15-0.78 (*m*, 4H), 0.96 (*s*, 3H), 0.94 (*s*, 3H), 0.88 (*s*, 3H). ^{13}C-NMR ($CDCl_3$, 75.4 MHz, 298K) δ: 171.3 (2C), 80.6 (2C) 71.8 (CH_2), 58.7 (CH_2), 55.0 (CH), 53.5 (CH_2), 47.4 (CH_2), 43.5 (CH_2), 39.1 (CH_2), 38.7 (C), 35.6 (CH_3), 32.0 (C), 28.25 (CH_3), 28.16 (CH_3), 27.9 (CH_3), 23.6 (CH_3). ESI-MS (+): m/z calcd for $C_{34}H_{62}N_2O_8$ (626.5), found 627.4 ($M+H^+$), 649.4 ($M+Na^+$).

2.2.2 - *Isophoronediamine-N,N,N',N'-tetraacetic acid* (*cis*-**IPDTA**)

cis-**IPDTA**-(*t*Bu)$_4$ (1.04 g, 1.66 mmol) was dissolved at room temperature in trifluoroacetic acid (10 mL) and the resulting reaction mixture was stirred at room temperature for 3 days. The solvent was removed under reduced pressure and the resulting oil was dissolved in methanol and precipitated with diethyl ether. This purification procedure was repeated 3 times, affording *cis*-**IPDTA** (900 mg, 1.43 mmol) as a white powder. ^{1}H-NMR (D_2O, 300 MHz, 298K) δ: 4.03 (*s*, 8H), 3.76 (*bt*, 1H), 3.19 (*s*, 2H), 1.88-1.77 (*m*, 2H), 1.50-1.18 (*m*, 6H), 1.22 (*s*, 3H), 0.98 (*s*, 3H), 0.94 (*s*, 3H). ^{13}C-NMR (D_2O, 75.4 MHz, 298K) δ: 169.21 (C), 169.17 (C), 70.2 (CH_2), 61.4 (CH), 59.4 (CH_2), 53.5 (CH_2), 45.9 (CH_2), 37.9 (C), 36.2 (CH_2), 35.3 (C), 34.1 (CH_3), 31.7 (CH_2), 26.6 (CH_3), 22.1 (CH_3). ESI-MS(-): m/z calcd for $C_{18}H_{30}N_2O_8$ (402.2), found 401.2 $[M\text{-}H^+]^-$.

2.3 Potentiometric titrations

The protonation and the stability constants of some metal complexes formed with *cis*-**IPDTA** ligand were determined by pH-potentiometric titration. The metal-to-ligand concentration ratios were 1:1 and 2:1 (the concentration of the ligand was generally 0.002 M). For the pH measurements and titrations, a *Metrohm 785 DMP Titrino* titration workstation and a *Metrohm-6.0233.100* combined electrode were used. Equilibrium measurements were carried out at a constant ionic strength (0.1 M KCl or KNO_3) in 6 mL samples at 25 °C. The solutions were stirred, and N_2 was bubbled through them. The titrations were made in the pH range of 1.7-11.7. KH-phthalate (pH=4.005) and borax (pH=9.177) buffers were used to calibrate the pH meter. For the calculation of $[H^+]$ from the measured pH values, the method proposed by *Irving et al.* was used.[15] A 0.01M HCl or HNO_3 solution was titrated with the standardized KOH solution in the presence of 0.1 M KCl or KNO_3 ionic strength. The differences between the measured (pH_{read}) and calculated pH (-

log[H^+]) values were used to obtain the equilibrium H^+ concentration from the pH values, measured in the titration experiments. The protonation and stability constants were calculated with the PSEQUAD software.[16]

Results and discussion

The structural features of **IPD** (5-amino-1,3,3-trimethylcyclohexanemethylamine) are represented by two primary amine groups on the central saturated six-membered ring, placed in different chemical environments. A first amine group is directly linked to the cyclohexane residue while the second one is linked to the ring through a single -CH_2- group. Three methyl groups complete the molecule introducing some steric hindrance. The molecule is chiral with C-1 and C-3 being the stereocentres and giving rise to an overall count of 4 stereoisomers. In principle **IPD** may appear to be a non-optimal candidate for the preparation of chelating agents, as the two donor nitrogen atoms are separated by 4 carbon atoms. Metal chelation would lead to the formation of 7-membered rings, reported to show lower stability compared with 5- or 6-membered chelate rings. Nevertheless, the presence of the cyclohexane ring introduces an element of strong structural rigidity that could counterbalance the unfavourable entropic factor represented by the long inter-nitrogen distance. Furthermore, Berkessel *et al.* reported a method to isolate selectively the *cis*-isomer of **IPD**, based on the selective absorption of carbon dioxide to form the alcohol-insoluble carbamic acid, subsequently decarboxylated by thermal treatment.[14] The *cis*-stereochemistry places the coordinating nitrogen atoms on the same side of the ring plane, possibly inducing the formation of chelates.

The amine groups in *cis*-**IPD** may be located in an equatorial-equatorial (*eq-eq*) or in an axial-axial (*ax-ax*) disposition as a consequence of ring-flipping phenomena (Scheme 1). The *eq-eq* disposition is not suitable for metal chelation due to the distance between the nitrogen atoms. The cyclohexane ring commutation leads the

two amines to reside in equatorial positions of the free chelating agent, while they are forced in the less-stable diaxial positions when implicated in the coordination of the metal.

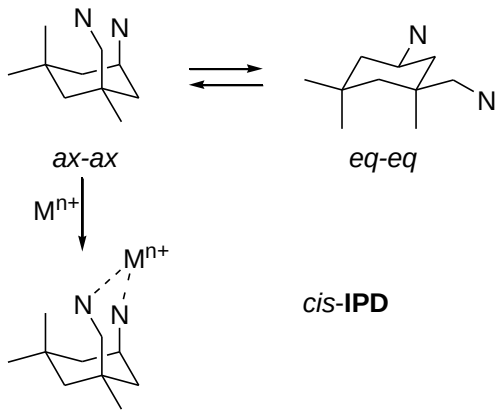

Scheme 1. Conformational equilibrium for *cis*-**IPD**.

In this work we report the functionalization of the nitrogen atoms with four carboxymethyl residues, completing the assembly of the potentially hexadentate original chelating agent (*cis*-)**IPDTA**. Functionalization is achieved by exhaustive alkylation with *t*-butyl bromoacetate in acetonitrile in the presence of potassium carbonate (Scheme 2). Standard removal of the *t*-butyl groups with neat TFA yields the desired ligand, whose behavior with a wide array of metal ions is studied by means of potentiometric techniques. The thermodynamic behavior of the cyclic *cis*-**IPDTA** was compared with that of the linear congener **BDTA** (1,4-butanediamine-*N,N,N',N'*-tetraacetic), sharing the same distance between the two iminodiacetic functions (*i.e.*: 4 carbon atoms). This comparison is intended to evaluate the contrasting effects on the metal chelation of the conformational issues. In principle, **IPDTA** (or its derivatives) can behave as heteroditopic coordinating agent, since the iminodiacetic moieties are located in a different chemical environment. Nevertheless, the resulting dinuclear complexes would be characterized by a considerable loss of stability due to the absence of the intermolecular "chelate effect".

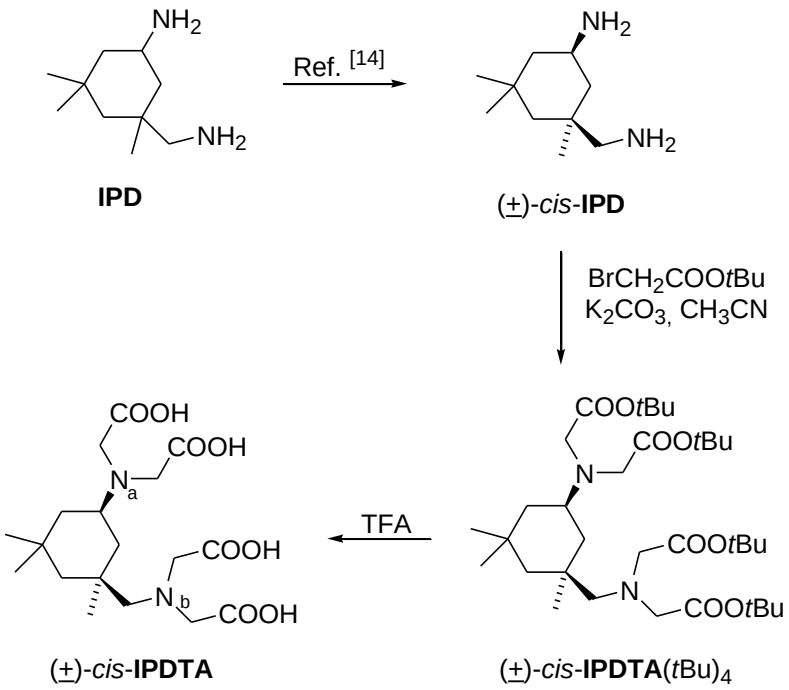

Scheme 2. Synthesis of *cis*-**IPDTA**. a) $BrCH_2COOtBu$, K_2CO_3, CH_3CN, r.t., 24h; b) TFA, r.t., 3d.

3.1 – Synthesis

The synthetic pathway employed for the preparation of *cis*-**IPDTA** is depicted in Scheme 2. The commercial mixture of **IPD** isomers was separated using the literature procedure reported by Berkessel *et al.*,[14] affording the racemic *cis*-**IPD** with good diastereomeric excess (*de* > 98%). *cis*-**IPD** was peralkylated with *tert*-butyl bromoacetate in the presence of potassium carbonate in acetonitrile, leading to *cis*-**IPDTA**-$(t\text{Bu})_4$. Treatment with trifluoroacetic acid and precipitation with diethyl ether led to the isolation of the tetraacetic acid *cis*-**IPDTA** as a bis(trifluoroacetate) salt.

3.2 Equilibrium studies

3.2.1 Protonation equilibria: The complexation properties and protonation equilibria of the *cis*-**IPDTA** ligand have not been studied previously. (The charges of ionic species will be used only when it is necessary). The protonation constants, defined by Equation (1), have been determined by pH-potentiometry (Fig. 1).

$$K_i^H = \frac{[H_iL]}{[H_{i-1}L][H^+]} \qquad (1)$$

where i=1, 2…5. The obtained $\log K_i^H$ values are listed and compared with those of H_4**BDTA** and H_2**Cy-IDA** (*N*-cyclohexyliminodiacetic acid) in Table 1. Standard deviations (3σ) are shown in parentheses.

Table 1. Protonation constants of *cis*-**IPDTA**, **BDTA** and **Cy-IDA** at 25°C.

	cis-**IPDTA**		**BDTA**[a]	**Cy-IDA**[b]
I	0.1 M KCl	0.1 M KNO_3	0.1 M KNO_3	0.1 M KNO_3
$\log K_1^H$	11.23 (1)	11.21 (2)	10.66	10.81
$\log K_2^H$	8.34 (1)	8.34 (2)	9.05	2.15
$\log K_3^H$	2.53 (1)	2.59 (2)	2.45	–
$\log K_4^H$	1.73 (2)	1.67 (3)	1.90	–
$\log K_5^H$	1.25 (3)	1.23 (4)	–	–
$\Sigma \log K_4^H$	23.83	23.81	24.06	

[a] Ref. [17], [b] Ref. [18]

Comparison of the protonation constants of *cis*-IPDTA with those of BDTA indicates that the $\log K_1^H$ value of *cis*-IPDTA is higher, whereas its $\log K_2^H$ value is somewhat lower than those of the BDTA. Since the $\log K_1^H$ value of *cis*-IPDTA is similar to that of Cy-IDA, it can be assumed that the first protonation takes place on the nitrogen atom (a) of the iminodiacetate moiety directly linked to cyclohexane ring, whereas the second protonation occurs at the non-protonated

distal nitrogen atom (b) of the ligand. The third, fourth and fifth protonation steps of *cis*-IPDTA are related to the protonation of the carboxylate groups. The $\Sigma\log K_4^H$ value of *cis*-IPDTA ligand is comparable with the same parameter of BDTA (Table 1). According to the $\Sigma\log K_4^H$ values presented in Table 1, it can be assumed that the complexes of *cis*-IPDTA and BDTA ligand are characterized by similar stabilities. However, in determining the stability constants of the *cis*-IPDTA complexes, the presence of the less flexible cyclohexyl group may also play an important role. So, the equilibrium study of the metal complexes formed with the *cis*-IPDTA may give some new information about the effect of the less flexible ligand backbone on the metal-donor atom interaction and the thermodynamic stability of the metal complexes.

3.2.2 Complexation properties of cis-IPDTA: The stability and protonation constants of the metal complexes formed with the *cis*-IPDTA ligand are defined by Equations (2) – (4).

$$K_{ML} = \frac{[ML]}{[M][L]} \qquad (2)$$

$$K_{MH_iL} = \frac{[MH_iL]}{[MH_{i-1}L][H^+]} \qquad i=0,\ 1,\ 2 \qquad (3)$$

$$K_{M_2L} = \frac{[M_2L]}{[ML][M]} \qquad (4)$$

The K_{ML}, K_{MHiL} and K_{M2L} values characterizing the formation of *cis*-**IPDTA** complexes with Ca^{2+}, Mn^{2+}, Zn^{2+}, Cu^{2+}, Pb^{2+}, Cd^{2+} and Ln^{3+} ions have been calculated from the pH-potentiometric titration data obtained at 1:1 and 2:1 metal to ligand concentration ratios. In calculating the equilibrium constants, the best fitting of the mL KOH – pH data has been obtained by assuming the formation of ML, MHL, MH_2L and M_2L complexes The formation of the deprotonated $[M(cis\text{-}\mathbf{IPDTA})H_{-1}]^{2-}$ complexes takes place at pH>9.5, indicated by the base consumption in the titration curves. This deprotonation occurs by the coordination of the OH^- ion

to the M^{2+}-ions in ZnL, CuL, PbL and CdL complexes. The pH-potentiometric titration curves of the *cis*-**IPDTA** ligand in the absence and presence of M^{2+} and Ln^{3+} ions at 1:1 metal to ligand concentration ratio are shown in Figures 2 and 3, respectively.

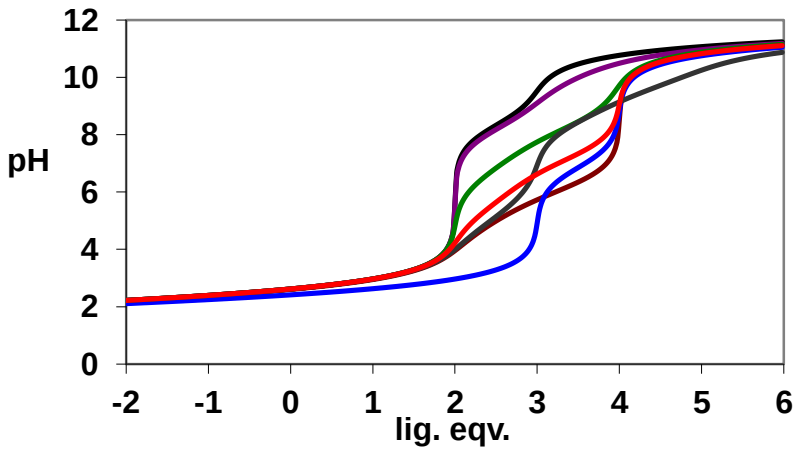

Figure 2. pH-potentiometric titration curve of H_4-*cis*-IPDTA in the absence and presence of Ca^{2+}, Mn^{2+}, Zn^{2+}, Cu^{2+}, Pb^{2+} and Cd^{2+} ions ([*cis*-IPDTA]= $[M^{2+}]$=2.00 mM, [HCl]=$[HNO_3]$=4.00 mM, 0.1 M KCl or KNO_3, 25°C)

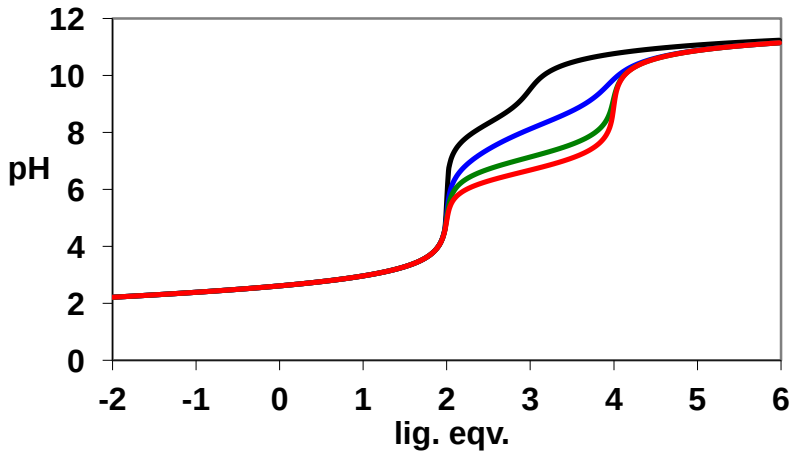

Figure 3. pH-potentiometric titration curve of H_4-*cis*-IPDTA in the absence and presence of La^{3+}, Gd^{3+} and Lu^{3+} ions ([*cis*-IPDTA]= $[Ln^{3+}]$=2.00 mM, [HCl]=4.00 mM, 0.1 M KCl, 25°C)

The stability and protonation constants of complexes of *cis*-IPDTA, BDTA and Cy-IDA (IDA) ligands with several metal ions, (investigated by pH-potentiometry) are reported in Table 2.

Table 2. The stability (logK_{ML}) and protonation (logK_{MHiL}) constants of metal complexes formed with *cis*-**IPDTA**, **BDTA**, **Cy-IDA** and **IDA** ligands (25°C).

	***cis*-IPDTA**	**BDTA**[a]	**Cy-IDA**[b]	**IDA**[a]
I	**0.1 M KCl**	**0.1 M KNO_3**	**0.1 M KNO_3**	**0.1 M KNO_3**
CaL	**4.28 (3)**	**5.54**	**3.34**	**2.59**
CaHL	9.46 (3)	8.65	–	–
Ca_2L	**1.39 (8)**	**1.42**	–	–
MnL	**7.54 (3)**	**9.46**	–	**4.72**[c]
MnHL	8.25 (3)	6.57	–	–
Mn_2L	**2.71 (5)**	**1.78**	–	–
CuL	**14.32 (2)**	**17.25**	**11.04**	**10.63**
CuHL	6.53 (2)	4.19	–	2.3
CuH_2L	2.36 (2)	**–**	–	–
$CuLH_{-1}$	11.28 (3)	**–**	8.07	8.5
Cu_2L	**7.34 (2)**	**–**	–	–
ZnL	**11.59 (2)**	**14.89**	**7.60**	**7.27**
ZnHL	6.05 (1)	3.10	–	–
ZnH_2L	3.66 (1)	**–**	–	–
$ZnLH_{-1}$	11.78 (4)	**–**	–	–
Zn_2L	**2.55 (3)**	**–**	–	–
***PbL**	**9.15 (4)**	**10.38**	–	**7.35**
PbHL	8.37 (3)	7.63	–	3.84
$PbLH_{-1}$	9.68 (5)	–	–	9.36
Pb_2L	**5.26 (8)**	**5.45**	–	–
***CdL**	**9.89 (3)**	**11.89**	**6.94**	**5.73**
CdHL	7.14 (3)	5.50	–	–
$CdLH_{-1}$	11.75 (5)	–	–	–

Cd_2L	**2.60 (5)**	**2.22**	–	–
LaL	**6.64 (5)**	**9.04**	–	**5.88**[d]
LaHL	8.43 (5)	7.70	–	–
GdL	**8.54 (4)**	**9.90**	–	**6.68**[d]
GdHL	6.81 (7)	6.70	–	–
LuL	**9.43 (5)**	**11.40**	–	**7.61**[d]
LuHL	6.09 (8)	6.60	–	–

[a] Ref. [17]; [b] Ref. [18]; [c] Ref. [19]; [d] Ref. [20]

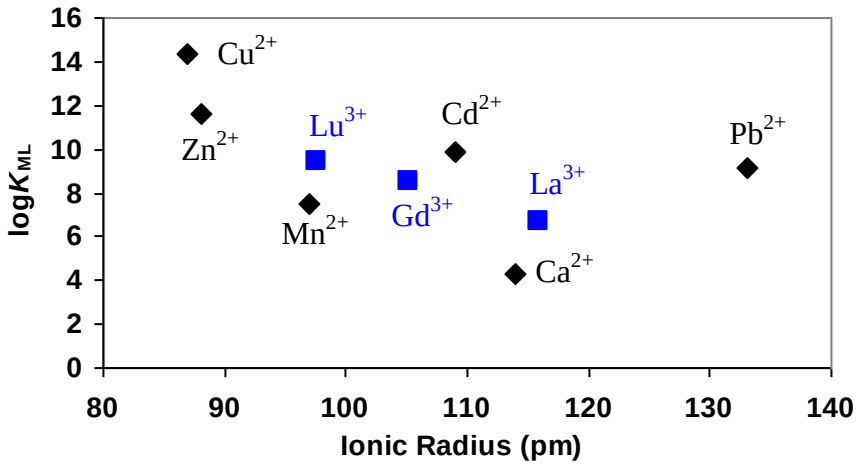

Figure 4. logK_{ML} values of the *cis*-IPDTA as a function of the ionic radius of the metal ions.

The stability constants of the metal complexes formed with *cis*-**IPDTA** (Table 2 and Figure 4) are generally about 2 – 3 orders of magnitude lower and higher than those of the corresponding **BDTA** and **Cy-IDA** or **IDA** complexes, respectively. The logK_{ML} values determined for the Ca^{2+} and Pb^{2+} complexes are lower than those of **BDTA** by 1 - 1.5 log$K$ unit, whereas $\Delta\log K_{ML}$ values of Cu^{2+} and Zn^{2+} complexes formed with **BDTA** and *cis*-**IPDTA** complexes are about 3 - 3.5. By taking into account the size of the investigated metal ions, it can be assumed that *cis*-**IPDTA** can form ML complex of higher stability with

the metal ions of lower size. However, the stability constants of the Cd^{2+} and Pb^{2+} complexes formed with *cis*-**IPDTA** are higher than it can be expected according to the trend of the logK_{ML} values presented in Figure 4.

The stability constants of the Ln(*cis*-**IPDTA**) complexes increase monotonously from La^{3+} to Lu^{3+} (Figure 4 and Table 2). This behaviour is similar to that found for the Ln(**BDTA**) and Ln(**IDA**) complexes. On the other hand, the stability constants of the Ln(*cis*-**IPDTA**) are significantly lower than those of Ln(**BDTA**) but the differences between the logK_{LnL} values significantly increase from the Gd^{3+} and it is 2 log$K$ unit for the Lu^{3+}. These data clearly indicate the effect of the rigid ligand backbone on the trend of the logK_{LnL} values across the lanthanide series.

The complexes formed with the *cis*-**IPDTA**, similarly to those of **BDTA**, can be protonated and the protonation constants have been determined by pH-potentiometry (Table 2). Two protonation constants could be determined for the complexes formed with Zn^{2+} and Cu^{2+} ions. According to the first protonation constants (logK_{MHL} = 6.0 - 9.5) it can be assumed that the metal ion is coordinated by the iminodiacetate moiety (*a*) attached to cyclohexyl-ring, whereas the protonation occurs at the nitrogen atom (*b*) of the non- or weakly-coordinated iminodiacetate fragment. The free or weakly coordinated iminodiacetate moiety in the ML complexes can lead to the formation of the dinuclear M_2L species in the presence of excess metal ion. In the Zn^{2+} and Cu^{2+} complexes there is evidence of one non-coordinated donor atom (carboxylate-O), which can be protonated at lower pH values.

Conclusions

cis-**IPDTA**, a new polyaminopolycarboxylic ligand from isophoronediamine, was prepared from the commercially available commodity isophoronediamine. The protonation constants of this hexadentate ligand were determined by pH-potentiometric analysis. The formation and protonation constants of the complexes with various metal ions were investigated, in order to characterize the complexation behavior of *cis*-**IPDTA**. The thermodynamic behavior of this ligand was compared with that of the linear congener **BDTA**. The results suggest a strong effect of the conformation of cyclohexane ring on the chelation of metal ions by mean of the two iminodiacetic moieties.

ACKNOWLEDGMENTS

Financial support by the Hungarian Scientific Research Found (OTKA K109029 and K84291) is also gratefully acknowledged.

REFERENCES

[1] B. Nowack, J.M. VanBriesen, "Chelating Agents in the Environment" in "Biogeochemistry of Chelating Agents", ACS Symposium Series 910 (2005) 1-18.
[2] J.R. Hart, "Ethylenediaminetetraacetic Acid and Related Chelating Agents", in "Ullmann's Encyclopedia of Industrial Chemistry", Wiley-VCH (2011).
[3] T.J. McMurry, K.N. Raymond and P.H. Smith; Science 244 (1989) 938-943.
[4] E. Bayer, H. Fiedler, K.L. Hock, D. Otterbach, G. Schenk and W. Voelter; Angew. Chem. Int. Ed. Engl. 3 (1964) 325-332.
[5] I.S.S. Pinto, I.F.F. Neto and H.M.V.M. Soares; Environ. Sci. Pollut. Res. 21 (2014) 11893-11906.

[6] S. Aime, L. Calabi, C. Cavallotti, E. Gianolio, G.B. Giovenzana, P. Losi, A. Maiocchi, G. Palmisano and M. Sisti; Inorg. Chem. 43 (2004) 7588-7590.

[7] Z. Baranyai, F. Uggeri, G.B. Giovenzana, A. Bényei, E. Brücher and S. Aime; Chem. Eur. J. 15 (2009) 1696-1705.

[8] Z. Baranyai, F. Uggeri, A. Maiocchi, G.B. Giovenzana, C. Cavallotti, A. Takács, I. Tóth, I. Bányai, E. Brucher and S. Aime; Eur. J. Inorg. Chem. (2013) 147-162.

[9] G.B. Giovenzana, Z. Baranyai, S. Aime, C. Cavallotti, D. Imperio and G. Palmisano; Polyhedron, 27 (2008) 3683-3687.

[10] L. Tei, M. Benzi, F. Kielar, M. Botta, C. Cavallotti, G.B. Giovenzana and S. Aime; Helv. Chim. Acta 92 (2009) 2414-2426.

[11] Z. Baranyai, L. Tei, G.B. Giovenzana, F.K. Kálmán and M. Botta; Inorg. Chem. 51 (2012) 2597-2607.

[12] K. Eller, E. Henkes, R. Rossbacher and H. Höke; "Amines, Aliphatic", in "Ullmann's Encyclopedia of Industrial Chemistry", Wiley-VCH (2000).

[13] A. Berkessel, K. Roland and J.M. Neudörfl; Org. Lett. 8 (2006) 4195-4198.

[14] A. Berkessel, K. Roland, M. Schröder, J.M. Neudörfl and J. Lex; J. Org. Chem. 61 (2006) 9312-9318.

[15] H.M. Irving, G.M. Miles and D.L. Pettit; Anal. Chimica Acta 38 (1967) 475-485.

[16] L. Zékány and I. Nagypál, in "Computational Method for Determination of Formation Constants" Ed. Legett D J, Plenum, New York (1985) p. 291.

[17] G. Anderegg; Helv. Chim. Acta 47 (1964) 1801-1814.

[18] H. Irving and J.J.R. Frausto da Silva; J. Chem. Soc. (1963) 3308-3320.

[19] R.J. Motekaitis and A.E. Martell; J. Coord. Chem. 14 (1985) 139-149.

[20] L. Thompson; Inorg. Chem. 1 (1962) 490-493.

CHAPTER 4

Determination of Thermodynamic and Kinetic Parameters for the Sc(III)-AAZTA System

Zsolt Baranyai,[a] Arianna Maria Giani,[a,b] Roberto Negri,[b] Giovanni Battista Giovenzana[b]

[a] – Department of Inorganic and Analytical Chemistry, University of Debrecen, H-4010, Debrecen, Egyetem tér 1 (Hungary)

[b] – Dipartimento di Scienze del Farmaco, Università degli Studi del Piemonte Orientale "A. Avogadro", Largo Donegani 2/3, I-28100 Novara (Italy)

Introduction

Noninvasive imaging modalities have recently allowed increased opportunities for molecular diagnostic and therapeutic procedures. Molecular imaging (MI) is the visualization, characterization, and measurement of biological processes at the molecular and cellular levels in humans and other living systems.[1] Specific MI agents are usually needed to generate a contrast useful for the diagnostic content of the images. The most sensitive molecular imaging techniques are positron emission tomography (PET) and single photon emission computed tomography (SPECT).[2] Classical PET isotopes such as ^{18}F and ^{11}C were incorporated into small molecules, but their often lengthy syntheses combined with short half-lives and rapid clearance lead to a limited time-window available for imaging, restricting the investigation of biological processes.[3] The enduring development of biological targeting agents such as proteins, peptides, antibodies and nanoparticles, stimulated the need to introduce radionuclides with half-lives matching their biological properties.[4] In this context, radiometals such as Ga, Cu, In, Y and Zr, were investigated as

radionuclide labels for biomolecules due to their longer and favorable decay characteristics.[3] In addition, the development of radionuclide portable generators and small biomedical cyclotrons able to produce radiometals allows to overcome the dependence on nuclear reactors and accelerators for the availability of radionuclides. Furthermore, the use of metal ions requires a single complexation step to prepare the diagnostic probe. This is exemplified by the recent development of PET agents based on ^{68}Ga (β^+, $t_{½}$ = 67.71 min), a radionuclide used for PET imaging that could be obtained with a portable ^{68}Ge/^{68}Ga generator.

In the last years ^{44}Sc raised a significant interest because it combines a relatively long half-life (3.97 hours, E_{mean} (β^+) = 632 keV) with its high positron branching of 94.27%, being of potential interest for PET applications.[5] The use of this nuclide may offer several advantages: its high positron fraction and nearly four times the half-life of ^{68}Ga, ^{44}Sc can be more easily employed to synthesise a wider variety of radiotracers with longer pharmacokinetic profiles, leaving more time to transport it to more distant PET facilities. ^{44}Sc is currently produced via cyclotronirradiation of ^{44}Ca targets through ^{44}Ca(p,n)^{44}Sc reaction[6-8] or more practically by ^{44}Ti/^{44}Sc generators.[8-11]

To date, a limited number of studies have been devoted to the coordination chemistry of this interesting metal ion, except for some report on organometallic derivatives. Its application as a PET radiopharmaceutical requires a chelating agent exhibiting a fast complex formation kinetic, in order to prepare the final probe with the minimum erosion in its useful emitting lifetime. Furthermore, to avoid the dissociation of the metal ion with concomitant toxic effects, the resulting chelate should show excellent thermodynamic stability and kinetic inertness. Scandium(III) complexes with DOTA and DTPA[5,12,13] displayed high formation constants; moreover, DOTA showed a valuable dissociation kinetic, with a $t_{½}$ = 44.9 hours (pH 0)[5]. The [Sc(DOTA)]$^-$ chelate was conjugated with a dimeric cyclic RGD peptide for the visualization of integrin $\alpha_v\beta_3$, an important factor linked to tumour aggressiveness and metastasis in several cancer types.[14]

The heptadentate ligand AAZTA is a recent entry in the realm of chelating agents. It is easily prepared in 3-4 synthetic steps, and its coordination properties towards a wide array of metal ions have been studied in detail, showing a remarkable affinity for lanthanides and transition-metal ions. Thermodynamic, kinetic and structural studies have been carried out with Ga^{3+}, In^{3+} and Cu^{2+}, three metal ions of PET interest, demonstrating good stability values for the resulting chelates. Lipophilic and tailored derivatives of this ligand have been studied, allowing to include AAZTA in lipid-based nanoparticles or to interact with proteins and molecular hosts.[15-18] Recent efforts were devoted to the development of bifunctional chelating agents (BFCAs)[19,20] based on the AAZTA platform,[21-24] paving the way for the conjugation of this versatile ligand to vectors for targeting purposes.

Prompted by the renewed interest toward ^{44}Sc as PET-imaging radiometal, we started a systematic study of the thermodynamic and kinetic properties of the interaction of AAZTA with this trivalent metal ion, in order to evaluate the suitability of the corresponding chelate as a PET tracer.

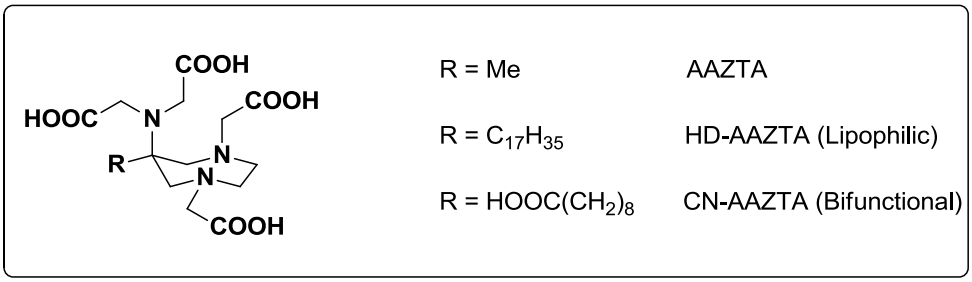

Figure X.1 AAZTA, lipophilic and bifunctional derivatives are reported.

Results and discussion

The thermodynamic and kinetic properties required to a chelating agent to be successfully employed in nuclear medicine applications may be summarized as

follows: i) high thermodynamic stability; ii) fast kinetic of complex formation; iii) slow kinetic of complex dissociation.

Thermodynamic parameters

The thermodynamic stability of the interaction between Sc^{3+} and AAZTA was assessed by a combination of analytical techniques. The formation of the $Sc(AAZTA)^-$ complex could be followed by both ^1H and ^{45}Sc-NMR spectrometry, operating in acidic conditions in order to reproduce the classical conditions of nuclear medicine (the radiometal is usually eluted from an ion exchange column and obtained as acidic eluate). The sequences of spectra registered for the system Sc^{3+}-AAZTA at different pH are reported in Figure X.2 (^1H-NMR) and Figure X.3 (^{45}Sc-NMR).

Figure X.2 ^1H-NMR spectra of the Sc^{3+}-AAZTA system: ($[Sc^{3+}]=[AAZTA]=10$ mM, $[H^+]=0.03 – 1.0$ M, $[H^+]\leq 0.1$ M $\rightarrow [K^+]+[H^+]=0.1$ M, 298 K)

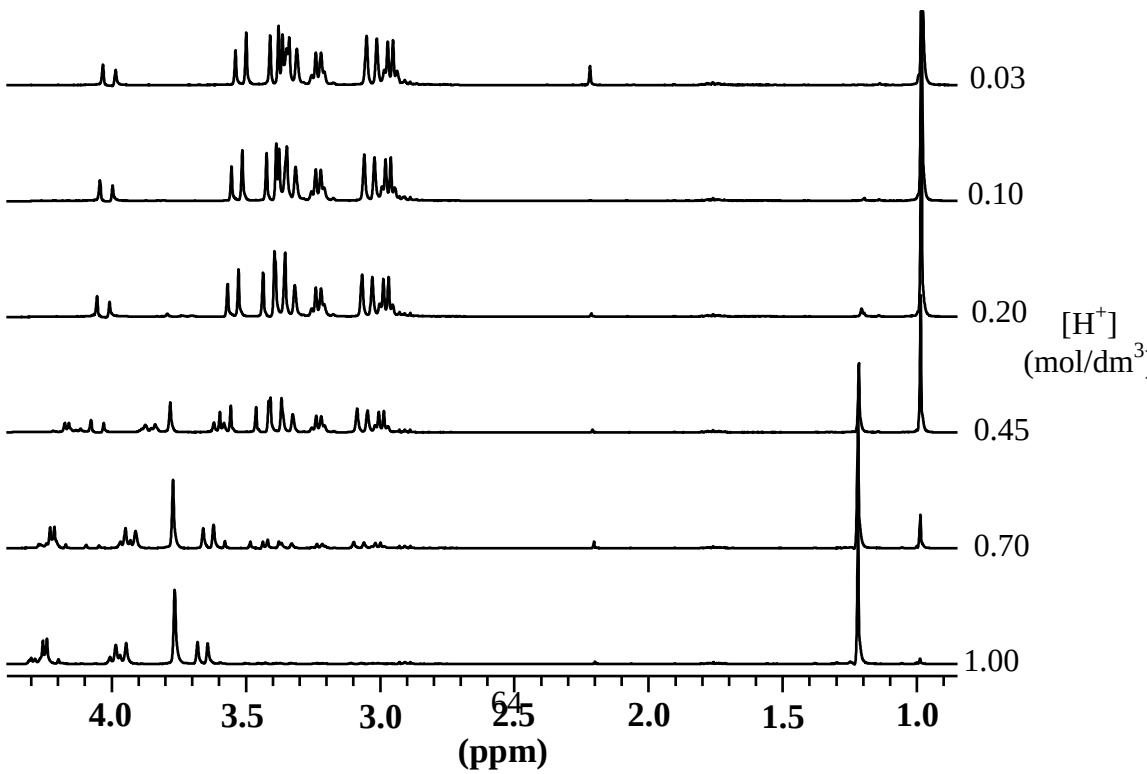

Figure X.3. ^{45}Sc-NMR spectra of the Sc^{3+}-AAZTA system: ([Sc^{3+}]=[AAZTA]=10 mM, [H^+]=0.03 – 1.0 M, [H^+]≤0.1 M → [K^+]+[H^+]=0.1 M, 298 K)

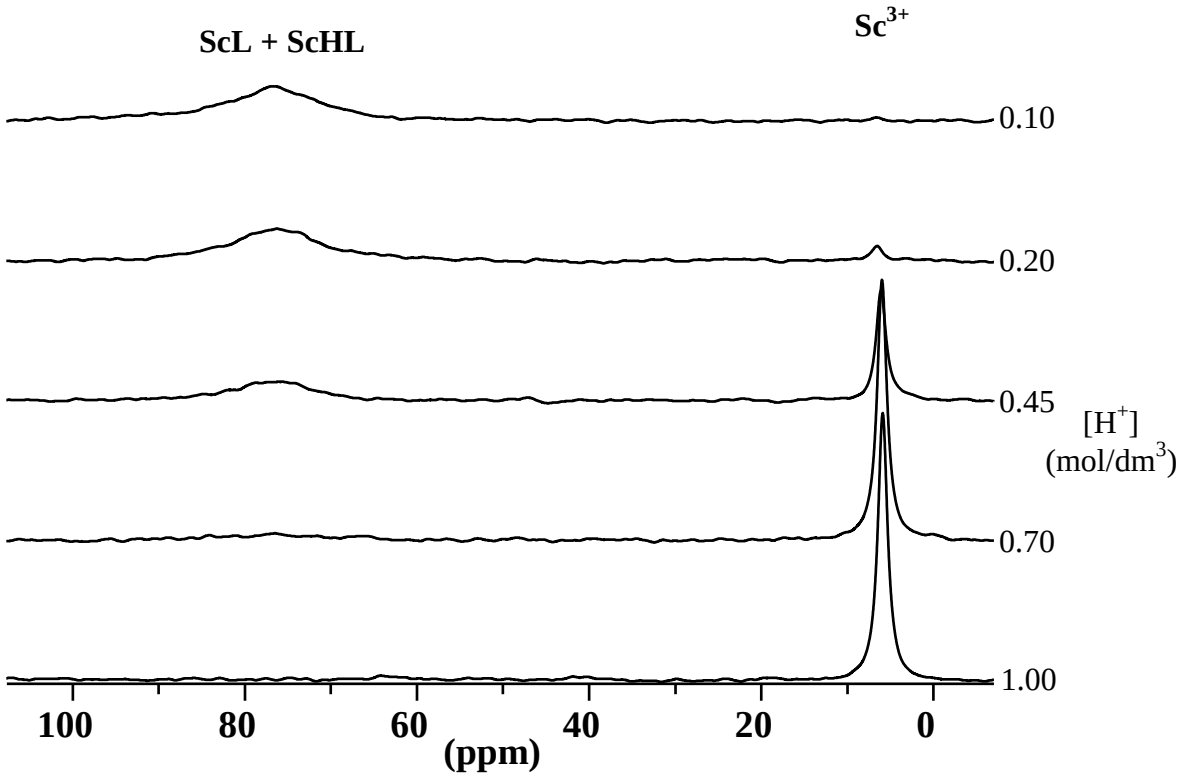

The formation of the Sc(AAZTA)$^-$ complex is clearly observed to occur, even in strongly acidic conditions. Signals of the chelate are detected starting from pH = 0 and regularly increasing with the pH. The formation of the complex is complete at the concentration of [H^+] 0.03M, showing the strong affinity of the metal ion for the coordination environment of AAZTA.

The plot of the relative concentration of the solution species (*i.e.*: the aquo-ion, the chelate and its protonated form) is reported in Scheme X.1.

Scheme X.1. Species distribution of Sc^{3+}-AAZTA system and the amount of the Sc^{3+} (◆) calculated from the ^{45}Sc-NMR studies ($[Sc^{3+}]=[AAZTA]=10$ mM, $[H^+]\leq 0.1$ M $\rightarrow I=[H^+]+[K^+]=0.1$ M, 25°C)

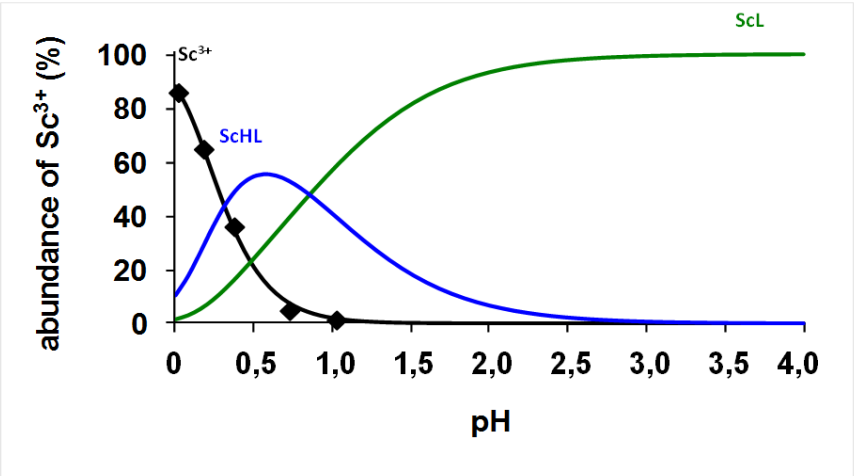

The analysis of these data allows to extract the stability constant for the formation of the $Sc(AAZTA)^-$ complex $\log K_{ScL}=27.69(4)$, and its protonation constant $\log K_{ScHL}=0.86(3)$. This value locates between the values recently reported for the Sc^{3+} complexes of the archetypal acyclic DTPA and macrocyclic DOTA ligands and well above the value reported for EDTA,[25] confirming the strong affinity of AAZTA for this trivalent cation.

Kinetics parameters

The determination of the kinetic parameters for the dissociation of the $Sc(AAZTA)^-$ complex had to be adapted to the significant inertness of the chelate, once formed. The study of the kinetic stability of $Sc(AAZTA)^-$ started with the kinetic studies of the transmetallation reactions between $Sc(AAZTA)^-$ and Cu^{2+} in the presence of citrate excess (0.15 M NaCl, 25°C) (Eq. X.1).

Eq. X.1 $Sc(AAZTA)^{-} + Cu(Cit)H_{-1} \rightleftharpoons Cu(AAZTA)^{2-} + Sc(Cit)H_{-1}$

In the pH range 5–7, the citrate prevents the hydrolysis of the exchangeing Cu^{2+} and the released Sc^{3+} ions. $Cu(Cit)H_{-1}$ and $Sc(Cit)H_{-1}$ species predominates in this pH range.[26] Some characteristical absorption spectra of the reacting system show below Figure X.4.

Figure X.4. UV spectra of Sc(AAZTA) –Cu^{2+}-Cit reacting system ([ScL]=0.01 M, [CuL]=0.2 mM, [Cu^{2+}]=0.2 mM, [Cit]=2.0 mM, pH=6.0, 0.15 M NaCl, l=0.874 cm, 25°C)

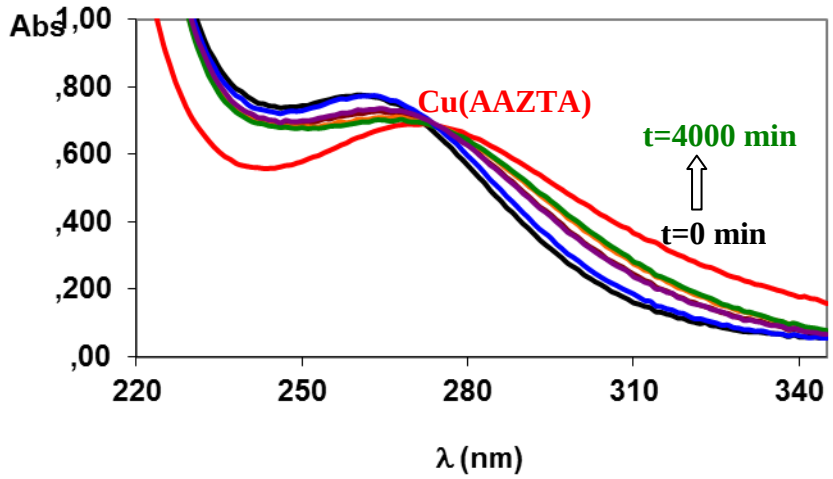

Dissociation of $Sc(AAZTA)^{-}$ is initially assumed to follow a first-order rate law (Eq. X.2), where k_d and $[ScL]_t$ are the pseudo-first-order rate constant and the total concentration of the $Sc(AAZTA)^{-}$, respectively.

Eq. X.2 $$-\frac{d[ScL]_t}{dt} = \frac{d[CuL]_t}{dt} = k_d[ScL]_t$$

During the progress of the transmetallation reactions the concentration of $Cu(AAZTA)^{2-}$ complex increases, while that of $Cu(Cit)H_{-1}$ decreases. By the use of 1.0 cm cells, the first-order rate constant, k_d can be expressed as it follows (Eq. X.3):

Eq. X.3

$$k_d = \frac{\Delta Abs}{\Delta t} \times \frac{1}{\varepsilon_{CuL} - \varepsilon_{Cu(Cit)H_{-1}}} \times \frac{1}{[\mathrm{ScL}]_t}$$

In Eq. X.3 the $\Delta Abs/\Delta t$ values (the increase of the absorbance during the time Δt) were calculated from the slope of the kinetic curves. $\varepsilon_{Cu(Cit)H-1}$ and ε_{CuL} are the molar absorptivities of the $Cu(Cit)H_{-1}$ (921 $M^{-1}cm^{-1}$) and $Cu(AAZTA)^{2-}$ (1875 $M^{-1}cm^{-1}$) complexes at 300 nm. The obtained pseudo-first-order rate constants for the reaction of $Sc(AAZTA)^-$ with Cu^{2+} in the presence of citrate are shown in Figure X.4.

Figure X.4. Plot of k_d values vs. pH for the reaction between $Sc(AAZTA)^-$ and Cu^{2+} in the presence of citrate excess. ([$Sc(AAZTA)^-$] = 10.0 mM, [Cu^{2+}]=0.2 mM (◆) and 0.4 mM (■), [Cit]=2.0 mM, [MES]=[HEPES] = 0.01 M, 0.15 M NaCl, 25°C).

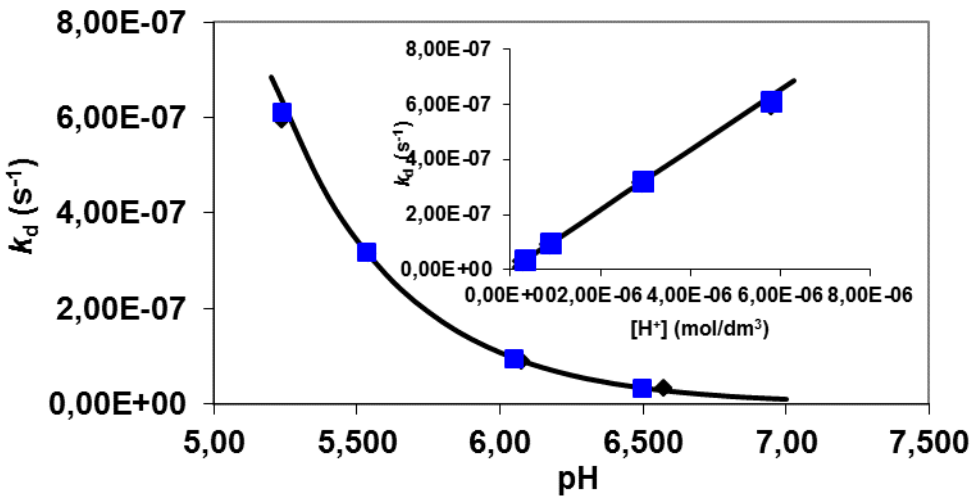

Mechanism

Since the reaction rate (k_d) is independent from the concentration of citrate and $Cu(Cit)H_{-1}$, it can be assumed that the rate determining step is the dissociation of $Sc(AAZTA)^-$, followed by a fast metal exchange reaction between $Cu(Cit)H_{-1}$ species and the free AAZTA ligand. The dissociation of the $Sc(AAZTA)^-$ might take place in a spontaneous pathway characterized with the rate constant k_0. The increase of k_d values with the increase of $[H^+]$ can be explained by the proton assisted dissociation (k_1) of $Sc(AAZTA)^-$ complex.

Eq. X.4 $Sc(AAZTA)^- \xrightarrow{k_0} Sc^{3+} + H_xAAZTA$

Eq. X.5 $Sc(AAZTA)^- + H^+ \xrightarrow{k_1} Sc^{3+} + H_xAAZTA$

Eq. X.6 $$-\frac{d[ScL]_t}{dt} = k_d[ScL]_t = k_0[ScL] + k_1[ScL][H^+]$$

Considering the total concentration of the complex ($[ScL]_{tot} = [ScL]$), the pseudo-first-order rate constant (k_d) can be expressed as follows:

Eq. X.7 $k_d = k_0 + k_1[H^+]$

The rate constants characterising the transmetallation reaction of $Sc(AAZTA)^-$ in the presence of citrate were calculated by fitting the k_d values presented in Figure X.4 into Eq. X.7 and the values obtained are shown and compared with those of $Gd(AAZTA)^-$ in Table X.1.

Table X.1 Rate, equilibrium constants and half-lives ($t_{1/2}=\ln 2/k_d$) for the transmetallation reactions of $Sc(AAZTA)^-$ and $Gd(AAZTA)^-$ complexes (25°C)

	$Sc(AAZTA)^-$	**$Gd(AAZTA)^-$ [27]**
$k_0\,(s^{-1})$	$(2 \pm 2)\times10^{-11}$	–
$k_1\,(M^{-1}s^{-1})$	0.1 ± 0.01	1.05
k_d (s^{-1}) at pH=7.4	4.0×10^{-9}	4.5×10^{-8}
$t_{1/2}$ (h) at pH=7.4	48364	4337

Conclusions

In this work we report a systematic evaluation of AAZTA as a potential chelating agent for the development of Sc-radiopharmaceuticals. The fast formation kinetics of $Sc(AAZTA)^-$ compares favourably with the slow complexation associated with macrocyclic derivatives exemplified by DOTA. The thermodynamic formation constant of $Sc(AAZTA)^-$ demonstrates the substantial stability of this complex, higher than those of corresponding acyclic ligands EDTA and DTPA, suggesting a significant contribution of the mesocyclic structure of AAZTA. The dissociation of $Sc(AAZTA)^-$ takes place through an acid catalysed mechanism, with a striking kinetic inertness exemplified by a half-life of over two thousand days (~ 5.5 years) at physiological pH.

The combination of the fast kinetics of complex formation, high thermodynamic stability and very slow kinetics of dissociation make AAZTA as one of the most promising chelating agents for the development of Sc-based radiopharmaceuticals.

REFERENCES

[1] N. Gourtsoyiannis , I. McCall , M. Reiser , B. Silberman , A. Bischof Delaloye , I. Carrió , A. Cuocolo and W. Knapp; Eur. Radiol. (2007), 17(8):1926-30.

[2] A. Rahmim and H. Zaidi; Nucl. Med. Commun. (2008), 29:193–207.

[3] T. J. Wadas, E. H. Wong, G. R. Weisman and C. J. Anderson; Chem. Rev. (2010), 110, 2858–2902.

[4] Y. Zhou, K.E. Baidoo, and M. W. Brechbiel; Adv. Drug Deliv. Rev. (2013) July; 65(8): 1098–1111.

[5] M. Pniok, V.Kubcek, J. Havlckov, Jan Kotek, Andrea Sabatie-Gogov, J. Plutnar, S. Huclier-Markai, and P. Hermann; Chem. Eur. J. (2014), 20, 7944 – 7955.

[6] M. Pruszynski, N. S. Loktionova, D. V. Filosofov and F. Roesch; Appl. Radiat. Isotop. (2010), 68, 1636 –1641.

[7] D. V. Filosofov, N. S. Loktionova and F. Roesch; Radiochim. Acta (2010), 98, 149–156.

[8] F. Roesch; Curr. Radiopharmaceuticals (2012), 5, 187 –201.

[9] S. Krajewski, I. Cydzik, K. Abbas, A. Bulgheroni, F. Simonelli, U. Holzwarth and A. Bilewicz; Radiochim. Acta (2013), 101, 333 –338.

[10] G. W. Severin, J. W. Engle, H. F. Valdovinos, T. E. Barnhart, R. J. Nickles; Appl. Radiat. Isot. (2012), 70, 1526 –1530.

[11] J. E. Duval, M. H. Kurbatov; J. Am. Chem. Soc. (1953), 75, 2246– 2248.

[12] S. Huclier-Markai, A. Sabatie, S. Ribet, V. Kubcek, M. Paris, C. Vidaud, P. Hermann and C. S. Cutler; Radiochim. Acta (2011), 99, 653– 662.

[13] M. Połosak, A. Piotrowska, S. Krajewski and A. Bilewicz; J. Radioanal. Nucl. Chem. (2013), 295, 1867–1872.

[14] Y. Zhou, S. Chakraborty, and S. Liu; Theranostics (2011); 1: 58–82.

[15] S. Aime, E. Gianolio, G. B. Giovenzana, D. Longo, I. Longo and I. Menegotto; Chem. Eur. J. 2007, 13, 5785–5797.

[16] K. C.Briley-Saebo, S. Geninatti, A. Barazza, D. Cormode, W. J. M. Mulder, W.Chen, G. B. Giovenzana, S. Aime and Z. A. Fayad; J. Phys. Chem. B (2009), 113, 6283–6289.

[17] E. Gianolio,; C. Cabella,; S. Colombo Serra, G. Valbusa, F. Arena, A. Maiocchi, L. Miragoli, F. Tedoldi, F. Uggeri, M. Visigalli, P. Bardini and S. Aime; J. Biol. Inorg. Chem. (2014), 19, 719–726.

[18] D.L. Longo, F. Arena, L. Consolino, P. Minazzi, S. Geninatti Crich, G.B. Giovenzana and S. Aime; Biomaterials (2016), 75, 47-57.

[19] L. Frullano and P. Caravan; Curr. Org. Synth. (2011), 8, 535–565.

[20] L. Lattuada, A. Barge, G. Cravotto, G. B. Giovenzana and L. Tei; Chem. Soc. Rev. (2011), 40, 3019–3049.

[21] P. Minazzi, L. Lattuada, I.G. Menegotto, G.B. Giovenzana; Org. Biomol. Chem. (2014); 12:6915-6921.

[22] L. Manzoni, L. Belvisi, D. Arosio, MP. Bartolomeo, A. Bianchi, C. Brioschi, F. Buonsanti, C. Cabella, C. Casagrande, M. Civera, M. De Matteo, L. Fugazza, L. Lattuada, F. Maisano, L. Miragoli, C. Neira, M. Pilkington-Miksa and C. Scolastico; Chem.Med.Chem. (2012); 7:1084-93.

[23] I. Mamedov, J. Engelmann, O. Eschenko, M. Beyerlein and N. K. Logothetis; Chem. Commun. (2012), 48, 2755–2757.

[24] R. Artali, G. Bombieri, G. B. Giovenzana, M. Galli, L. Lattuada and F. Meneghetti; Inorg. Chim. Acta, (2013), 407, 306–312.

[25] S. Huclier-Markai, C. Alliot, J. Sebti, B. Brunel, J. Aupiais; RSC Adv., (2015), 5, 99606-99617.

[26] A. E. Martell, R. M. Smith, Critical Stability Constants, Vol. 4., Plenum Press, New York, (1974).

[27] Zs. Baranyai, F. Uggeri, G. B. Giovenzana, A. Bényei, E. Brücher and S. Aime; Chem. Eur. J. (2009), 15, 1696-1705.

CHAPTER 5

Fluorescence studies on 2-(het)arylperimidine derivatives

Arianna Maria Giani,[1] Marco Lamperti,[2] Angelo Maspero,[3] Alessandro Cimino,[3] Roberto Negri,[1] Giovanni Battista Giovenzana,[1] Giovanni Palmisano,[3] Luca Nardo[2*]

[1] - Dipartimento di Scienze del Farmaco, Università degli Studi del Piemonte Orientale "A. Avogadro", Largo Donegani 2/3, I-28100 Novara, Italy

[2] - Dipartimento di Medicina e Chirurgia, Università degli Studi di Milano-Bicocca, Via Cadore 48, I-20900 Monza, Italy

[3] - Dipartimento di Scienza e Alta Tecnologia, Università degli Studi dell'Insubria, Via Valleggio 11, I-22100 Como, Italy

Abstract

Perimidines are extensively studied for their different therapeutic properties, including antiulcer, antifungal, antimicrobial, immunosuppressive and anticancer activity. Moreover, their heterocyclic structure embodies the naphthalene moiety, exploited in bio-imaging and biomolecules staining due to its high fluorescence. Although the concomitance of both biologically active moieties and a chromophore in the same molecule virtually discloses applications in state-of-art theranostics protocols, this aspect of the (photo)chemistry of this otherwise widely studied class of compounds were extensively investigated so far. In this work we present the spectroscopic characterization of a family of perimidine derivatives, in order to obtain useful information potentially useful for the design of compounds combining biological activity and detectable fluorescence in physiological environment.

Keywords: perimidines; fluorescence; intra-tissue drug localization, theranostics

Introduction

Perimidines are diazaheterotricyclic compounds extensively studied for their versatile chemical properties as well as their intense and heterogeneous biological activities.[1] Among their multiple applications in pharmaceutics, including also activity as antiulcer,[2] antifungal,[3,4] antimicrobial,[5] immunosuppressive[6] agents and enzyme inhibitors,[7] a particular interest is assumed by the established chemotherapeutic, anti-cancer and anti-proliferative properties of perimidine derivatives,[8,9] connected to their DNA-binding properties.[10] Perimidine belongs to the class of DNA-targeting antitumor drugs intercalating to DNA, including also several pharmaceutical compounds widely used in current medical practice, such as anthracyclines, actinomycins, amsacrine, and mitoxantrone. A significant correlation has been demonstrated for intercalating agents between *in vitro* cytotoxic potency on one side and both binding affinity and fast binding kinetics on the other. Extensive efforts were devoted since the 80's towards the synthesis of compounds maximizing these aspects of the interaction with DNA. These studies have shown how planar polycyclic aromatic compounds optimally intercalate and that the binding affinity is enhanced by higher nuclearity. However, at the same pace as our knowledge of the molecular basis of chemotherapy progressed, a growing consciousness matured that maximization of *in vitro* cytotoxicity, although being an important aspect, is not the main design goal for an effective anticancer drug substance. Namely, the fundamental properties to be sought are broad-spectrum activity, reduced induction of resistance and the ability of reaching remotely sited solid tumours. While the former two virtues are assured by drugs endowed with the ability of inducing cell death through several diverse pathways, which might be triggered by the co-existence of multiple different DNA-binding modes, the latter requires optimization of the distributive properties and might be

favoured by a low binding constant, since a higher proportion of free ligand will be delivered at the systemic level in such instance.

Perimidine has a very peculiar interaction with DNA in that its structure has been identified as very close to that ideally bearing the minimal features indispensable for base intercalation.[10] For this reason, the binding affinity of perimidine for DNA is lower with other intercalating anticancer ($10^{\wedge 5}$-$10^{\wedge 6}$ M^{-1}). Moreover, its binding mode is liable to be more easily shifted, and its binding parameters more effectively tuned, by acting on the substituents of the heterotricyclic system. Historically, compounds substituted at either nitrogen 1 or carbon 2 position have been experimented, but the former were proven not to intercalate to DNA (although conserving fairly high binding constants), thereby loosing most of their cytotoxic potential.[10-11] 2-Substituted perimidines are most straightforwardly synthesized from 1,8-diaminonaphthalene and a large number of derivatives thereof were evaluated as to their physico-chemical properties, DNA binding affinity and cytotoxicity[9-10]. Although most of them exhibit DNA-binding constants comparable to that of the parent compound, retaining to variable extents an intercalative character (evidenced by the capacity of unwinding supercoiled plasmid DNA, and quantifiable through the pertaining unwinding angles), and induce cell death *in vitro* with IC_{50} values in the μM range, only a few selected derivatives are effective *in vivo*. The propensity of these compounds to oxidative degradation, pivoted by the highly π-excessive nature of the naphthalene moiety, was suggested as the cause of *in vivo* inefficacy[10]. However, this explanation is not consistent with the high cytotoxicity of virtually all the tested compounds *in vitro*, where oxidation should also take place. Moreover, π-excessive nature, and thus tendency to oxidation, is a feature common also to unsubstituted perimidine and to the substituted compounds displaying anti-proliferative properties in mice. To this regard, it is worth to mention that cyclic substituents (*e.g.* aryl rings) appear to preserve the *in vivo* activity better than linear ones. A subtler source of tuning of

the *in vivo* effectiveness of perimidine derivatives might be linked to the differential capacity of penetrating cell membranes (cell uptake), as well as to localize within different cell compartments (*e.g.* mitochondrial instead of nuclear DNA) or to react with alternative intracellular targets (*e.g.* RNA). Indeed, while *in vitro* the latter features should barely result in modulations of the IC_{50} value, *in vivo* they are liable to severely modify the systemic distribution.

From the above discussion it is clear that our comprehension of the molecular mechanisms underlying to the perimidines-DNA interactions on the one side and of the cellular uptake, bioavailability and bio-distribution at the cellular and systemic level on the other side remain still elusive.

Spectrophotometric titration has been widely and successfully applied to elucidation of the binding specificities of small polycyclic ligands to DNA. The main requirement preliminary to implementation of this technique is an absorption band spectrally separated from that of DNA bases (which is peaked at 260 nm). The UV-Vis absorption spectra of several perimidines have been reported in the literature up to now, and their main absorption peak typically falls in the band 320-360 nm.[12]

Fluorescence is an even more sensitive tool in order to perform binding studies[13]. Moreover, nowadays there exist several fluorescence techniques based on confocal [14] or multi-photon[13] excitation which allow non-invasive acquisition of maps of the intracellular and intra-tissue distribution of fluorescent compounds endowed with few tens of nanometers resolution as well as quantitative assessments of their local concentration and binding status. Because their molecular structure encompasses a notably performing fluorophore, 1,8-diaminonaphthalene, whose tabulated fluorescence quantum yield is ≈0.2, slightly depending on the environment[15,16], perimidines might in principle lend themselves to such analysis. In spite of this, the fluorescence properties of perimidine analogues have been so far scarcely investigated. The fluorescence quantum yield of these compounds appears generally much lower than that of naphthalenes, although highly solvent

dependent. While the latter feature might be promising of large fluorescence differences from the free to the bound state in titration experiments, the loss in quantum yield with respect to the isolated fluorophore might arise from perturbation of the naphthalene charge distribution. Indeed, it has been ascertained that the lone-pair of the pyrrole-like nitrogen of the perimidine moiety participates to the π-system through an electronic-charge transfer from the heterocyclic ring to the naphthalene[9,12]. Actually, saturation of the heterocyclic ring bonds has been reported to induce an increment in fluorescence quantum yield.[17] However, the proclivity to act as both a π-excessive and a π-deficient system, which would be lost upon saturation, has likely a primary role in determining the intercalating character.[9]

In this work we studied a family of perimidines, with the aim of selecting model compounds conserving the DNA-binding features of perimidine and suitable for spectrophotometric/spectrofluorimetric binding assays and/or fluorescence microscopy studies.

Figure 1

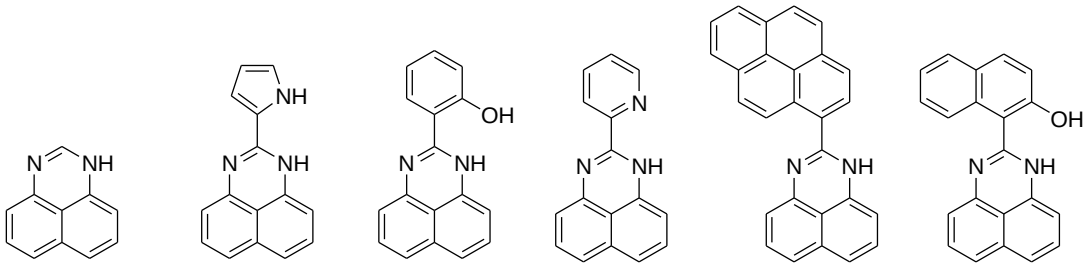

1 **2** **3** **4** **5** **6**

A total of six perimidines (Figure 1) containing (het)aromatic 2-substituents (in addition to the parent unsubstituted 1*H*-perimidine) were synthesized according to previously published procedures or synthesized *ex novo*. Their UV-Vis absorption and fluorescence emission properties were studied in a panel of organic solvents differing in polarity and H-bonding affinity, and compared to those of the parent compound. We also probed the above spectroscopic properties in pseudo-

physiological environment (phosphate buffered saline), assessed their DNA-binding affinity by means of spectrophotometric assay and preliminary tested the sensitivity of their fluorescence emission to the presence of excess calf thymus DNA.

Materials and methods

General

All chemicals of the highest purity grade were purchased from Sigma-Aldrich, Alfa Aesar or TCI Europe, were, and were used without further purification. ^{1}H- and ^{13}C-NMR were recorded on a JEOL Eclipse ECP 300 operating at 7.05 T. Chemical shifts were reported relative to tetramethylsilane (TMS) and were referenced by using the residual proton resonances of the solvent. Melting points were obtained with a Stuart Scientific SMP3 apparatus and are uncorrected.

Chemistry

The parent unsubstituted 1*H*-perimidine was prepared from the condensation of 1,8-naphthalenediamine with formic acid, according to a reported procedure.[18] All the other compounds were prepared in a two-step procedure (Scheme 1) starting with the condensation of 1,8-naphthalenediamine with the suitable aldehyde to give 2-(het)aryl-2,3-dihydro-1*H*-perimidines, usually isolated by simple filtration from the reaction mixture. Following oxidative dehydrogenation[19] to the desired 2-(het)aryl-1*H*-perimidines was performed with sodium pyrosulphite in hot alcoholic solution.

Scheme 1

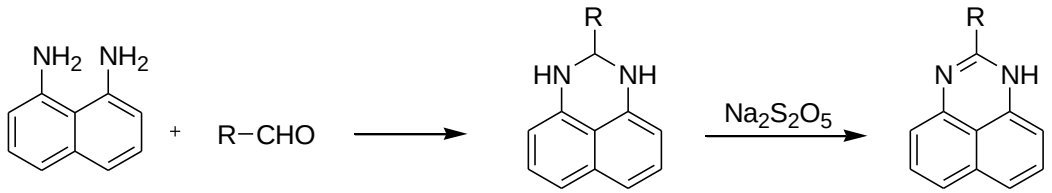

General procedure for the synthesis of 2-substituted 2,3-dihydro-1*H*-perimidines: 1,8-Diaminonaphthalene (1.0 mmol) and the appropriate aromatic aldehyde (1.0 mmol) were sequentially dissolved in dichloromethane (10 mL) and stirred at room temperature. A solid started to separate after 10-15 minutes. The reaction mixture was stirred for ≈1h to ensure complete precipitation. The product was filtered and washed with dichloromethane, affording the 2-substituted 2,3-dihydro-1*H*-perimidine as a light coloured solid. These products were used for the next step without any further purification.

2-(2-Pyridyl)-2,3-dihydro-1H-perimidine: 26%; light brown solid; ^{1}H-NMR ($CDCl_3$, 300MHz, 298K) δ: 8.60 (dt, 1H, J_d=4.6Hz, J_t=0.6Hz), 7.68 (td, 1H, J_t=7.7Hz, J_d=1.8Hz), 7.59 (d, 1H, J=7.4Hz), 7.32-7.19 (m, 5H), 6.59 (dd, 2H, J=6.7, 1.5Hz), 5.58 (s, 1H), 5.30 (s, 1H, exch. with D_2O); ^{13}C-NMR ($CDCl_3$, 75.4MHz, 298K) δ: 159.4 (C), 149.4 (CH), 141.1 (C), 137.4 (CH), 134.8 (C), 127.0 (CH), 123.7 (CH), 120.9 (CH), 118.2 (CH), 114.1 (C), 106.8 (CH), 67.8 (CH); m.p. = 113-114°C.

2-(2-Pyrrolyl)-2,3-dihydro-1H-perimidine: 74%; light grey solid; ^{1}H-NMR (DMSO-d_6, 300MHz, 298K) δ: 11.08 (bs, 1H, exch. with D_2O), 7.15 (t, 2H, J=7.8Hz), 6.98 (d, 2H, J=8.0Hz), 6.80-6.74 (m, 1H), 6.65 (s, 2H, exch. with D_2O), 6.51 (d, 2H, J=7.4Hz), 6.19 (bs, 1H), 6.02 (bq, 1H), 5.43 (s, 1H); ^{13}C-NMR (DMSO-d_6, 75.4MHz, 298K) δ: 143.9 (C), 135.0 (C), 131.9 (C), 127.4 (CH), 118.5

(CH), 115.8 (CH), 113.3 (C), 107.46 (CH), 107.45 (CH), 104.9 (CH), 61.5 (CH); m.p. = 195-196°C.

2-(2-Hydroxy-1-phenyl)-2,3-dihydro-1H-perimidine: 68%; light grey powder; ^{1}H-NMR (CD_3OD, 300MHz, 333K) δ: 9.55 (bs, 1H, exch. with D_2O), 7.48 (dd, 1H, J=7.7, 1.8Hz), 7.20 (td, 1H, J_t=7.6Hz, J_d=1.8Hz), 7.18 (t, 2H, J=7.8Hz), 7.03 (d, 2H, J=7.8Hz), 6.92 (dd, 1H, J=8.3, 0.9Hz), 6.85 (td, 1H, J_t=7.3Hz, J_d=0.9Hz), 6.58 (dd, 2H, J=7.4, 0.9Hz), 6.44 (bs, 2H, exch. with D_2O), 5.71 (s, 1H); ^{13}C-NMR (CD_3OD, 75.4MHz, 333K) δ: 156.1 (C), 143.6 (C), 135.0 (C), 129.6 (CH), 128.9 (CH), 127.8 (C), 127.4 (CH), 119.5 (CH), 116.2 (CH), 116.1 (CH), 113.2 (C), 105.3 (CH), 62.0 (C); m.p. = 198-199°C.

2-(2-Hydroxy-1-naphthyl)-2,3-dihydro-1H-perimidine: 50%; light brown powder; ^{1}H-NMR ($CDCl_3$, 300MHz, 323K) δ: 9.68 (bs, 1H, exch. with D_2O), 7.93 (d, 1H, J=8.6Hz), 7.80 (d, 2H, J=8.6Hz), 7.43 (t, 1H, J=7.7Hz), 7.38-7.26 (m, 5H), 7.20 (d, 1H, J=8.9Hz), 6.60 (d, 2H, J=6.8Hz), 6.42 (s, 1H), 4.66 (bs, 2H, exchanged with D_2O); ^{13}C-NMR ($CDCl_3$, 75.4MHz, 323K) δ: 156.9 (C), 141.5 (C), 135.0 (C), 132.3 (C), 131.8 (CH), 129.1 (CH), 128.7 (C), 127.4 (CH), 126.9 (CH), 123.3 (CH), 120.5 (CH), 119.9 (CH), 119.4 (CH), 114.4 (C), 112.8 (C), 107.7 (CH), 63.8 (CH); m.p. = 172-173°C.

2-(1-Pyrenyl)-2,3-dihydro-1H-perimidine: 67%; light yellow powder; ^{1}H-NMR (DMSO-d_6, 300MHz, 298K) δ: 8.95 (d, 1H, J=9.2Hz), 8.50-8.14 (m, 7H), 8.07 (t, 1H, J=7.3Hz), 7.21 (t, 2H, J=7.5Hz), 7.07 (d, 2H, J=8.0Hz), 7.01 (s, 2H, exch. with D_2O), 6.57 (d, 2H, J=7.0Hz), 6.31 (s, 1H); ^{13}C-NMR (DMSO-d_6, 75.4MHz, 323K) δ: 144.2 (C), 135.2 (C), 134.6 (C), 131.7 (C), 131.4 (C), 130.9 (C), 129.6 (C), 128.3 (CH), 127.9 (CH), 127.7 (CH), 127.6 (CH), 127.4 (CH), 126.8 (CH), 125.9 (CH), 125.8 (CH), 125.3 (CH), 125.0 (CH), 124.9 (C), 124.7 (C), 116.2 (CH), 113.3 (C), 105.2 (CH), 66.1 (CH); m.p. = 230-231°C.

General procedure for the synthesis of 2-substituted-1*H*-perimidines: 2-Substituted 2,3-dihydro-1*H*-perimidine (1.0 mmol) was dissolved in hot ethanol. For some substrates few drops of *N,N'*-dimethylformamide were added to completely dissolve the reagent. Sodium metabisulfite (1.0 mmol) was added in one portion at room temperature under vigorous stirring. A solid product started to separate after 10-15 minutes. The reaction mixture was stirred overnight, then the product was filtered and sequentially washed with cold ethanol and water to give 2-substituted-1*H*-perimidine as coloured powders.

2-(2-Pyridyl)-1H-perimidine: 76%; red powder; ^{1}H-NMR (DMSO-d_6, 300MHz, 298K) δ: 10.95 (s, 1H, exch. with D_2O), 8.73 (dq, 1H, J_d=4.6Hz, J_q=0.8Hz), 8.30 (dt, 1H, J_d=8.0Hz, J_t=1.1Hz), 8.01 (td, 1H, J_t=7.7Hz, J_d=1.6Hz), 7.62 (ddd, 1H, J=7.5, 4.7, 1.2Hz), 7.19 (t, 1H, J=7.7Hz), 7.16 (t, 1H, J=7.1Hz), 7.09 (t, 2H, J=7.2Hz), 7.01 (dd, 1H, J=8.3, 0.9Hz), 6.78 (dd, 1H, J=7.4, 0.9Hz), 6.72 (dd, 1H, J=7.4, 0.9Hz); ^{13}C-NMR (DMSO-d_6, 75.4MHz, 298K) δ: 151.4 (C), 149.9 (C), 149.0 (CH), 145.4 (C), 138.6 (C), 138.1 (CH), 135.7 (C), 129.4 (CH), 128.7 (CH), 126.7 (CH), 122.9 (C), 122.2 (CH), 120.4 (CH), 118.3 (CH), 114.7 (CH), 104.1 (CH); m.p. = 175-176°C.

2-(2-Hydroxy-1-phenyl)-1H-perimidine: 92%; yellow powder; ^{1}H-NMR (DMSO-d_6, 300MHz, 298K) δ: 10.66 (bs, 1H, exch. with D_2O), 7.98 (dd, 1H, J=8.4, 1.4Hz), 7.42 (td, 1H, J_t=7.7Hz, J_d=1.4Hz), 7.20 (t, 2H, J=7.8Hz), 7.12 (d, 2H, J=8.0Hz), 6.95 (t, 1H, J=7.5Hz), 6.94 (d, 1H, J=8.0Hz), 6.70 (dd, 2H, J=7.4, 0.9Hz); ^{13}C-NMR (DMSO-d_6, 75.4MHz, 298K) δ: 161.7 (C), 155.3 (C), 139.5 (C), 135.4 (C), 133.9 (CH), 129.1 (CH), 126.8 (CH), 121.6 (C), 119.9 (CH), 118.6 (CH), 113.4 (C), 109.5 (bs, CH); m.p. = 266-267°C.

2-(2-Pyrrolyl)-1H-perimidine: 86%; yellow powder; ^{1}H-NMR (DMSO-d_6, 300MHz, 298K) δ: 12.46 (bs, 1H, exch. with D_2O), 7.64 (bs, 1H, exchanged with D_2O), 7.30-7.13 (m, 6H), 7.02-6.88 (m, 2H), 6.31 (bs, 1H). ^{13}C-NMR: 153.9 (C),

147.0 (C), 135.2 (C), 134.7 (C), 128.8 (CH), 127.5 (CH), 121.0 (CH), 119.7 (CH); 118.8 (C), 111.5 (CH), 108.1 (CH).

2-(1-Pyrenyl)-1H-perimidine: 90%; orange powder; ^{1}H-NMR (DMSO-d_6, 300MHz, 298K) δ: 11.08 (s, 1H, exch. with D_2O), 8.61 (d, 1H, J=9.2Hz), 8.45-8.24 (m, 7H), 8.14 (t, 1H, J=7.7Hz), 7.23 (t, 1H, J=7.7Hz), 7.18-7.04 (m, 3H), 6.72 (d, 1H, J=7.4Hz), 6.43 (d, 1H, J=7.1Hz); ^{13}C-NMR (DMSO-d_6, 75.4MHz, 323K) δ: 155.2 (C), 135.9 (C), 132.4 (C), 131.4 (C), 130.9 (C), 130.5 (C), 129.0 (CH), 128.9 (CH), 127.8 (CH), 127.2 (CH), 126.7 (CH), 126.5 (CH), 126.3 (CH), 125.2 (CH), 125.0 (CH), 124.5 (C), 124.3 (C), 122.3 (C); m.p. = 292-293°C.

2-(2-Hydroxy-1-naphthyl)-1H-perimidine: 79%; yellow powder; ^{1}H-NMR (DMSO-d_6, 300MHz, 298K) δ: 10.55 (bs, 1H, exch. with D_2O), 7.93-7.82 (m, 3H), 7.48 (t, 1H, J=7.7Hz), 7.34 (t, 1H, J=7.3Hz), 7.27 (d, 1H, J=8.9Hz), 7.14 (t, 2H, J=7.2Hz), 7.05 (d, 2H, J=8.3Hz), 6.44 (d, 2H, J=7.4Hz); ^{13}C-NMR (DMSO-d_6, 75.4MHz, 298K) δ: 153.7 (C), 153.1 (C), 142.8 (C), 135.9 (C), 132.8 (C), 131.2 (CH), 128.9 (CH), 128.5 (CH), 128.1 (C), 127.5 (CH), 124.1 (CH), 123.5 (CH), 122.4 (C), 118.9 (CH), 118.8 (CH), 115.7 (C), 108.2 (bs, CH); m.p. = 197-198°C.

Spectroscopic characterization

The UV-VIS absorption spectra were measured by a Perkin Elmer Lambda 2 UV-VIS spectrophotometer. For each compound, stock solutions in HPLC-grade toluene, acetonitrile (ACN), dimethylsulfoxyde (DMSO) and methanol (MeOH) of 1mM concentrations were prepared by weighing the powders previously desiccated overnight under vacuum. Three more solutions for each sample were prepared by dilution of the stocks, their absorption spectra in the 270 nm - 650 nm range were acquired and the molar extinction coefficients at the main absorption peak were evaluated by linear regression of the absorbance *vs* concentration plots. The fluorescence emission spectra were acquired with a PTI Fluorescence Master System spectrofluorimeter. The acquisition software provided on-line correction for both the excitation lamp and the detector spectral responses. Fluorescence

quantum yields were determined by comparison with a solution of dimethyl-POPOP in cyclohexane (Φ_{Fl}=0.93)[20], excited at the 343 nm absorption peak, by normalizing with respect to the relative absorption and solvent refractive index.

Due to the relatively low quantum yield of some of the compounds, careful correction for the solvent signal was necessary. The latter was performed by exploiting a home-written Matlab routine: the fluorescence signal was first corrected for the absorbance of the sample at the emission spectra wavelengths, considering the absorption due to an average optical path of the fluorescence light of 5 mm inside the cuvette (whose optical path is 10 mm), then the background signal measured on the solvent was subtracted and a smoothing with the Savitzki-Golay algorithm was performed.

Results and discussion

Spectroscopic characterization in organic solvents.

The UV-Vis absorption spectra of **1-6** were recorded in the non-polar solvent toluene (TOL), in the polar, weakly hydrogen-bonding solvent acetonitrile (ACN), in the strongly hydrogen-bonds acceptor dimethylsulfoxide (DMSO) and in the protic solvent methanol (MeOH) in the band 270 nm-650 nm. In the most transparent solvents, *i.e.*, ACN and MeOH, absorption was measured also in the UVB band between 200 nm-270 nm, whereas in the remaining two solvents such measurement was prevented due to high solvent absorbance. In ACN and MeOH the absorption band peaked at ≈235 nm that was previously observed for several perimidine derivatives and attributed to excitation from the bonding π_2 configuration to the corresponding antibonding orbital, π_3^*, within the naphthalene system [20], was punctually detected for all the compounds. However, because this band, besides being not easily measurable in some of the selected benchmark solvents, corresponds to a local electronic transition and is thus liable of being less environment and substitution sensitive, we focused our analysis on the UVA band.

In this spectral region, the peak around 340 nm falls, which was also early reported for several perimidine derivatives and attributed to intramolecular charge transfer of the excess electron back from the naphthalene system to the perimidine moiety (see introduction). In inert environment (*e.g.*, TOL), such band is expected to be the more red-shifted and intense the more mobile and prone to be withdrawn from the naphthalene system is the electron. Interaction with solvent molecules of the perimidine moiety can either enhance or inhibit the electron withdrawing character of such moiety. We note that the removal of the excess electronic charge donated by the perimidine heterocycle from the naphthalene system would restore the original aromatic character of the fluorophore, hopefully leading to the recovery of fluorescence.

Table 1: Spectroscopic properties of compounds 1-6 in organic solvents.λ_{peak}: absorption peak wavelength; ϵ: molar extinction coefficient; λ_{fluo}: fluorescence peak wavelength (--: no detectable fluorescence signal); Φ: fluorescence quantum yield.

Compound	**Solvent**	$\boldsymbol{\lambda_{peak}}$ **[nm]**	$\boldsymbol{\epsilon}$ **[$M^{-1}cm^{-1}$]**	$\boldsymbol{\lambda_{fluo}}$ **[nm]**	**Φ**
1	ACN	329	12660	476	0.00126
	DMSO	333	22936	482	0.00307
	MeOH	329	9480	485	0.00052
	TOL	331	12355	472	0.00544
2	ACN	341	20860	531	0.0025
	DMSO	345	13100	533	0.021
	MeOH	340	16480	424	0.005

	TOL	342	19300	381	0.036
3	ACN	342	18402	400	0.00036
	DMSO	345	19197	393	0.00039
	MeOH	343	24876	396	0.00030
	TOL	343	18955	370	0.00329
4	ACN	348	13880	411	0.00026
	DMSO	352	16600	--	
	MeOH	347	19800	400	0.0002
	TOL	351	13400	384	0.0077
5	ACN	342	31720	--	
	DMSO	346	30530	--	
	MeOH	341	28636	406	0.00045
	TOL	346	16989	373	0.01604
6	ACN	357	15966	--	
	DMSO	364	16550	477	0.00414
	MeOH	334	16143	438	0.00075
	TOL	351	17680	382	0.03259

In Table 1 we report the main spectroscopic properties of compounds **1-6** in organic solvents. The wavelength of the absorption peak of the charge-transfer band and the pertaining molar extinction coefficient value, determined as described

in the experimental section, are tabulated in the third and fourth column from left, respectively . In Fig. 1a) we compare the spectra of the different compounds in TOL, while in Fig. 1b) we exemplify the procedure used to determine the extinction coefficient values by showing the plots of absorbance as a function of concentration obtained for **1** in the different solvents, and the pertaining linear fits.

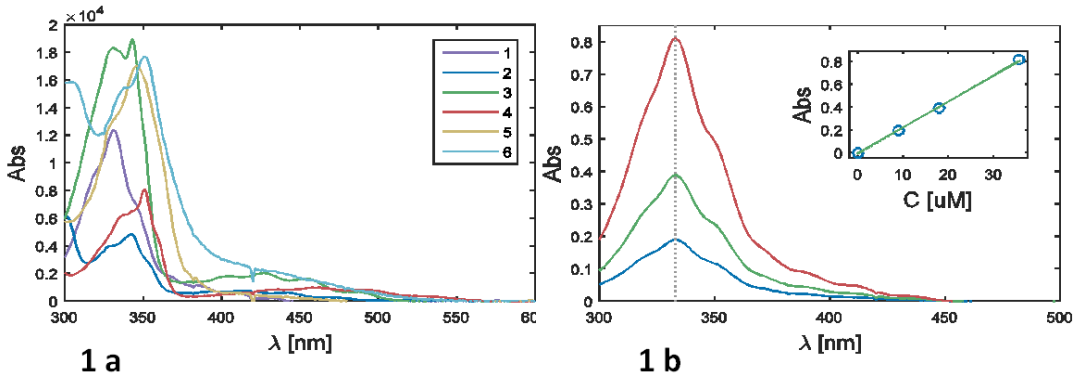

Figure 1a) Absorption spectra of compounds 1-6 in TOL. Absorbance is normalized for concentration equal to 1 M. **1b)** Absorption spectra of compound 1 in DMSO at various concentrations for the determination of the molar extinction coefficient. The grey dotted line is drawn in correspondence to the peak wavelength. (Inset) The molar extinction coefficient is determined as the slope of the best fit line of the absorbance versus concentration graph.

Similar plots were built up for compounds **2-6** (data not shown). It can be observed that all the 2-substitutions induce a bathochromic shift in the charge transfer band. This result agrees with previous finding on compound **3**[21] as well as on 2-phenylperimidine.[12] In the quoted reference, it was interpreted as the effect of enhanced electron withdrawal from the naphthalene system, due to charge conjugation between such group and the aromatic 2-substituents through the perimidine heterocycle. Moreover, in TOL the extinction coefficient values are higher than that measured for perimidine, **1**, for all compounds with the exception of **4**. We remind that the intensity of an absorption band is proportional to the

dipole moment of the corresponding transition, i.e. to the propensity of the molecule to undergo such transition. Due to the peculiar behaviour of **4**, charge transfer seems thus to be not univocally favoured compared to **1** by addition of cyclic 2-substituents. The observation that the extinction coefficient value of **4** is very similar to that of unsubstituted perimidine might be explained by the fact that, as previously attested by molecular dynamics calculations, the six-membered heterocyclic ring of perimidine is a rather poor conductor of electronic charge in the ground state.[20] Thus, in order for the excess electronic charge to be exchanged between the naphthalene system and the added 2-substituents a fairly high potential barrier must likely be overcome. In other words, in order to make the charge migration energetically favourable and thus the corresponding transition probable notably electron withdrawing substituents are required. Indeed, the polyaromatic structure of the **5** 2-substituent promises high conjugation, while the superior electron withdrawing properties of the 2-hydroxyphenyl substituent of **3** with respect to the very similar one exhibited by **4** might be a consequence of the formation of a further six-membered quasi-aromatic ring due to intramolecular H-bonding (IHB) between the hydroxyl group of the hydroxyl-phenyl substituent and the unsaturated nitrogen of the perimidine heterocycle. For **6**, both polyaromaticity of the substituent and IHB formation might play a role. It is worth noting that the formation of the above-claimed IHB in **3** is widely supported by the work of several authors. [21]

As testified by the parameters detailed in Table 1, the absorption properties are only slightly affected by the solvent properties. There are only a few variations that are worth to be commented. First, charge transfer from the naphthalene system to the cyclic substituent appears to be sensitive to solute-solvent H-bonding interactions for both **1** and **6**. Namely, interaction with the pure H-bond acceptor DMSO seems to enhance the transition probability, whereas interaction with the H-bond donating MeOH inhibits the charge flux. For **1**, such behaviour is denounced by an increase of the extinction coefficient in DMSO and a decrease in MeOH with

respect to the very similar values measured in both non-polar (TOL) and polar (ACN) weakly H-bonding environment. The spectra of **1** in all the solvents are plotted in Fig. 2a).

In 6, comparable values of the extinction coefficient suggest that the potential barrier is comparable in all the benchmark solvents we tested. However, a consistent hypsochromic shift with respect to TOL (17 nm) for the compound dissolved in protic environment is the symptom of a significant reduction in conjugation. Conversely, in DMSO a comparable (13 nm) bathochromic shift is observed, which stems in support of enhanced intramolecular charge mobility. The spectra of 6 in all the solvents are plotted in Fig. 2b). The second sizeable perturbation of the absorption properties due to environmental changes is the increment in extinction coefficient, thus in transition dipole moment, measured for 5 by effect of increasing the solvent polarity, independent of the H-bonding character. The spectra of 5 in all the solvents are plotted in Fig. 2c).

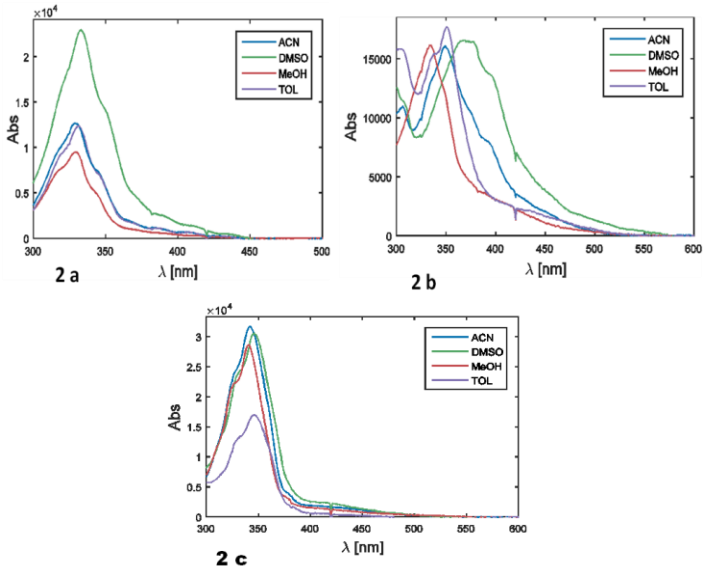

Figure 2a) Absorption spectra of compound **1** in ACN, DMSO, MeOH and TOL.

Absorbance is normalized for concentration equal to 1 M. **2b)** Absorption spectra of compound **5** in ACN, DMSO, MeOH and TOL.Absorbance is normalized for concentration equal to 1 M. **2c)** absorption spectra of compound **6** in ACN, DMSO, MeOH and TOL. Absorbance is normalized for concentration equal to 1 M.

The spectra of compounds **2**, **3**, and **4** are provided in Figs. S1a), S1b) and S1c) and in Figs. S2a)-S2c) we compare the spectral line-shapes of the different compounds in ACN, MeOH, and DMSO, respectively.

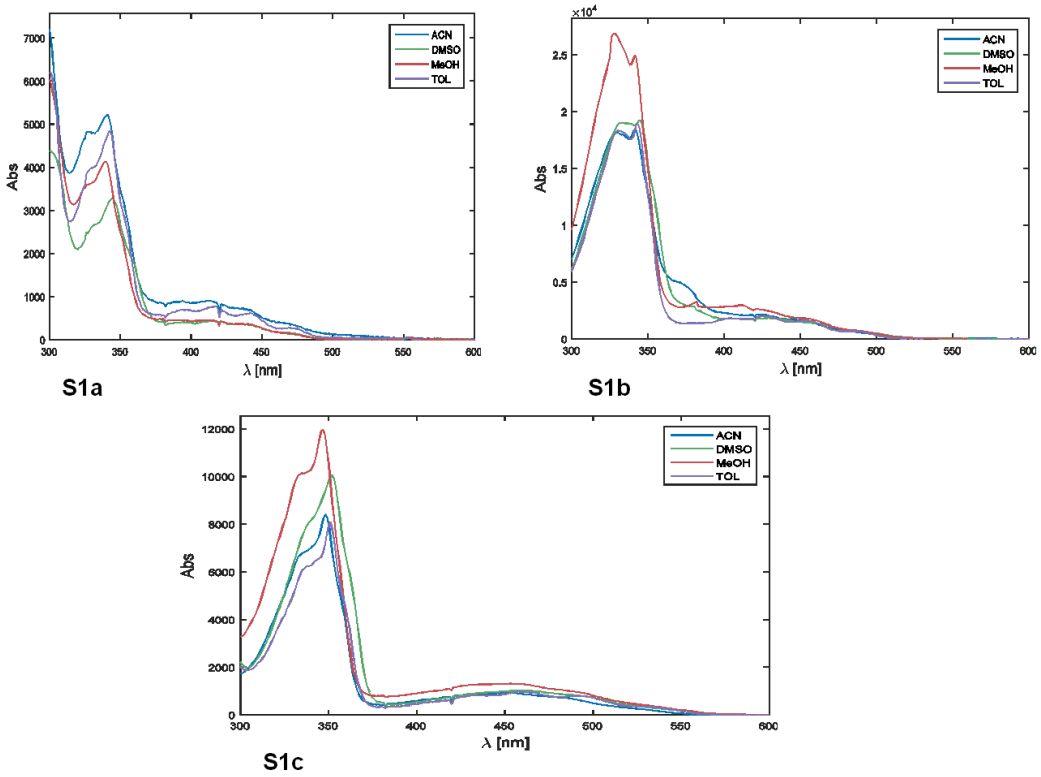

Figure S1 a) absorption spectra of compound **2** in ACN, DMSO, MeOH and TOL. Absorbance is normalized for concentration equal to 1 M. **b)** absorption spectra of compound **3** in ACN, DMSO, MeOH and TOL. Absorbance is normalized for concentration equal to 1 M. **c)** absorption spectra of compound **4** in ACN, DMSO, MeOH and TOL.Absorbance is normalized for concentration equal to 1 M.

In the fifth and sixth column of Table 1 we report the fluorescence emission peak wavelength and the fluorescence quantum yield values, respectively, of compounds **1**-**6** in the different solvents. By comparing the emission properties of perimidine, **1**, with those of its 2-substituted analogues, **2**-**6**, in TOL, a first evidence is immediately apparent. As shown in Fig. 3, the spectra of **2**-**6** are systematically blue-shifted by as much as 90-100 nm compared to that of the parent compound.

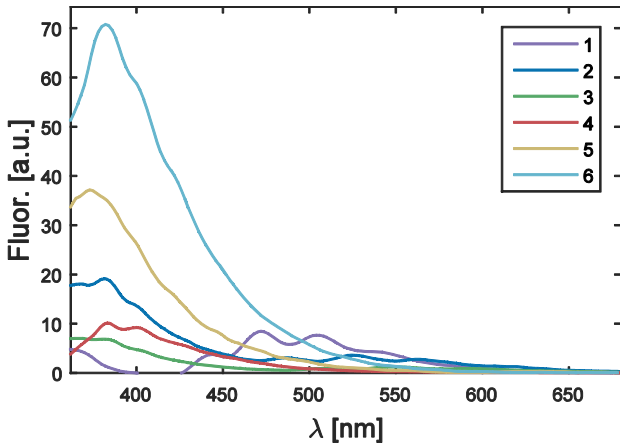

Figure 3: Fluorescence spectra of compounds **1**-**6** in TOL.

In this regard, they tend to resemble much more to that of the isolated naphthalene fluorophore, peaking at 330 nm in cyclohexane. This observation stems in support of the hypothesis that introduction of the cyclic substituents in 2- position capable of draining part of the excess electronic charge of the six-membered heterocycle out of the naphthalene system has the effect of partially restoring its original electronic configuration. According with our assumption that in **1** the fluorescence is quenched mainly because of perturbation of the aromatic system of naphthalene through donation of an excess electron by the *peri*-fused six-membered heterocycle, an enhanced tendency to expel such an electron in the excited state should correlate with a fluorescence increase at least in inert environment, where solvent-rearrangement driven excited-state deactivation pathways should be

negligible. Indeed, the fluorescence quantum yield in TOL increases by as much as roughly 50% from **1** to **4**, a compound which exhibits increased intramolecular charge conjugation (evidenced by bathochromic shift) but a comparable transition probability (similar extinction coefficient). The increase in fluorescence quantum yield is even more evident in **2**, **5** and **6**, three compounds combining large bathochromic shifts of the charge-transfer absorption band with high increment in the corresponding extinction coefficient. The latter have quantum yields exceeding that of **1** by at least a factor of four. However, for **3** we measured a quantum yield value comparable, and even somewhat lower than that measured for **1**. The quantum yield value measured for **3** in TOL is very similar to that reported by other authors for the same compound in cyclohexane, a solvent sharing very similar polarity and H-bonding properties.[21] In the same reference, the authors demonstrate that the hypothesis that the unexpectedly low fluorescence quantum yield of **3** can be ascribed to an excited-state proton transfer phenomenon occurring between the enol moiety and the unsaturated nitrogen must be ruled out. Indeed, the notable decrease in quantum yield observed both by us and the above authors as a result of IHB quenching by means of polarity and H-bonding interactions with solvent molecules would be hardly compatible with such hypothesis. Thus, it must be concluded that, although significant, the enrichment in electronic charge of the naphthalene system is not the only mechanism dictating the steep reduction in fluorescence emission in perimidines with respect to the isolated fluorophore, and that specific features of the 2-substituents are also liable to play substantial and hardly predictable roles.

Interaction with a non-inert environment generally quenches the fluorescence emission of compounds **1**-**6**, typically by as much as one or more orders of magnitude.

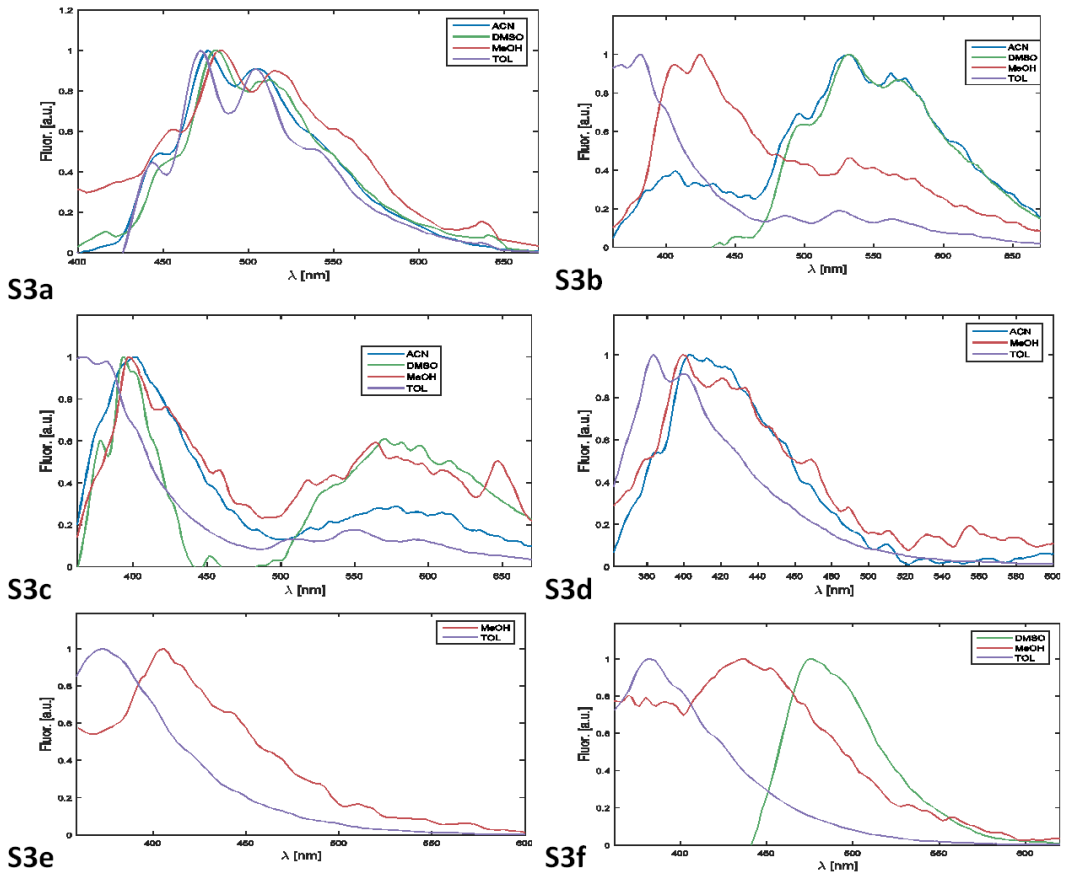

Figure S3 a) fluorescence spectra of compound **1** in ACN, DMSO, MeOH and TOL. Spectra are normalized to a peak value of 1. **b)** Fluorescence spectra of compound **2** in ACN, DMSO, MeOH and TOL. Spectra are normalized to a peak value of 1. **c)** Fluorescence spectra of compound **3** in ACN, DMSO, MeOH and TOL. Spectra are normalized to a peak value of 1. **d)** Fluorescence spectra of compound **4** in ACN, MeOH and TOL. Spectra are normalized to a peak value of 1. **e)** Fluorescence spectra of compound **5** in MeOH and TOL. Spectra are normalized to a peak value of 1. **f)** Fluorescence spectra of compound **6** in DMSO, MeOH and TOL. Spectra are normalized to a peak value of 1.

Interestingly (see Table 1 and Fig. S3 a-f), the compounds showing the largest dependence from the environment are the ones that were concluded to be endowed

with the higher intramolecular charge mobility, *i.e.* **5** and **6**. In any case, however, there is no straightforward dependence from the polarity of the solvent, suggesting that specific solute-solvent interactions, possibly mediated by intermolecular H-bonding, are of major importance in tuning the excited-state dynamics. Moreover, the effects of such interactions are not univocal in the different compounds, but depend from the substituent in position 2 of the perimidine.

Spectroscopic characterization in pseudo-physiological environment.

We now explore the spectroscopic properties of compounds **1-6** in pseudo-physiological environment. Their absorption spectra in phosphate buffered saline (PBS) at pH 7.4 and 150 mM ionic strength are reported in Fig. 4.

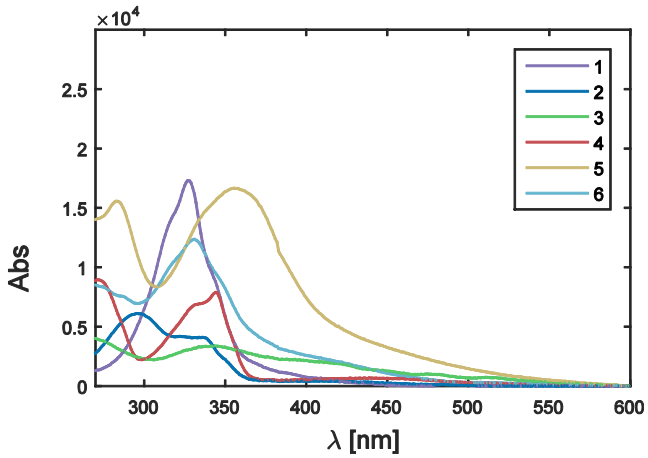

Figure 4: Absorption spectra of compounds **1-6** in PBS. Absorbance is normalized for concentration equal to 1 M.

For the great majority of the compounds, virtually excluding only **3** and **5**, the features of the absorption spectrum in aqueous environment closely resemble those of the spectrum measured in MeOH, consistently with the highly polar, H-bonding and protic nature of both solvents.

Perimidine, **1**, exhibits a peak molar extinction coefficient value, ≈18000 $M^{-1}cm^{-1}$, which is intermediate between those measured in MeOH (≈9500 $M^{-1}cm^{-1}$) and

DMSO (≈23000 $M^{-1}cm^{-1}$), suggesting that water can react as an H-bond acceptor with respect to **1** more effectively than MeOH.

For **2**, which exhibited a markedly red-shifted π-π^* transition band also in organic solvents (≈290 nm, see Fig. 2), the π-π^* and charge-transfer bands are only slightly broadened, but this is sufficient to make the charge transfer band resemble a bare shoulder, and the complex of the two transitions appears as a unique, though structured, band.

Compounds **4** and **6** are only slightly hypochromic in water than in alcohol, otherwise producing almost superimposable absorption spectral line-shapes in the two solvents.

At difference, compound **5** exhibits considerably red-shifted and hypochromic absorption in aqueous environment than in alcohol. Moreover, the spectrum loses its structural features and becomes notably broader. These characteristics suggest that in PBS the intramolecular charge transfer mechanism producing the UVA band requires less energy and that the electronic charge results more conjugated. Instead, the potential barrier to be overcome increases.

Finally, for compound **3** we assist to a dramatic reduction in the UV absorption cross section (the molar extinction coefficient at the charge-transfer band peak wavelength reduces from (≈20000 $M^{-1}cm^{-1}$ in MeOH to ≈3000 $M^{-1}cm^{-1}$ in water), at the advantage of the spectral features in the visible band around 420 nm, which were present but minor in organic solvents. This phenomenon might be a symptom of enhanced intramolecular conjugation in aqueous medium.

Coming to the fluorescence properties, all the compounds emit very deem fluorescence in water upon excitation at the peak of the charge-transfer band. This feature might be beneficial in view of applications of the compounds as DNA stains in fluorescence microscopy, provided that measurable fluorescence is recovered upon dye binding to the biopolymer and consequent shielding from the solvent molecules.

Assessment of DNA-binding affinity and sensitivity of fluorescence to the binding status.

The DNA-binding affinity of the compounds was probed by means of spectrophotometric titrations. First, the absorption spectra of **1**-**6** in PBS added with calf thymus DNA (ligand-to-base pair concentration ratio 1:20) were measured. They are represented in Fig. 5, while Figs. S4 a)-f) provide direct comparison of the absorption spectra of isoconcentrated (15 μM) samples of **1**-**6**, respectively, in PBS in the presence (data reproduced from Fig. 5) and absence of excess DNA (from Fig. 4).

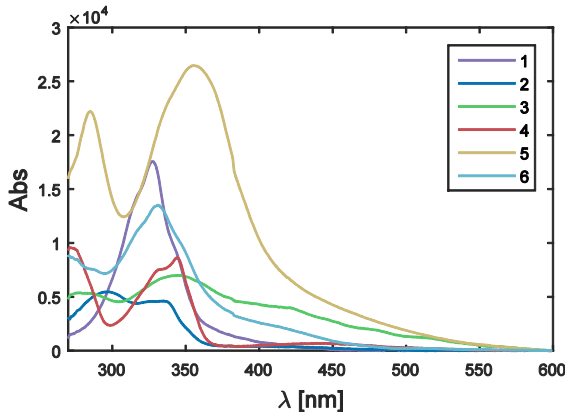

Figure 5: Absorption spectra of compounds **1**-**6** in PBS in the presence of 300 uM DNA. Absorbance is normalized for compound concentration equal to 1 M.

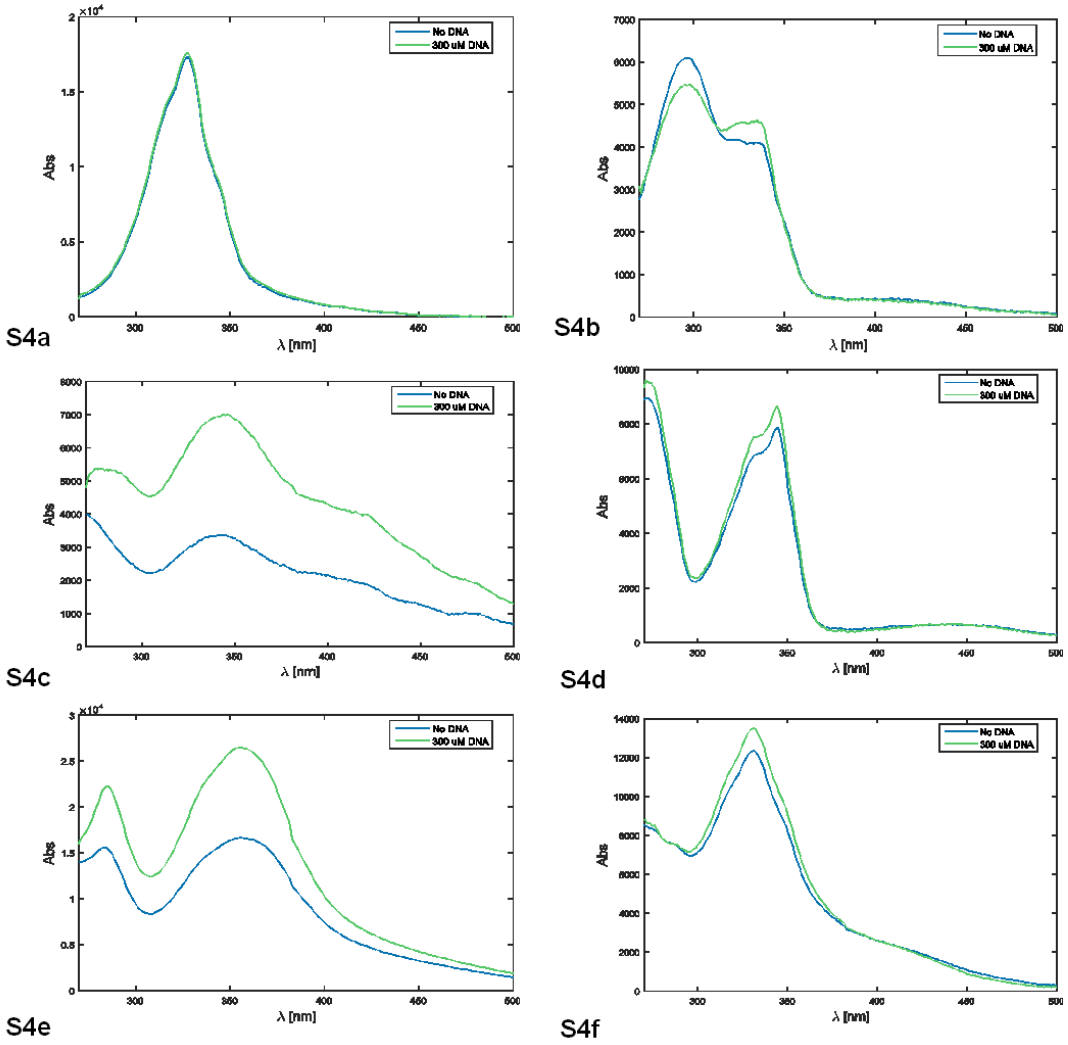

Figure S4 a) Absorption spectra of **1** in PBS (blue line) or PBS + 300 uM DNA (green line). Absorbance is normalized for concentration equal to 1 M. **b)** Absorption spectra of **2** in PBS (blue line) or PBS + 300 uM DNA (green line). Absorbance is normalized for concentration equal to 1 M. **c)** Absorption spectra of **3** in PBS (blue line) or PBS + 300 uM DNA (green line). Absorbance is normalized for concentration equal to 1 M. **d)** Absorption spectra of **4** in PBS (blue line) or PBS + 300 uM DNA (green line). Absorbance is normalized for concentration equal to 1 M. **e)** Absorption spectra of **5** in PBS (blue line) or PBS +

300 uM DNA (green line). Absorbance is normalized for concentration equal to 1 M. **f)** Absorption spectra of **6** in PBS (blue line) or PBS + 300 uM DNA (green line). Absorbance is normalized for concentration equal to 1 M.

It can be observed that binding to DNA produces significant modifications to the absorption spectral features in all cases excluded compound **1**. Namely, for **3**-**6** a more or less pronounced hyperchromic effect is detected throughout all the absorption range, while in the case of **2** it appears that the charge-transfer band is corroborated and the π-π^* transition band depressed in intensity as a consequence of binding.

The sizeable modifications in the 2-substituted perimidine derivatives spectral properties upon binding were exploited to perform spectrophotometric binding titrations in which the DNA base-pairs concentration was varied in the range 0-300 μM while fixing the ligand concentration to 15 μM. Obviously, it was not possible to perform spectrophotometric titrations of the binding of **1** to DNA, due to the negligible effect of binding on the absorption properties.

An exemplary plot (obtained with **5** as a ligand) of the value of absorbance at the charge transfer band peak as a function of DNA concentration is sketched in Fig. 6.

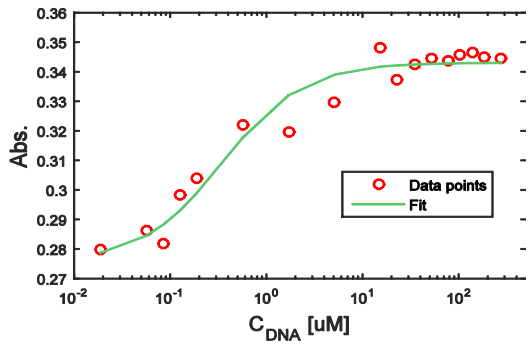

Figure 6. Titration curve for the binding of compound **5** to DNA. Points correspond to experimental data, solid line corresponds to the best fit line obtained with the model of Eq. (1)

This experimental binding isotherm was fitted to the independent binding sites model [13,22], i.e., to the following equation:

$$Abs(C_{DNA}) = Abs_0 + \frac{\delta Abs}{2}\left[(K_{app})^{-1} + D + C_{DNA} - \sqrt{\left((K_{app})^{-1} + D + C_{DNA}\right)^2 - 4DC_{DNA}}\right]$$

(Eq.1).

In Eq.(1) $Abs(C_{DNA})$ represents the predicted absorbance at the charge transfer band peak for a sample in which DNA was added in concentration C_{DNA}, Abs_0 represents the predicted absorbance of a 15 mM solution of **5** in the absence of DNA, K_{app} is the apparent binding constant for the **5**-DNA complex, D is the total concentration of **5**, either free or bound, i.e., 15 μM in our instance and δAbs×D is the enhancement in absorbance which would be measured if the same concentration of **5** were completely DNA-bound. Eq. (1) models an initial hyperchromicity due to progressive shift of the chemical equilibrium towards the bound complex and a subsequent absorbance saturation corresponding to DNA concentrations at which virtually all the ligand molecules are bound.

In Table 2 we report the K_{app} values as estimated by applying the above procedure to compounds **2**-**6**. Notably, they range from ≈6×10^4 M^{-1} to ≈5×10^6 M^{-1}, the value for typical intercalators such as ethydium bromide[23] and quinacrine dihydrochloride being around ≈10^5 M^{-1}at similar salt concentrations. [20] Moreover, addition of more aromatic rings in 2-position (as for **5** and **6**) and enhancement of conjugation by formation of intramolecular H-bonds (in the case of **3** and **5**) enhance the DNA-binding affinity. These data agree with the early findings of Herbert et al., [20] and stem in support of their hypothesis that, having perimidine a structure very close to that ideally bearing the minimal features indispensable for base intercalation, perimidine derivatives are susceptible to effective tuning of DNA binding parameters by means of substitutions.

Table 2: apparent binding constants of compounds **1-6** to DNA. *: Binding constant for compound **1** was determined through spectrofluorimetric titration, while for compounds **2-6** it was determined via spectrophotometric titration.

Compound	$\boldsymbol{K_{app}}$ $[\mathbf{M^{-1}}]$
1	$(2.5 \pm 0.5) \cdot 10^5 *$
2	$(6 \pm 1) \cdot 10^4$
3	$(3 \pm 1) \cdot 10^6$
4	$(9 \pm 3) \cdot 10^4$
5	$(3.2 \pm 0.5) \cdot 10^6$
6	$(5 \pm 2) \cdot 10^6$

Finally, we performed measurements of the fluorescence emission of **1-6** upon excitation at the charge transfer band peak in the presence of excess calf thymus DNA (ligand-to-base pair concentration ratio 1:20). Unfortunately, only compounds **1**, **5**, and **6** emit detectable fluorescence in the above conditions. The pertaining emission spectra are shown in Fig. 7a-c, respectively.

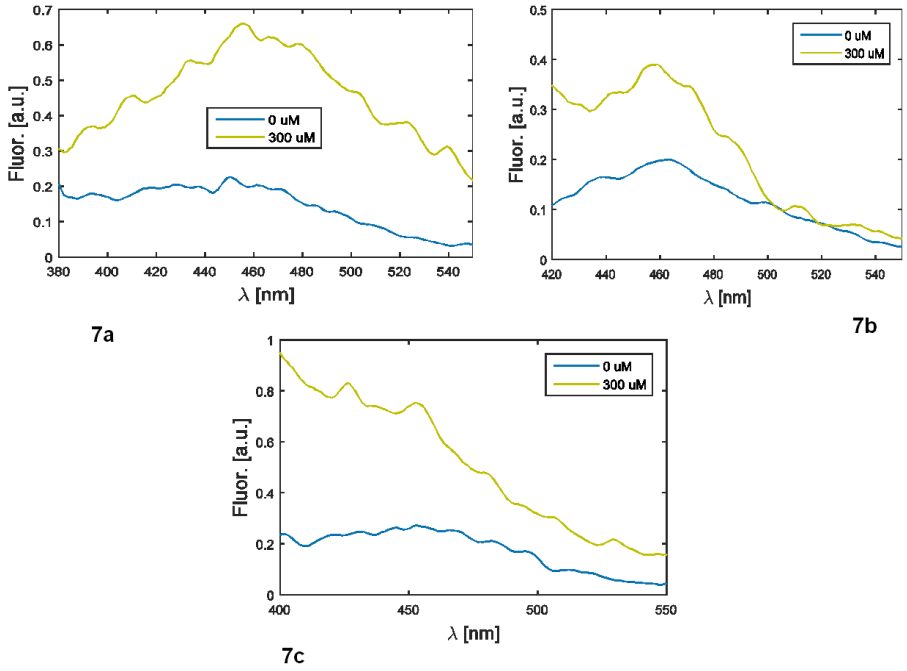

Figure7 a) Fluorescence spectrum of compound **1** in PBS (blue line) or PBS + 300 uM DNA (yellow line). **b)** Fluorescence spectrum of compound **5** in PBS (blue line) or PBS + 300 uM DNA (yellow line). **c)** Fluorescence spectrum of compound **6** in PBS (blue line) or PBS + 300 uM DNA (yellow line).

The corresponding emission spectra in PBS in the absence of DNA are also reproduced. It can be observed that, for all these three compounds, binding to DNA results in a roughly three-fold increase in the fluorescence intensity, with no relevant modifications in the spectral line-shapes. On the other side, it must be said that the fluorescence quantum yield of the three compounds bound to DNA in pseudo-physiological environment is too low to allow them be applied as DNA stains in fluorescence imaging experiments.

Nonetheless, the notable fluorescence increase measured for **1** as a consequence of binding allowed to assess its DNA-binding affinity by means of spectrofluorimetric titration. Practically, an experiment similar to those described above, but in which the fluorescence emission spectra were recorded as a function of DNA concentration instead of the absorption spectra, was undertaken. The resulting

binding isotherm was fitted to a suitably modified equation (XXX), in which the values of absorbance were substituted by peak fluorescence intensities, and the obtained K_{app} value is reported in Table 2. Notably, it is in the middle of the range of values obtained for the substituted compounds, suggesting that substitutions can lead to both enhancement and depression of the binding affinity.

Conclusions

Perimidine and five 2-substituents were synthesized according to either previously reported or novel procedures, and their electronic state transition spectroscopy (namely UV-Vis absorption and fluorescence emission) features were characterized at varying the environmental properties. The binding affinity to DNA was also determined by means of spectrophotometric or spectrofluorimetric titrations. The compounds show binding constants spanning from 10^4 M^{-1} to 10^6 M^{-1}, confirming that the binding properties of perimidines are exceptionally tuneable by means of chemical substitutions. However, although some of the derivatives show higher fluorescence quantum yields in organic solvents with respect to the parent compound, none of them conserves this desirable properties in aqueous environment. Thus, the analysed compounds demonstrated to be not optimal for theranostic purposes.

REFERENCES

[1] A.F. Pozharskii and V.V. Dal’nikovskaya; Russ. Chem. Rev. 50 (1981) 816-835.

[2] M. Ikeda, K. Maruyama, Y. Nobuhara, T. Yamada and S. Okabe; Chem. Pharm. Bull. 44 (1996) 1700-1706.

[3] V.N. Novikov, A.F.Pozharskii and V. N. Doron'kin; Chem. Het. Comp. 12 (1976), 210-217.

[4] U. Burkhardt, S. Johne, M. Klenel, S. Kuehne, H. Lehmann, DD Patent 238908 (1986).

[5] T.A. Farghaly, M.A. Abdallah, Z.A. Muhammad, Res. Chem. Intermed. 41 (2015) 3937-3947.

[6] K. Matsumoto, US Pat. 4224326 (1980).

[7] E. Mentese, F. Yilmaz, N. Karaali, S. Ulker, B. Kahveci, Russ. J. Bioorg. Chem. 40 (2014) 336-342.

[8] T. Farghaly, E.M.H Abbas, K.M. Dawood, T.B.A. El-Naggar, Molecules 19 (2014) 740-755.

[9] T.A. Farghaly, H.K. Mahmoud, Arch. Pharm. 346 (2013) 392-402.

[10] J.M. Herbert, P.D. Woodgate, W.A. Denny, J. Med. Chem. 30 (1987) 2081-2086.

[11] W. Wasulko, A.C. Noble, F.D. Popp, J. Med. Chem. 9 (1966), 599-601.

[12] V.I. Minkin, Y.A. Zhdanov, I.D. Sadekov, O.A. Raevskii, A.D. Garnovskii, Chem. Heteroc. Comp. 3 (1967) 1100-1108.

[13] A. Abbotto, G. Baldini, L. Beverina, G. Chirico, M. Collini, L. D’Alfonso, A. Diaspro, R. Magrassi, L. Nardo and G.A. Pagani; Biophys. Chem. 114 (2005) 35-41.

[14] M. Gregori, D. Bertani, E. Cazzaniga, A. Orlando, M. Mauri, A. Bianchi, F. Re, S. Sesana, S. Minniti, M. Francolini, A. Cagnotto, M. Salmona, L. Nardo, D.

Salerno, F. Mantegazza, M. Masserini and R. Simonutti; Macromol. Biosci. 15 (2015) 1687-1697.

[15] G. Grabner, K. Rehcthaler, B. Mayer and G. Köhler; J. Phys. Chem. A 104 (2000), 1365-1376.

[16] F.P. Schwarz and S.P. Wasik, Anal. Chem. 48 (1976), 524-528.

[17] G. Varsha, V. Arun, P.P. Robinson, M. Sebastian, D. Varghese, P. Leeju, V.P. Jayachandran and K.K.M. Yusuff; Tetrahedron Lett. 51 (2010) 2174–2177.

[18] E. Gehrer and W. Harder; DE Patent 19536403.

[19] N.M. Starshikov and A.F. Pozharskii; Chem. Het. Comp. 16 (1980), 81-85.

[20] I.B. Berlman, Handbook of Fluorescence Spectra of Aromatic Molecules, Academic Press, N.Y., 1971

[21] G. Grabner, K. Rehcthaler, B. Mayer and G. Köhler; J. Phys. Chem. A 104 (2000), 1365-1376.

[22] L. Nardo, M. Bondani and A. Andreoni; Spectroscopy 23 (2009) 11-28.

[23] J.B. Birks, M. Salete and S.C.P. Leite; J. Phys. B: At. Mol. Phys. 3 (1970) 417-424.

CHAPTER 6

Unprecedented Formation of 2,5-Diaminoquinones from the Reaction of Vanillin with Secondary Amines in Aerobic Conditions

Arianna M. Giani, Valentina Papillo, Roberto Negri, Fabiano Travaglia,
Marco Arlorio*, Giovanni B. Giovenzana*

Introduction

Vanillin (4-hydroxy-3-methoxybenzaldehyde) is one of the most important flavoring compounds used in foods, beverages, perfumes and pharmaceuticals. This compound is extracted from orchid of the genus *Vanilla* [1]. However, being the extraction very expensive and covering just a little percentage of the market request, synthetic vanillin is nowadays the most used. Vanillin was recognized as suitable for food use by FDA since 1977 [2]. Additionally, several studies on bioactivity of this aromatic compound were produced, displaying potential anti-bacterial [3], anti-mutagen [4,5] and anti-oxidant [6] activities.

Extensive studies have been devoted to the identification of the compounds formed during thermal treatments related to the cooking of aliments like, for example, the Maillard reaction of carbohydrates in the presence of biogenic amines, finally leading to Amadori products.[7] Even if the annual worldwide production and use of vanillin is in excess of $1.5 \cdot 10^4$ tons, it is surprising that few or no investigations have been reported on the possible byproducts that could be formed during the use of this flavoring agent.[8]

While performing a series of reaction on vanillin, initially addressed to the preparation of quinomethides, we observed the nearly exclusive formation of unexpected products from its reaction with secondary amines. In detail, treatment

of vanillin (**1**) with excess pyrrolidine (**2a**) in alcoholic solution at room temperature originated an initially complex mixture of coloured compounds (detected by TLC), ultimately evolving overnight towards the copious precipitation of a brick red precipitate. Isolation of the latter and analytical characterization by NMR and ESI-MS spectrometry led to the identification of this product as 2,5-dipyrrolidino-1,4-benzoquinone (**3a**). Comparison of the product with a sample prepared by an independent procedure[9] confirmed its identity.

Puzzled by this result, we started a systematic investigation of this curious reaction by exploring its versatility towards different amines. Different secondary aliphatic amines (**2a-e**, Scheme 1) were found to react in a similar fashion, leading to the isolation of good to excellent yields of the corresponding substituted 2,5-diamino-1,4-benzoquinones (**3a-e**). Secondary aromatic amines did not react significantly. Primary amines, either aliphatic or aromatic, gave limited yields of "simple" imines in these conditions (no drying agents were used).

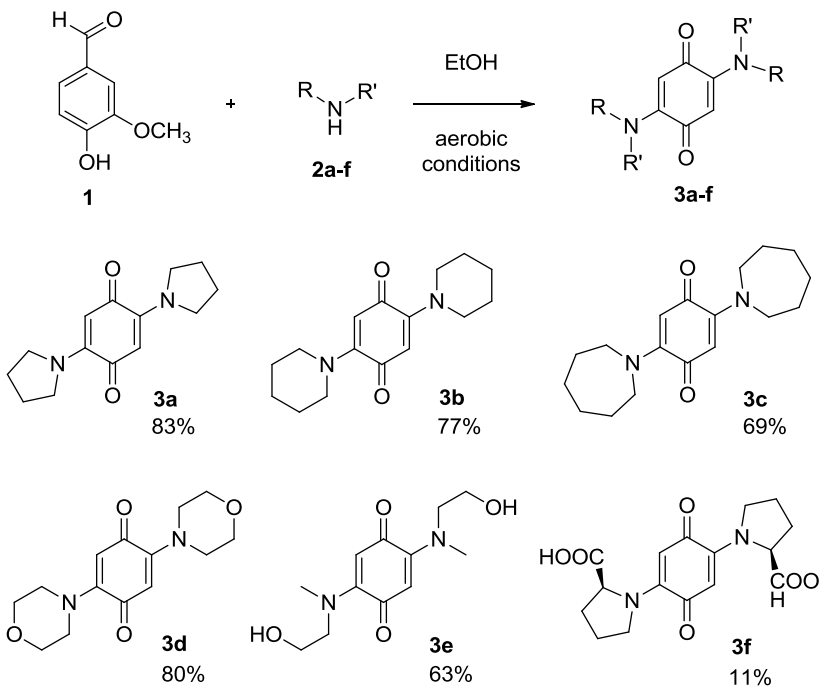

The experimental conditions were then examined in order to gain additional information on the mechanism. Heating the reaction mixture (60°C or reflux) accelerated the formation of 2,5-diamino-1,4-benzoquinones. Changing the solvent led to different results, mainly driven by the limited solubility of the reagents in apolar solvents such as diethyl ether or more polar ones as water. Interestingly, the reaction proceeded sluggishly under an inert atmosphere and reached almost complete conversion after restoring aerobic conditions, suggesting the direct intervention of oxygen in an oxidative step.

Simple reaction mapping allowed to trace back the quinone skeleton to the aromatic ring of vanillin, with the evident exclusion of the carbon atom of the aldehyde group. Chromatographic separation performed on the residual mother liquor of the reaction originally leading to **3a** enabled to separate significant amount of *N*-formylpyrrolidine (**4a**), finally identifying the fate of the missing carbon atom.

Scheme 2

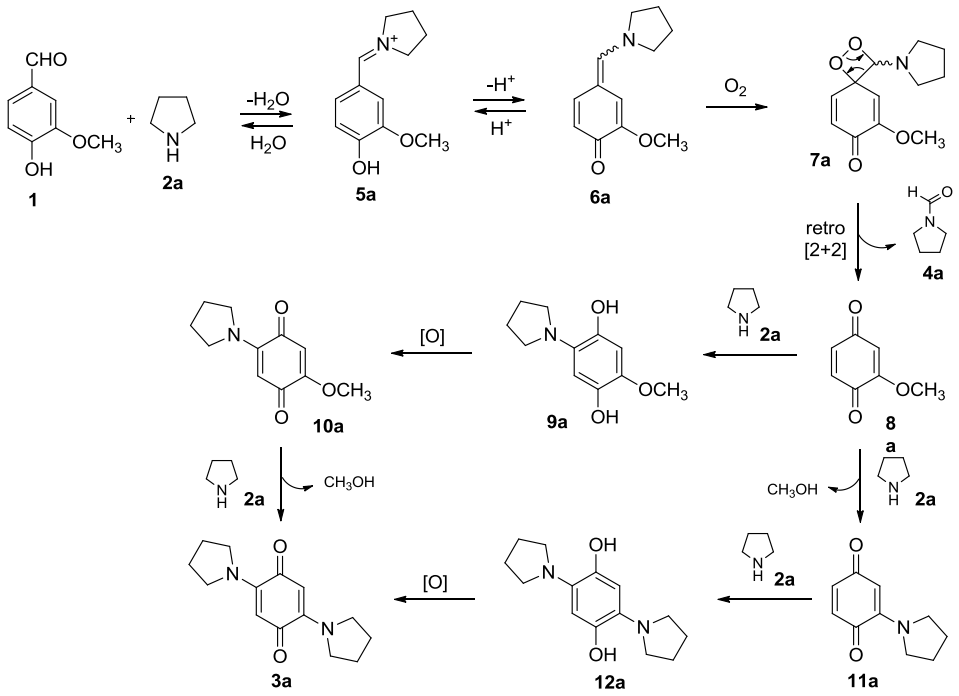

On the base of the experimental evidences collected in this preliminary investigation, we propose the following mechanism for this reaction (Scheme 2).

The conversion of vanillin to 2,5-diamino-1,4-benzoquinones starts with the dehydrative condensation of the aldehyde with the secondary amine (exemplified by pyrrolidine **2a** in Scheme 2) to give the intermediate iminium ion **5a**, that loses a proton to give the pyrrolidinoquinomethide **6a**. Structural analogues of **6a** were either invoked as intermediates in cycloadditions[10] or even isolated.[11] Aerobic oxidation of the enamine moiety[12] of the quinomethide takes place through a SET mechanism[9] leading to the formation of the dioxetane **7a**. The unstable four-membered ring immediately fragments likely through a retro[2+2] cycloaddition generating 2-methoxy-1,4-benzoquinone **8a** and the observed byproduct N-formylpyrrolidine **4a**. The quinone **8a** may be converted to the final 2,5-diamino-1,4-benzoquinone **3a** through two different and converging pathways, involving standard quinone chemistry[13]: i) conjugate addition of the secondary amine to give a 2-amino-5-methoxyhydroquinone **9a**, readily oxidised to the corresponding 1,4-benzoquinone **10a**, finally converted to **3a** with an *ipso*-substitution of the methoxy group operated through an addition-elimination mechanism;[13] ii) initial *ipso*-substitution of the methoxy group by the nucleophilic secondary amine yielding the 2-amino-1,4-benzoquinone **11a**, followed by addition of another molecule of amine to give the intermediate 2,5-diaminohydroquinone **12a**, finally oxidised to the stable end product **3a**.

Further support to this mechanism came from two additional experiments. Treatment of commercially available **8a** with a slight excess of pyrrolidine in ethanol at room temperature in aerobic conditions overnight gave as expected good yields of **3a**, confirming its involvement as intermediate in the reaction pathway. Additionally, ethylvanillin (3-ethoxy-4-hydroxybenzaldehyde, largely employed in virtue of its stronger flavouring note and persistance), gave the same reaction products on reaction with amines **2a-e**, even if slightly longer reaction times were needed in order to reach complete conversion.

The reaction of vanillin with secondary amines appears to be an efficient transformation, taking place in mild conditions and with good to excellent yields. Safety concerns may be raised by the possibility of this reaction to take place during cooking processes in the hot aerobic environment of baking ovens, with foods on which vanillin is usually sprayed as an ethanolic solution. Indeed, we observed the formation of 2,5-diprolino-1,4-benzoquinone **3f**, from the reaction of vanillin with excess proline (taken as a model of biogenic secondary amine), even if basic mixed aqueous-ethanolic conditions were needed to solubilize proline and low yield were registered.

Preliminary toxicity tests were undertaken in order to evaluate the potential biological effect of 2,5-diamino-1,4-benzoquinone, for which no literature data are available except for the 2,5-diaziridino analogues, where cytotoxicity and mutagenicity is well documented[14] but clearly related to the presence of the strained aziridine heterocyclic three-membered rings rather than to the benzoquinone moiety. The first results indicate that even at high concentration 2,5-diamino-1,4-benzoquinones do not show clear toxic effects, though more detailed investigation are needed.

Experimental section

The appropriate secondary amine (4 eq) was added at room temperature to a stirred solution of vanillin (1 eq) in ethanol. The resulting reaction mixture was stirred at room temperature, checking periodically by TLC. The precipitate was filtered and the residual solvent was removed under reduced pressure. The reaction with L-proline was carried out using the same procedure, adding potassium carbonate (4 eq) to the reaction mixture. The same procedures were used to perform the reaction on ethyl-vanillin (3-ethoxy-4-hydroxybenzaldehyde).

Coclusions

In this work we report the observation of an unprecedented reaction of vanillin with secondary amines in aerobic conditions, leading to the highly efficient formation of 2,5-diamino-1,4-benzoquinones. The reaction involves several steps and intermediates, as exemplified by the reaction mechanism, proposed on the base of literature evidences and suitably designed experiments. The importance of this reaction stems resides in the possibility of this transformation to occur more frequently than considered until now, due to the large use of vanillin (and derivatives thereof, as ethylvanillin) and the occurrence of secondary amines, either biogenic or thermally/chemically generated in the experimental conditions encountered in food processing.

REFERENCES

[1] A. K.. Sinha, U. K. Sharma and N. Sharma; International J. of Food Sciences and Nutrition (2008) 59(4), 299–326.

[2] D.L.J. Opdyke; Food Cosmet. Toxicol. (1977)15, 633–638.

[3] H.P.V. Rupasinghe, J. Boulter-Bitzer, , A. Taehyun and J.A. Odumeru; Food Res. Int. (2005) 39, 575–580.

[4] Y.F. Sasaki, T. Ohta, H. Imanishi, M. Watanabe, K. Matsumoto, T. Kato and Y. Shirasu; Mutat. Res. (1990) 243, 299–302.

[5] K. Ho, L.S. Yazan, N. Ismail and M. Ismail; Cancer Epidemiol. (2009) 33, 155–160.

[6] A. Tai, T. Sawano, F. Yazama and H. Ito; Biochim. Biophys. Acta (2011)1810, 170–177.

[7] V.A. Yaylayan and A. Huyghues-Despointes; Crit. Rev. Food Sci. Nutr. (1994), 34(4), 321-369.

[8] W. Chobpattana, I.J. Jeon and J. Scott Smith; J. Agric. Food Chem. 2000, 48, 3885-3889.

[9] A. Marxer; Helv. Chim. Acta (1955), 38, 1473-89

[10] L. Y. Ukhin, L. V. Belousova, Zh. I. Orlova, S. V. Shishkina, and O. V. Shishkin; Russ. Chem.
Bull. 2002, 51(7), 1262-1269.

[11] M. B. Gazizov, R. K. Ismagilov, L. P. Shamsutdinova, R. F. Karimova, and O. G. Sinyashin;
Russ. J. Gen. Chem. 2006, 76(7), 1176-1177.

[12] B. Tiwari, J. Zhang and Y. R. Chi; Angew. Chem. Int. Ed. 2012, 51, 1911 – 1914.

[13] R. N. Harger; J. Am. Chem. Soc. 1924, 46, 2540-2551.

[14] R.H.J. Hargreaves, J.A. Hartley, J. Butler; Frontiers in Bioscience (2000), 5, E172-E180

CHAPTER 7

CONCLUSIONS

The PhD activity was dedicated to a wide range exploration of the chemistry of imaging probes. The large number of diagnostic techniques developed in the last decades stimulated a vast research activity in the field of imaging probes. Imaging probes are useful and sometimes necessary for the acquisition of the diagnostic images. The work of the PhD period tackled various aspects of the chemistry of imaging probes, spanning from chelating agents for MRI and PET applications, to π-extended luminescent heterocycles for potential use in Optical Imaging. The work on chelating agents was concretized in the design of a novel diaminotetracarboxylic ligand, whose coordination ability towards metal ions of diagnostic interest and biologically relevant ones was studied. The synthesis, involving two simple steps from a commodity chemical, allowed to prepare multigram samples of the chelating agents and to perform a systematic study of the affinity towards metal ions by means of potentiometric techniques.

Furthermore, a chelating agent originally developed for lanthanoids, was devised for possible application to long-lived positron emitting radionuclides, recently gaining interest for metabolic multi-day imaging. In detail, thermodynamic and kinetic parameters for the interaction of AAZTA (a ligand originally developed on our research group for Gd^{3+} with Sc^{3+}), were determined by a combination of potentiometric, multinuclear NMR and spectrophotometric techniques. The results were striking, with the observation of a noteworthy stability constant that, joined with an exceptionally slow dissociation kinetic represent an extremely positive combination for the development of probes for nuclear medicine.

The research towards Optical Imaging probes involved the scrutiny of structures combining favourable photophysical properties (*e.g.*: intense luminescence) with additional features, useful for biological applications. In this context we choose the diazaheterotricyclic nucleus of perimidines in order to prepare and to study selected substitutes derivatives. The easy synthetic access to 2-substituted perimidines was exploited for the preparation of a total of six members of this heterocyclic family, all of them with a substantial fluorescence, modulated by the nature of the different substituents. This property and the reported DNA-binding ability of perimidines, confirmed in our study, lead to interesting potential development of targeted imaging probes based on this heterotricyclic scaffold.

Finally, the research activity devoted to Optical Imaging probes led to a serendipitous discovery. While performing synthetic approaches en route to push-pull quinomethides, we observed the unexpected highly efficient formation of 2,5-diamino-1,4-benzoquinones from the reaction of vanillin with excess secondary amines in aerobic conditions. Puzzled by this unusual observation, a systematic study was undertaken in order to elucidate the mechanism and the substrate versatility of this reaction. The experiments performed allowed to draw a likely hypothesis of the mechanistic pathway, involving a complex multistep sequence. The reaction appears to be limited to secondary aliphatic amines and the involvement of 2-methoxybenzoquinone as an intermediate was demonstrated. The study of this transformation, even if not directly related to the chemistry of Imaging probes, was nevertheless worthwhile for its implications in food chemistry, due to the large use of vanillin and to the superimposability of the reaction conditions to those usually encountered in the baking oven environment.

List of publications

- ✓ Arianna Maria Giani[a,b], Adrienn Vágner[a] Roberto Negri[b], Zsolt Baranyai[a], Giovanni Battista Giovenzana[b]*

  ***cis*-IPDTA: an Original Polyaminopolycarboxylic Chelating Agent from Isophoronediamine. Synthesis and Thermodynamic Characterization of Metal Complexes**

  Accepted for publication in *"Polyhedron"*

- ✓ Zsolt Baranyai,[a] Arianna Maria Giani,[a,b] Roberto Negri,[b] Giovanni Battista Giovenzana[b]

  Determination of Thermodynamic and Kinetic Parameters for the Sc(III)-AAZTA System

  Unpublished

- ✓ Arianna Maria Giani,[1] Marco Lamperti, [2] Angelo Maspero,[3] Alessandro Cimino,[3] Roberto Negri,[1] Giovanni Battista Giovenzana,[1] Giovanni Palmisano,[3] Luca Nardo[2]*

  Fluorescence studies on 2-(het)arylperimidine derivatives

  Submitted: *Journal of Luminescence*

- ✓ Arianna M. Giani, Valentina Papillo, Roberto Negri, Fabiano Travaglia, Marco Arlorio*, Giovanni B. Giovenzana*

  Unprecedented formation of 2,5-diaminoquinones from the reaction of vanillin with secondary amines in aerobic conditions

  Unpublished

Acknowledgements

It is a pleasure to thank the many people who helped me in my Phd road.

I would like to express special thanks to the people in the laboratory of Inorganic and Analytical Chemistry of the University of Debrecen. All of you are fantastic and I remember you with a big smile because you have transformed a difficult period for me (far from home) in one of the best experiences of my life.
I would like to thank Roberto for his critical point of view!
A special thought for friends of DISCAFF and "CAPANNONE". My appreciation goes to Tracey, Chiara and Simona for "special canteen moments"…Paolo and Ivan for hilarity moments … I love you all so much!!!
A big acknowledgement to my special friends Saretta and Valentina: I'm sure I will miss you but fortunately we have a WhatsApp group entitled "desiderio di ciccionate".
I would like to express my special thank to Claudia: my collegue but above all my big friend...
A big thank to my special Mom Tiziana and my dear "Plicketta" always there for me.

Lastly I wish to thank my husband Davide, he supported me every day. To he I dedicate this three years and this thesis...

…..Arianna